NAVAL POSTGRADUATE SCHOOL

MONTEREY, CALIFORNIA

THESIS

DYNAMIC RESPONSE OF A CATAMARAN-HULL SHIP SUBJECTED TO UNDERWATER EXPLOSIONS

by

Hakan Ucar

December 2006

Thesis Advisor:	Young S. Shin
Co-Advisor:	Jarema M. Didoszak

Approved for public release; distribution is unlimited

THIS PAGE INTENTIONALLY LEFT BLANK

REPORT DOCUMENTATION PAGE		*Form Approved OMB No. 0704-0188*
Public reporting burden for this collection of information is estimated to average 1 hour per response, including the time for reviewing instruction, searching existing data sources, gathering and maintaining the data needed, and completing and reviewing the collection of information. Send comments regarding this burden estimate or any other aspect of this collection of information, including suggestions for reducing this burden, to Washington headquarters Services, Directorate for Information Operations and Reports, 1215 Jefferson Davis Highway, Suite 1204, Arlington, VA 22202-4302, and to the Office of Management and Budget, Paperwork Reduction Project (0704-0188) Washington DC 20503.		
1. AGENCY USE ONLY *(Leave blank)*	**2. REPORT DATE** December 2006	**3. REPORT TYPE AND DATES COVERED** Master's Thesis
4. TITLE AND SUBTITLE Dynamic Response of a Catamaran-Hull Ship Subjected to Underwater Explosions		**5. FUNDING NUMBERS**
6. AUTHOR(S) Hakan Ucar		
7. PERFORMING ORGANIZATION NAME(S) AND ADDRESS(ES) Naval Postgraduate School Monterey, CA 93943-5000		**8. PERFORMING ORGANIZATION REPORT NUMBER**
9. SPONSORING /MONITORING AGENCY NAME(S) AND ADDRESS(ES) N/A		**10. SPONSORING/MONITORING AGENCY REPORT NUMBER**
11. SUPPLEMENTARY NOTES The views expressed in this thesis are those of the author and do not reflect the official policy or position of the Department of Defense or the U.S. Government.		
12a. DISTRIBUTION / AVAILABILITY STATEMENT Approved for public release; distribution is unlimited		**12b. DISTRIBUTION CODE** A
13. ABSTRACT (maximum 200 words) Surface Ship Shock trials play an essential role in ship test and evaluation (T&E), and Live Fire Test and Evaluation (LFT&E) requirements for the lead ship of each new construction shock-hardened ship class. While these trials are necessary in order to evaluate the vulnerability and survivability of the ship, they are very expensive, require extensive time for planning and coordination, and pose serious danger to the crew, ship and marine environment. Thus, computer modeling of the ship structure, surrounding fluid, and virtual shock environment by utilizing finite element method offers a valuable design tool and an alternative to these tests. This thesis investigates the response of a catamaran-hull ship subjected to an underwater explosion by creating a virtual UNDEX environment based on the modeling and simulation methodology established by the Shock and Vibration Computational Laboratory at the Naval Postgraduate School (NPS). In previous works, all of the structural models were monohull ships and there have been concerns about the feasibility of creating the coupled fluid and catamaran-hull model. This thesis studies the effect of an additional hull and gap between two hulls on the dynamic response of the ship as well as the effect of the charge location.		
14. SUBJECT TERMS Underwater Explosion, Shock and Vibration, Modeling and Simulation, M&S, Ship Shock, UNDEX, Shock Response, Ship Shock, Sea TENTACLE	**15. NUMBER OF PAGES** 158	
	16. PRICE CODE	
17. SECURITY CLASSIFICATION OF REPORT Unclassified	**18. SECURITY CLASSIFICATION OF THIS PAGE** Unclassified	**19. SECURITY CLASSIFICATION OF ABSTRACT** Unclassified	**20. LIMITATION OF ABSTRACT** UL

THIS PAGE INTENTIONALLY LEFT BLANK

DYNAMIC RESPONSE OF A CATAMARAN-HULL SHIP SUBJECTED TO
UNDERWATER EXPLOSIONS

Hakan Ucar
Lieutenant Junior Grade, Turkish Navy
B.S. ME, Turkish Naval Academy, 2001

Submitted in partial fulfillment of the
requirements for the degree of

MASTER OF SCIENCE IN MECHANICAL ENGINEERING

from the

**NAVAL POSTGRADUATE SCHOOL
December 2006**

Author: Hakan Ucar

Approved by: Young S. Shin
                 Thesis Advisor

                 Jarema M. Didoszak
                 Co-Advisor

                 Anthony J. Healey
                 Chairman, Department of Mechanical and Astronautical
                 Engineering

iii

THIS PAGE INTENTIONALLY LEFT BLANK

ABSTRACT

Surface Ship Shock trials play an essential role in ship test and evaluation (T&E), and Live Fire Test and Evaluation (LFT&E) requirements for the lead ship of each new construction shock-hardened ship class. While these trials are necessary in order to evaluate the vulnerability and survivability of the ship, they are very expensive, require extensive time for planning and coordination, and pose serious danger to the crew, ship and marine environment. Thus, computer modeling of the ship structure, surrounding fluid, and virtual shock environment by utilizing finite element method offers a valuable design tool and an alternative to these tests.

This thesis investigates the response of a catamaran-hull ship subjected to an underwater explosion by creating a virtual UNDEX environment based on the modeling and simulation methodology established by the Shock and Vibration Computational Laboratory at the Naval Postgraduate School (NPS). In previous works, all of the structural models were monohull ships and there have been concerns about the feasibility of creating the coupled fluid and catamaran-hull model. This thesis studies the effect of an additional hull and gap between two hulls on the dynamic response of the ship as well as the effect of the charge location.

THIS PAGE INTENTIONALLY LEFT BLANK

TABLE OF CONTENTS

LIST OF FIGURES

xi

THIS PAGE INTENTIONALLY LEFT BLANK

LIST OF TABLES

THIS PAGE INTENTIONALLY LEFT BLANK

ACKNOWLEDGMENTS

There are many people I would like to thank for a huge variety of reasons.

I would first like to thank Research Assistant Prof. Jarema M. Didoszak for his overwhelming support and understanding throughout my thesis. With his enthusiasm, and his great efforts, he helped to make this thesis fun for me.

I would also like to thank Professor Young Shin for his support and vision. Throughout my thesis period, he provided encouragement, sound advice, and excellent teaching. I am very proud that I had the chance to work with them.

I am grateful to Mr. Dibyendu Datta for assisting me during the ABAQUS simulation of this research.

I am forever indebted to my parents for their understanding, endless patience, and encouragement when it was most required.

Finally, I would like to thank my loving wife Neslihan, most of all for her love, support, patience, and understanding during our time at the Naval Postgraduate School, especially during my hard work in this research.

THIS PAGE INTENTIONALLY LEFT BLANK

I.   INTRODUCTION

A.   BACKGROUND

Prior to World War II, almost all underwater explosive damage to naval ships was caused by contact explosions. At that time, one of the best ways to destroy a ship was to open a hole in the hull under the waterline by a direct hit and wait for flooding to reduce the stability of the ship so that the ship would sink. Aside from this, only a direct hit to a weapons magazine, an engine room or fuel tanks would result in the devastating loss of a ship. Since the result of a contact explosion is the destruction of the ship's structure in the immediate area of the explosion, only very slight effect of the explosion is transmitted to the other parts of the ship [Ref. 1].

In the late 1930s, the Bureau of Ships performed experiments on small structural models of the naval vessels in the Norfolk Naval Shipyard in order to determine the underwater explosions (UNDEX) effects. In the early 1940s, the test group in the shipyard designed and manufactured the Underwater Explosions Barge (UEB-1) in order to expand the experimental testing capabilities. Several tests were made in order to learn how to improve the strength of the hull to withstand the severe effects of underwater explosions. Early in World War II, the non-contact explosion was introduced. This type of explosion was later found to cause severe underwater shock to the ships. When the non-contact underwater explosion occurred, the ship's back was broken as it was raised up and then struck down into the water. As a consequence, the ship sank into the gap left by the explosion. Increasing the charge weight resulted in more damage to the ship. Thus, it was understood that a direct hit was not necessary to disable the ship capabilities. According to the analysis of the wartime ship losses suffered during the first half of the twentieth century, it was determined that the incident shock wave and gas bubble pulse forces caused severe structural damage and material failure, and resulted in the sinking of several ships [Ref. 2].

Research on the effects of underwater explosions was increased by the U.S. Navy and as a result the Underwater Explosions Research Division (UERD) was established on December 18, 1946, in Portsmouth, Virginia. UERD undertook experiments focused on

improving the resistance of the ships and submarines subjected to underwater weapons, evaluating the effects of underwater explosions on ships. UERD has worked with many other Navy and Department of Defense divisions and support contractors in executing full scale ship and submarine shock trials, weapons effects trials, equipment shock hardening and qualification tests. They also performed precision experiments with scale-model targets and free field phenomena experiments [Ref. 2].

During the past 50 years, ongoing research efforts in the field of UNDEX shock phenomena have resulted in a wide knowledge base in this phenomenon. Thus, guidelines and specifications were developed for the shock testing and hardening of shipboard equipment and systems. NAVSEA 0908-LP-000-3010A [Ref. 3] and MIL-S-901D [Ref. 4] are examples of this guidance. The ship system design is validated through shock trials as required in OPNAVINST 9072.2 [Ref. 5]. The DDG-81 Ship Shock Trials, which were completed in the summer of 2001, are the latest set of Live Fire Testing & Evaluations (LFT&E) to be executed in completion of these requirements.

The shock trials, a series of underwater explosions, are necessary in order to obtain a sufficient knowledge of the problem due to the complexity of the shock problem. The variety of equipment, the different locations of these equipments and the diversity of the sources of the shock itself, all contribute to the complexity of the shock trials [Ref. 1]. Shock measurements and observations of the response of the ship, weapons systems, specific equipment, and crew are made. The data obtained from the tests is recorded in order to assess their individual and system performance in a shock environment. After analyzing the data obtained from one of the ships in the same class or from a ship having major design changes during construction, recommendations are made for the modification of existing ships or for a change in the design of follow-on ships to be built within that same ship class.

Due to the difficulty and complexity associated with the conduct of the shock trial, these tests are very expensive and dangerous. They require comprehensive planning and coordination as well as sensitive equipment for measurement. Possible damage to the ship structure, electronics and multi-million dollar weapons systems is also an ever-present consequence. Although these tests give an accurate account of the system response, they are limited to testing only two-thirds of the ships' design limits due to the

safety concerns for the ship, equipment and crew. In the situation of the USS JOHN PAUL JONES (DDG-53) ship shock trials conducted in 1994, planning of the test took four years and involved over 50 government agencies and a shock team of 300 personnel. Due to the lawsuit brought by the environmentalist groups, the shock trials of DDG-53 were postponed three months. The shock tests were executed in June 1994, but only two of the four planned tests could be accomplished due to rough weather and post-delivery schedule considerations [Ref. 6]. The cost of shock trials ranged as high as 5% of the $950 million delivery cost of USS JOHN PAUL JONES (DDG-53) [Ref. 7]. The cost of shock trials of USS WINSTON S. CHURCHILL (DDG-81) conducted in May and June 2001 was $20million and the same limitations were also applied to these shock trials [Ref. 8].

In the last few years, extraordinary advances in computer modeling and simulation have introduced the shock tests in a virtual shock environment in order to reduce some of the costs associated with the LFT&E activities [Ref. 9]. By accomplishing these technologies, simulations can accurately predict the initial peak response of a ship subjected to an underwater shock event and allow for faster improvements in design and less cost. Besides, the simulations can be executed beyond the design limits providing more design information than that obtained by real shock trials [Ref. 8]. Thus, creating a virtual UNDEX environment for the ship system will be an effective method for shock trials without harming the ship crew or the environment.

The finite element method is used for meshing the structural and fluid model. In order to obtain accurate results, the finite element models must be strictly detailed and the surrounding fluid mesh must be coupled with the wetted surface of the structural mesh. Since the UNDEX environment is very complex due to the effects of cavitation, bubble pulse and structural whipping, the coupled fluid and structural model must be almost perfect. The computational time step must be very small, on the order of microseconds while the ship response lasts on the order of seconds.

This method can be used during the ship design, integrating predictive results gained from the simulations into the final stages of the design. Making the changes while the ship is still in the construction phase, helps reduce the overall cost.

Even though this approach is not sufficiently reliable enough at this time to completely replace the LFT&E process, it can be used as a predictive design tool. Through the knowledge obtained in the virtual UNDEX environment and further improvements in computer processing technology, virtual shock trials may eliminate the requirement for the LFT&E process and the need for broad scope shots and stimulate the investigation of UNDEX events with the use of scalable charges located at specified locations related to the points of concern determined in previous shock trial simulations.

B.   SCOPE OF RESEARCH

This thesis investigates the response of a catamaran-hull ship subjected to an underwater explosion by creating a virtual UNDEX environment based on the modeling and simulation methodology established by the Shock and Vibration Computational Laboratory at the Naval Postgraduate School (NPS). In previous works, all structural models were monohull ships and there have been concerns about the feasibility of creating the coupled fluid and catamaran-hull model. This thesis studies the effect of an additional hull and gap between two hulls on the dynamic response of the ship. The effect of the gap between the hulls will be investigated by comparing the responses of selected equivalent nodes on each hull. It also investigates the effect of the standoff distance from the charge on the response of the model.

The structural model is constructed using the TrueGrid finite element mesh generation program whereas the fluid model is generated using the ABAQUS finite element solver. Ship shock simulation of the Sea TENTACLE model is conducted using the ABAQUS/Explicit finite element analysis module.

The results from the ship shock simulations will validate the fluid modeling and UNDEX analysis in ABAQUS/CAE, and provide the basis for further investigation of the dynamic response of the catamaran-hull ships.

II. UNDERWATER EXPLOSIONS

Underwater explosions (UNDEX) occurring in the water near the ship hull are of great concern to naval surface ships and submarines since they can result in major hull damage. Analyzing this phenomenon requires understanding a complex sequence of events, shock wave propagation, bulk cavitation and fluid-structure interaction phenomena. Underwater explosions may be classified in two categories [Ref. 1].

a) Contact underwater explosions: This type of explosion occurs in the water adjacent to or in contact with the hull of the ship, such as an impact-fused torpedo hit or the explosion of a contact mine. These explosions result in severe local damage to the hull.

b) Non-contact underwater explosions: This type of explosion occurs at a given distance from the ship in water that is not in contact with the hull of the ship. The detonation of depth charges consisting of high explosives such as HBX-1, RDX, TNT and PETN is an example of non-contact underwater explosions. These explosions result in the most serious and severe shock damage to the ships.

Non-contact underwater explosions are the type considered in this work.

A. SEQUENCE OF EVENTS

It is very important to understand the sequence of events that occurs in the water as a result of an underwater explosion. The sequence begins with the detonation of a high explosive such as TNT, HBX-1, RDX, or PETN. After the detonation of the explosive, a shock wave travels through the charge material at a constant, high speed of approximately 25,000 ft/sec, converting the solid charge to a dense gas at great temperatures and pressures on the order of 3000° C and 50,000 atm pressure, without change in volume [Ref. 10]. This event happens very rapidly in order to prevent the energy from having enough time to escape. The water is assumed to be compressible and homogeneous in UNDEX analysis. Assuming an ideal fluid, the water in UNDEX analysis does not support shear stresses and no heat transfer is considered. The high pressure gas compresses the surrounding water, that layer of water then compresses the

5

adjacent layer, and so on. As the gas expands, the water is forced radially outward, and this radial flow modifies the pressure distribution at points relatively close to the bubble [Ref. 2]. Therefore, a shock front is propagated radially outward at a velocity that exceeds the velocity of sound in the uncompressed water as shown in Figure 1.
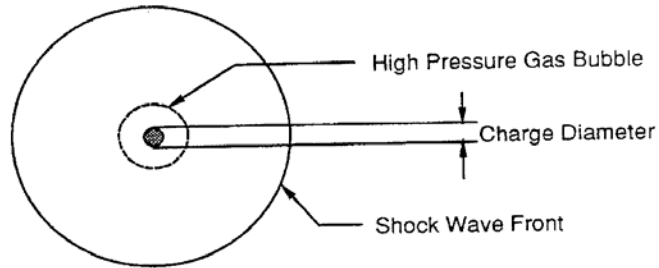
Figure 1. Gas Bubble and Shock Wave from an Underwater Explosion [Ref.10]

A shock wave is characterized by a discontinuous change in pressure, particle velocity, and density in a direction normal to the front. Figure 2 shows this type of pressure distribution for a 300 lb TNT underwater explosion [Ref. 10].
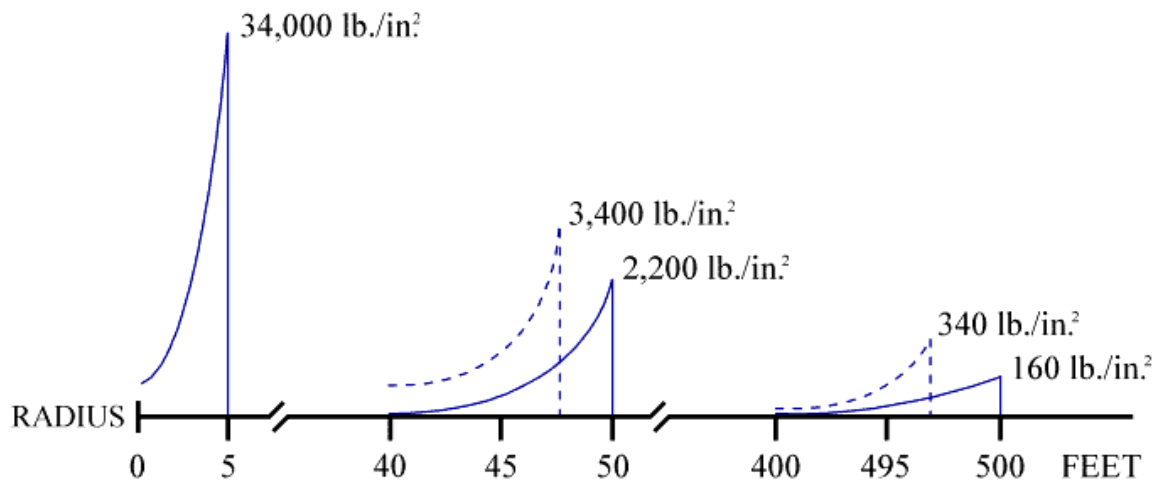
Figure 2. Shock Wave Pressure Profile for a Radially Expanding Wave From a 300 lb TNT Charge [Ref. 10]

Since the shock front is spherical, the pressure drops as the wave moves outward as seen in Figure 2. Thus, the resulting shock wave pressure profile is proportional to the inverse of the distance from the charge, 1/d.

6

Empirical equations are derived in order to characterize the shock wave pressure profile, P(t). These equations are accurate at distances between 10 and 100 charge radii, and for a duration of up to one decay constant in time after the initial detonation [Ref.10].

$$P(t)=P_{max}e^{-\frac{t-t_1}{\theta}} \qquad (psi) \qquad (2.1)$$

$$P_{max}=K_1\left(\frac{W^{\frac{1}{3}}}{R}\right)^{A_1} \qquad (psi) \qquad (2.2)$$

$$\theta=K_2 W^{\frac{1}{3}}\left(\frac{W^{\frac{1}{3}}}{R}\right)^{A_2} \qquad (msec) \qquad (2.3)$$

$$A_{max}=K_6\frac{W^{\frac{1}{3}}}{(D+33)^{\frac{1}{3}}} \qquad (ft) \qquad (2.4)$$

$$T=K_5\frac{W^{\frac{1}{3}}}{(D+33)^{\frac{5}{6}}} \qquad (sec) \qquad (2.5)$$

$$E = K_4 W^{\frac{1}{3}}\left(\frac{W^{\frac{1}{3}}}{R}\right)^{A_4} \qquad (lb\text{-}in/in^3) \qquad (2.6)$$

where P_{max} = the peak magnitude of the pressure in the shock front (psi)

$t-t_1$ = the time elapsed after the arrival of the shock (msec)

θ = the decay constant (msec)

R = standoff distance, radial (ft)

W = the weight of the explosive (lb)

D = charge depth (ft)

$K_1, K_2, K_4, K_5, K_6, A_1, A_2$ = constants depending on the explosive type

A_{max} = maximum bubble radius (ft)

T = the bubble oscillation period (sec)

E = energy per unit volume (lb-in/in^3)

The shock wave parameters are tabulated in Table 1. [Ref. 10]

Table 1.   Shock Wave Parameters [Ref. 10]

	CONSTANTS	HBX-1	TNT	PENTOLITE	NUKE
P_{max}	K_1	22347.6	22505	24589	4380000
	A_1	1.144	1.18	1.194	1.18
DECAY CONSTANT	K_2	0.056	0.058	0.052	2.274
	A_2	-0.247	-0.185	-0.257	-0.22
BUBBLE PERIOD	K_5	4.761	4.268	4.339	515
BUBBLE RADIUS	K_6	14.14	12.67	12.88	1500
ENERGY	K_4	3,086.5	3,034.9	3,135.2	3.313×10^8
	A_4	2.039	2.155	2.094	2.04

After generation of the shock wave, approximately 50% of the energy of the explosion is emitted in the shock wave. Since the bubble uses about half of the energy, the bubble pulse pressure can result in as severe damage as the shock wave itself. The gas bubble loses energy by the radiation. The shock wave moves outward as long as the gas bubble pressure is higher than hydrostatic pressure using its own energy. At some time, the gas pressure drops to the hydrostatic pressure prior to the explosion at some time when the gas bubble reaches its maximum diameter. Since the adjacent water still has an outward velocity, the gas bubble does not rest and continues to expand until the pressure becomes smaller than hydrostatic pressure. At this instant, the gas bubble reaches its maximum radius and the internal energy of the gas bubble is so small that it can be

neglected. Equation (2.4) is used to determine the maximum gas bubble radius. As shown from Equation (2.4), the maximum bubble diameter mostly depends on the charge type, depth and weight.

After reaching the maximum radius, the gas bubble pressure becomes so small that the hydrostatic pressure causes the gas sphere to be contracted and recompressed to a high pressure determined by the inward velocity of the water at the time the pressure returns to the hydrostatic pressure. Due to this recompression, a second wave forms and radiates into the water. The second bubble again reaches its equilibrium state and a maximum radius which is smaller than initial maximum radius. The gas sphere undergoes several compressions and re-expansions until it loses all of its energy or the bubble reaches the surface of the water [Ref. 1]. Figure 3 shows the oscillation of the gas bubble [Ref. 10].
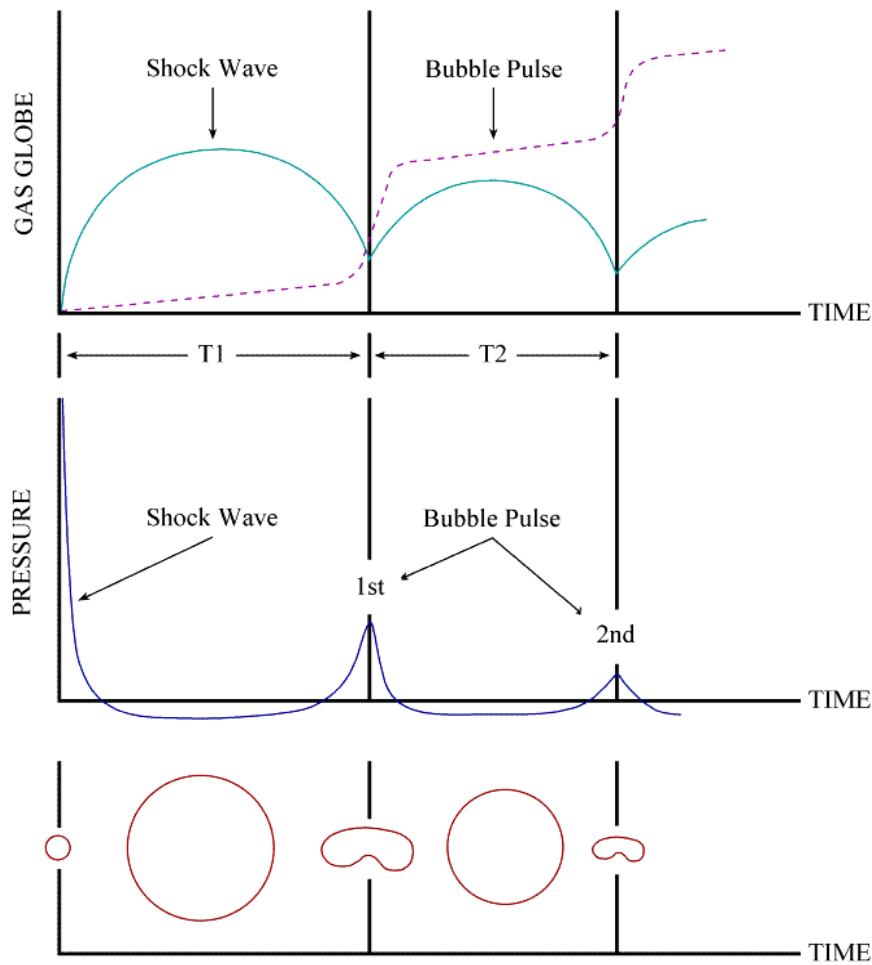
Figure 3.   Migration Pathway and Gas Bubble Oscillation [Ref. 10]

The gas bubble oscillation period can be calculated by Equation (2.5). As shown in Figure 3, the peak pressure of the shock wave is very big and decays very rapidly. Due to the energy loss, the maximum pressure of first bubble pulse is approximately 10-20% of shock wave pressure [Ref. 11]. The shock wave energy depends on the charge properties and standoff distance. Equation (2.6) is used to determine the shock wave energy.

Gravity has an important effect on bubble migration. It causes the gas bubble to migrate upward while it rises due to the buoyancy of the bubble [Ref. 10]. Using the impulse-momentum change theorem, the vertical bubble velocity (U) can be calculated by using Equation (2.7)

$$U = \frac{2g}{a^3(t)} \int_0^t a^3(t) \qquad \text{(ft/sec)} \qquad\qquad (2.7)$$

where g = gravitational acceleration constant

a = gas bubble radius

Since the vertical bubble velocity is proportional to the inverse of the third power of the bubble radius, it can be stated that the bubble rises faster when its size is minimum.

As seen in the empirical equations, the charge depth is of considerable interest. In shallow water, the gas pressure is less than atmospheric pressure when the gas bubble radius is about maximum. The air enters in the cavity very rapidly when the gas bubble reaches the surface and acts as a cushion in order to allow the closure and eliminate any closure pressure pulse. Therefore, it can be stated that the explosion depth should be less than the maximum bubble radius. The results will be acceptable if the charge depth is between 50% and 80% of maximum radius. [Ref. 10]

B.   CAVITATION

Cavitation is defined as the phenomenon that occurs in water led by the reflection of a shock wave at the surface. A tensile reflected wave, which is called rarefaction wave, occurs when the compressive shock wave is reflected from the free surface. Water cannot support the tensile force and cavitation occurs, leading to a pressure rise up to the vapor

pressure of water. There are two types of cavitation in an UNDEX event: bulk cavitation and local cavitation. Bulk cavitation can be regarded as the large area of low pressure at the free surface whereas local cavitation can be regarded as the small area of low pressure occurring at the fluid-structure interface. Cavitation has a tremendous effect on the overall response of the surface ships so that it must be taken into consideration in the simulation process [Ref. 12].

1.   Bulk Cavitation

In an UNDEX event, a three-dimensional spherical pressure wave forms and propagates outward from the detonation center. The underwater explosion attack geometry is shown in Figure 4. In an UNDEX event, the incident shock wave, which is compressive and the strongest wave, hits the target first and reaches the free surface. The rarefaction wave is formed by the reflection of the incident shock wave at the free surface. The direction of the rarefaction wave is opposite to the direction of propagation. Since the air-water interface is not a rigid boundary, it occurs as a tensile wave and poses a tensile force to water. As stated before, the water cannot support the tensile force and forms cavities which are filled with water vapor. The vapor pressure of water is about 0.3 psi. The rarefaction wave reaches the image after the incident wave as illustrated in Figure 5. After the arrival of the rarefaction wave, the pressure drops to zero or negative value. This is called "cut-off" in the pressure. The cavitation pressure is a negative pressure of three to four psi [Ref 13].

A bottom reflection wave is also formed due to the reflection of the shock wave at the sea bottom. However, this type of wave is of less interest in an UNDEX event due to the dependence on the sea bottom characteristics and its closeness to the target [Ref. 10].
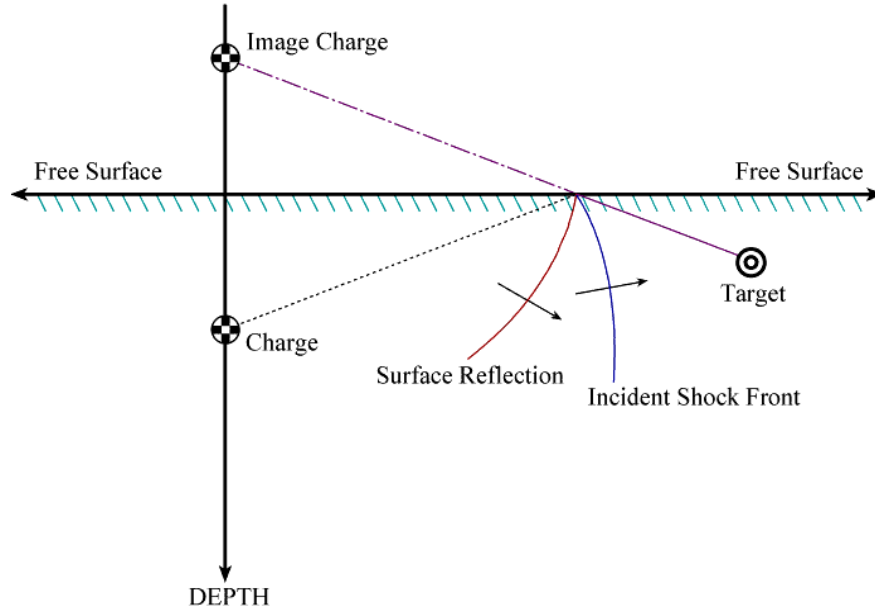
Figure 4.   Underwater Explosion Geometry [Ref. 10]
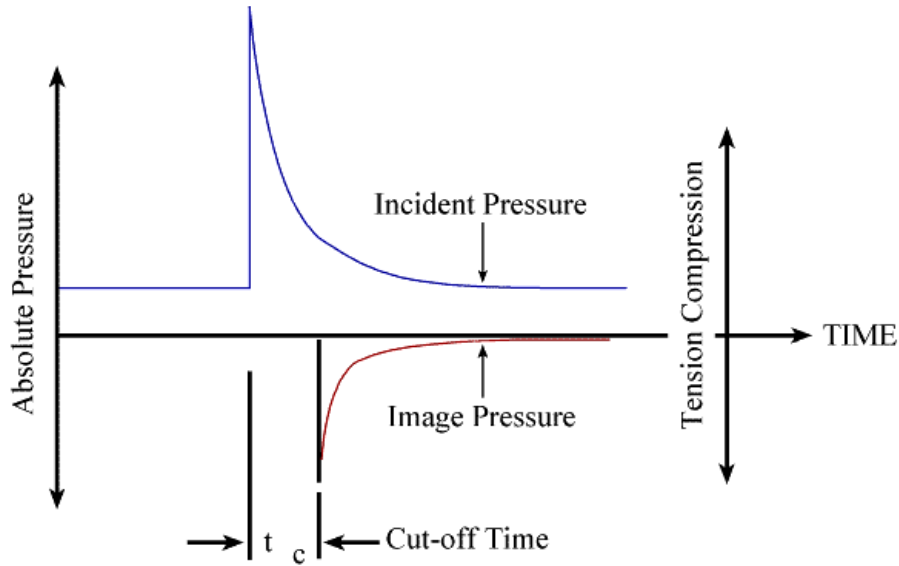
Figure 5.   Shock Wave Pressure Profile with Cut-off [Ref. 10]

The cavitated region formed by the rarefaction wave is called the bulk cavitation zone. It consists of two boundaries: the upper cavitation boundary and the lower cavitation boundary. The upper cavitation boundary is the region where the net pressure due to incident and reflected waves is zero. In point of fact, the net pressure below the surface is not zero at the cut-off time. The calculated net pressure may be less than zero

depending on the depth. As stated before, cavitation occurs where the total pressure is negative. Total pressure consists of compressive incident wave pressure, tensile rarefaction wave pressure, atmospheric pressure and hydrostatic pressure. Equation (2.8) with Equation (2.9) and (2.10) is used to determine the upper cavitation boundary by setting the total pressure to zero.

$$F(x, y) = K_1 \left(\frac{W^{\frac{1}{3}}}{r_1} \right)^{A_1} e^{-\frac{(r_2 - r_1)}{C\theta}} + P_A + \gamma y - K_1 \left(\frac{W^{\frac{1}{3}}}{r_2} \right)^{A_1} = 0 \qquad (2.8)$$

$$r_1 = \sqrt{(D - y)^2 + x^2} \quad \text{and} \quad r_2 = \sqrt{(D + y)^2 + x^2} \qquad (2.9) \text{ and } (2.10)$$

where x,y = the horizontal range and vertical depth of the point

r_1 = standoff distance from the charge to the point

r_2 = standoff distance from the image charge to the point

C = acoustic velocity in the water

D = charge depth

θ = decay constant (Equation (2.3))

P_A = atmospheric pressure

γ = weight density of water

W = charge weight

K_1, A_1 = shock wave parameters (see in Table 1)

The lower cavitation boundary is determined by equating the decay rate of breaking pressure and the decay rate of absolute pressure. The breaking pressure is defined as the rarefaction wave pressure that reduces the absolute pressure to the cavitation pressure [Ref. 10]. Equation (2.11) with Equation (2.12) is used to determine the lower cavitation boundary.

$$G(x, y) = -\frac{P_i}{C\theta}\left\{1 + \left[\frac{r_2 - 2D\left(\dfrac{D+y}{r_2}\right)}{r_1}\right]\left[\frac{A_2 r_2}{r_1} - A_2 - 1\right]\right\}$$

$$-\frac{A_1 P_i}{r_1^2}\left[r_2 - 2D\left(\frac{D+y}{r_2}\right)\right] + \gamma\left(\frac{D+y}{r_2}\right) + \frac{A_1}{r_2}(P_i + P_A + \gamma y) = 0 \qquad (2.11)$$

$$P_i = P_{max}\, e^{-\left[\frac{(r_2 - r_1)}{C\theta}\right]} \qquad (2.12)$$

where P_i = incident wave pressure at cut-off

A_1, A_2 = shock wave parameters (see in Table 1)

The MATLAB® code is used to determine these boundaries and plot the zone by solving the Equation (2.8) and (2.11). The results of the code depend on the user's input and analysis type. The code is provided in Appendix A.

The cavitation boundaries are highly dependent on the charge type, weight and depth as seen in the equations. Figure 6 illustrates that the charge depth has a very important effect on the cavitation region as stated before. The plots are generated for 150 lb Trinitrotouluene (TNT) charge at varying depths. As shown in Figure 6, the cavitation region (shown in red) stretches as the charge depth increases and the vertical depth of the region decreases due to the stretching. Therefore, the cavitation area is the largest when the charge is at 75 ft for a 150 lb charge. As a consequence, it can be stated that the cavitation area increases with increasing charge depth.
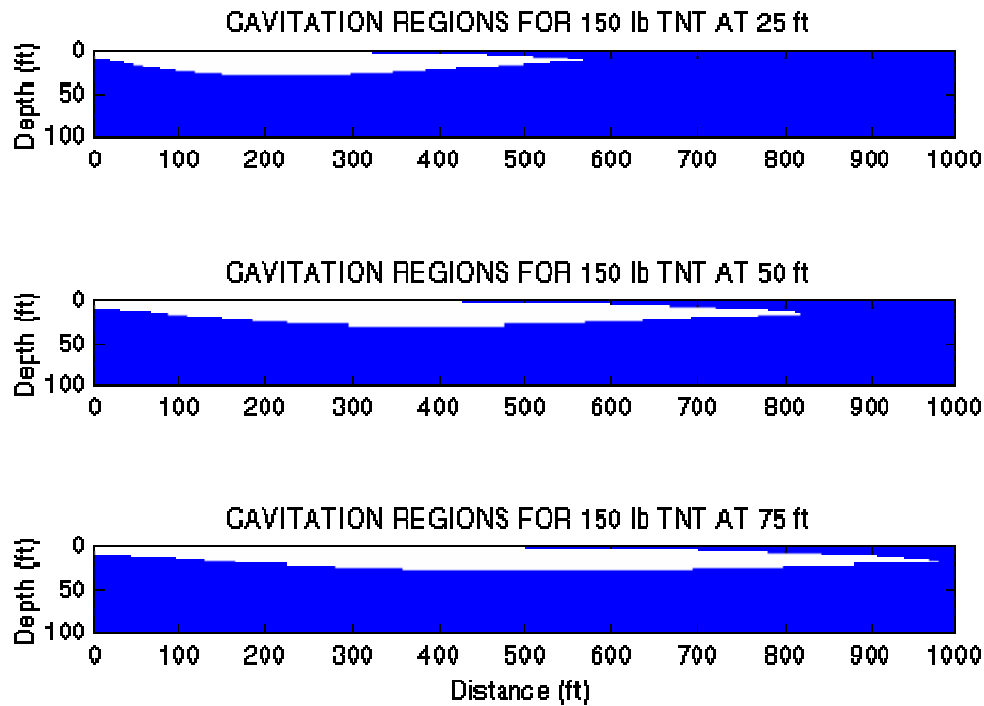
Figure 6. Bulk Cavitation Zone for 150 lb TNT Charge Detonated at Varying Depths

Figure 7 illustrates the effect of charge weight on the bulk cavitation zone. The plots are generated for HBX-1 at 50 ft depth with varying weights. As shown in Figure 7, the cavitation region for 300 lb HBX-1 is the largest, and the region for 100 lb the smallest, among them. It can be stated that the cavitation area increases with increasing charge weight while the region stretches. These effects can be combined such as increasing the weight but decreasing the depth. The cavitation region certainly changes due to the combined effects.
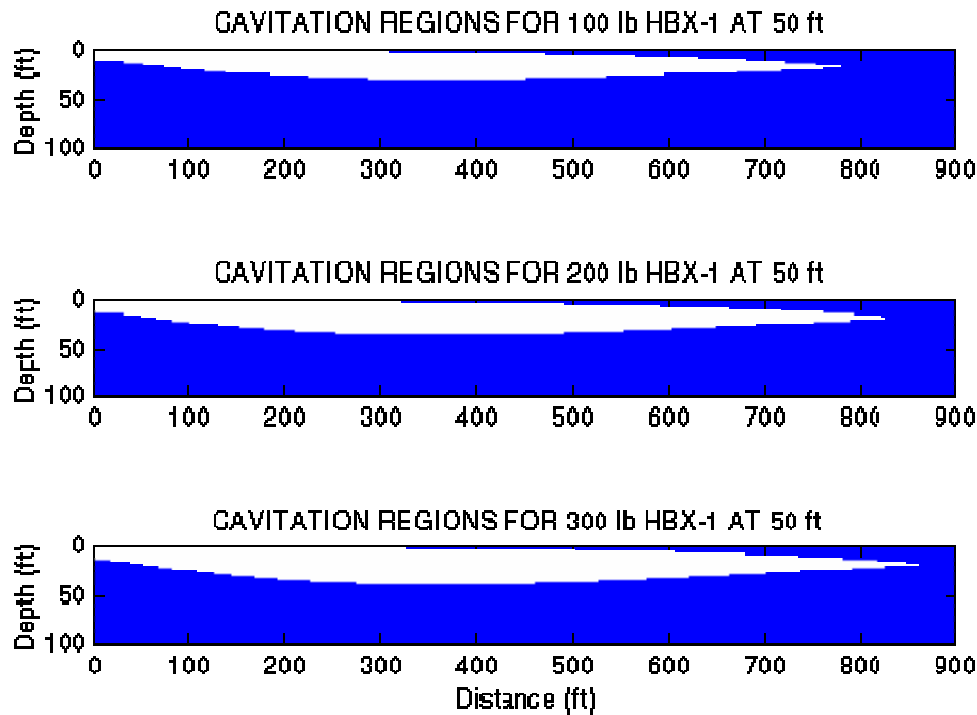
Figure 7.   Bulk Cavitation Zone for HBX-1 Charge Detonated at 50 ft with Varying Weights

Figure 8 illustrates the effect of charge type on the bulk cavitation zone. The plots are generated for TNT and HBX-1 charges detonated at the same depth (25 ft) and weight (200 lb). Each charge type has different shock wave coefficients that affect the cavitation region. Since the coefficients of HBX-1 are close to those of TNT, it is difficult to determine which explosive creates a larger cavitation area.

As shown in Figure 8, the cavitation region is more stretched when the TNT charge is used. For this situation, it can be stated that the cavitation region stretches when a charge having bigger P_{max} and decay constant coefficients is used. Many trials have been made in order to check the accuracy of this statement. For instance, increasing the charge depth gives the opposite result. For larger depths, the cavitation region is more

16

stretched when HBX-1 is used. Therefore, for larger depths it can be stated that the cavitation region increases when a charge having smaller P_{max} and decay constant coefficients is used.

The results for several trials are tabulated in Table 2 where the charge type that creates a larger cavitation region depending on the charge weight and depth is shown.
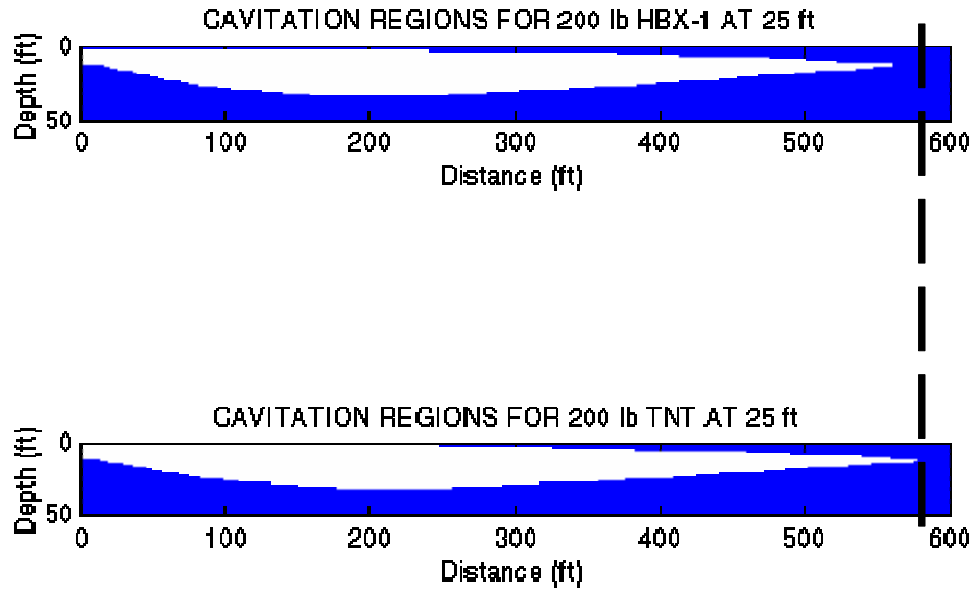
Figure 8. Bulk Cavitation Zone for 200 lb HBX-1 and TNT Charge Detonated at 25 ft

Table 2. Comparison of TNT and HBX-1 Charges

Charge Weight (lbs)	Charge Depth (ft)				
	10	30	50	100	200
25	TNT	TNT	HBX-1	HBX-1	HBX-1
50	TNT	TNT	TNT	HBX-1	HBX-1
100	TNT	TNT	TNT	HBX-1	HBX-1
200	TNT	TNT	TNT	TNT	HBX-1

As shown in Table 2, the cavitation region is greater when the TNT charge is used in shallow water. Otherwise, the cavitation region is greater when the HBX-1 charge is used. As a consequence, the charge types affect the cavitation region due to their shock wave parameters.

Although the plots exhibit a two-dimensional bulk cavitation region, it is actually a three-dimensional one that is generally symmetric about an imaginary vertical axis passing through the charge as shown in Figure 9. The shape of the bulk cavitation zone is similar to a cardioid just below the air-water interface. The bulk cavitation zone in Figure 9 is created by 100 lb Pentaerythritol Tetranitrate (PETN) at 75 feet depth [Ref 14].
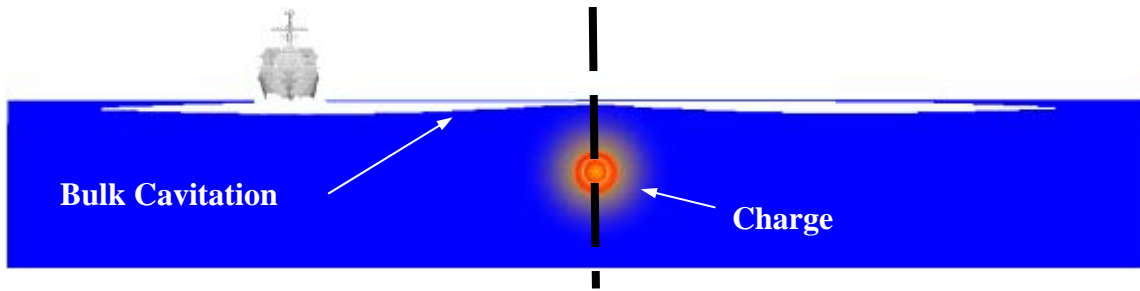
Figure 9.   Bulk Cavitation Zone in an UNDEX event [Ref. 14]

The vertical kick-off velocity of the surface ship can be determined by the fluid particle velocities near the free surface. According to Archimedes Law, the water particle velocity near the free surface is equal to the vertical kick-off velocity of the ship. After determining the centerline, the calculated water particle velocity can be used as an average vertical kick-off velocity of the ship.

2.   Local Cavitation

Local cavitation is the phenomenon that occurs at the fluid-structure interface due to the results of the interaction of the pressure pulse and the flexible surface of the structure. The shock pressure pulses that are produced by an UNDEX event excite the ship causing dynamic responses while they impinge on the ship and a fluid-structure

18

interaction occurs. Total pressure turns out to be negative along the hull. Since the water cannot support tensile pressure, the water pressure drops to the vapor pressure of water and local cavitation occurs.

Taylor flat plate theory, which was presented by G. I. Taylor, is the simplest fluid-structure interaction example. In this theory, an infinite, air-backed plate is used as the hull in order to illustrate the reaction of the hull subjected to the shock wave, as shown in Figure 10.
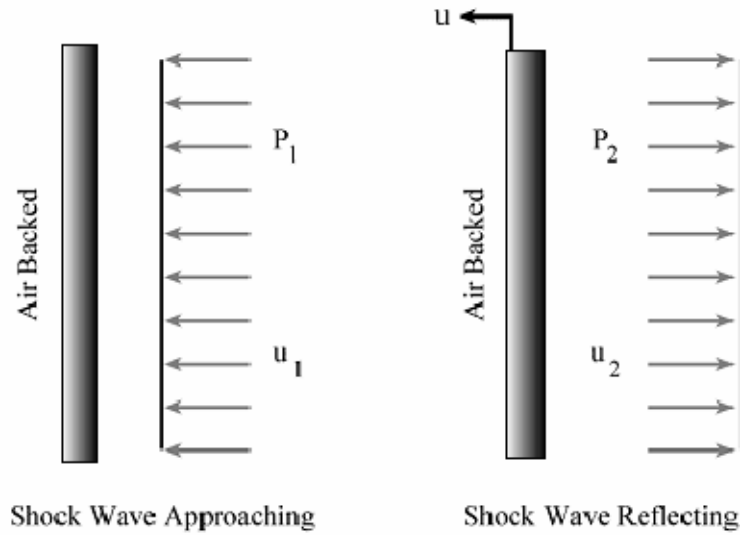
Figure 10.   Taylor Plate Subjected to a Plane Wave [Ref. 10]

As shown in Figure 10, the Taylor plate is subjected to the incident plane shock wave of pressure $P_1(t)$. After interacting with the plate, the reflected plane shock wave of pressure $P_2(t)$ is created and reflected off the plate. According to Newton's 2nd Law, the equation of motion of the plate can be written as

$$m\frac{du(t)}{dt} = P_1(t) + P_2(t) \tag{2.13}$$

where m = the mass of the plate per unit area

   $u(t)$ = the velocity of the plate

19

The velocities of the fluid particle behind the incident and reflected shock waves are defined as $u_1(t)$ and $u_2(t)$, respectively. Thus, the velocity of the plate can be defined as

$$u(t) = u_1(t) - u_2(t).$$ (2.14)

For one-dimensional incident and reflected shock waves, the wave pressures can be expressed as

$$P_1(t) = \rho C u_1(t)$$ (2.15)

$$P_2(t) = \rho C u_2(t)$$ (2.16)

where ρ = the fluid density

C = the acoustic velocity

Substituting Equations (2.15) and (2.16) into Equation (2.14) gives the relationship between the plate velocity and shock wave pressures.

$$u(t) = u_1(t) - u_2(t) = \frac{P_1(t) - P_2(t)}{\rho C}$$ (2.17)

The incident shock wave pressure $P_1(t)$ can be calculated by using Equation (2.1). Equation (2.1) is substituted into Equation (2.17) in order to obtain an expression for the reflected wave pressure $P_2(t)$.

$$P_2(t) = P_{max} e^{-\left(\frac{t-t_1}{\theta}\right)} - \rho C u(t)$$ (2.18)

The equation of motion, Equation (2.13) can be rewritten by substituting Equation (2.18).

$$m\left(\frac{du}{dt}\right) + \rho C u(t) = 2 P_{max} e^{-\left(\frac{t-t_1}{\theta}\right)}$$ (2.19)

20

Equation (2.20) is determined after solving the first order linear differential equation, Equation (2.19).

$$u(t) = \frac{2P_{max}\theta}{m(1-\beta)}\left\{ e^{-\left[\frac{\beta(t-t_1)}{\theta}\right]} - e^{-\left[\frac{(t-t_1)}{\theta}\right]} \right\} \qquad (2.20)$$

where $\beta = \dfrac{\rho C\theta}{m}$ and $t > 0$. Since the expression for the plate velocity is defined, the reflected shock wave pressure $P_2(t)$ and the net pressure at the plate can be described as

$$P_2(t) = \frac{P_{max}}{1-\beta}\left[(1+\beta)e^{-\left(\frac{t-t_1}{\theta}\right)} - 2\beta e^{-\left[\frac{\beta(t-t_1)}{\theta}\right]} \right] \qquad (2.21)$$

$$P_1 + P_2 = P_{max}\left\{ \frac{2}{1-\beta}e^{-\left[\frac{(t-t_1)}{\theta}\right]} - \frac{2\beta}{1-\beta}e^{-\left[\frac{\beta(t-t_1)}{\theta}\right]} \right\} \qquad (2.22)$$

As shown in Equation (2.20), the net pressure becomes negative at a very early time as β increases, which correlates to a lightweight plate. Local cavitation occurs when the tensile pressure turns out to be the vapor pressure of water and separates the plate from the water [Ref. 10]. The plate has maximum velocity at the cut-off time when the pressure in front of the plate occurs. The time at which the plate reaches its maximum velocity, t_0 can be determined by setting Equation (2.22) equal to zero and solving for t.

$$t_0 = \frac{\ln\beta}{\beta-1}\theta \qquad (2.23)$$

The maximum velocity of plate, u_{max} can be expressed by substituting t_0 into Equation (2.20).

$$u_{max} = \frac{2P_{max}\theta}{m(1-\beta)}\left[e^{-\left(\frac{\beta t_0}{\theta}\right)} - e^{-\left(\frac{t_0}{\theta}\right)} \right] \qquad (2.24)$$

The equations used in the Taylor plate theory are appropriate up to the beginning of the cavitation. After cavitation begins, the problem turns into a nonlinear and non-conservative problem and the equations are no longer valid. For light plate weights, a second loading occurs and increases the plate velocity due to the fact that the momentum of the light plate is equal to a fraction of the impulse in the shock wave. This loading can be more extreme than the first loading.

C.   FLUID-STRUCTURE INTERACTION

The fluid-structure interaction between the water and the hull due to the underwater explosion mainly occurs in the vertical direction. Since the shock wave impinges on the ship hull causing dynamic responses on the ship structure, the fluid-structure interaction has a great importance in an UNDEX event.

A matrix of differential equations is used to determine the approximate response of the ship with some acceptable degree of accuracy. This approximation is called the Doubly Asymptotic Approximation (DAA) and is applicable at both low and high frequencies and at early and late times [Ref. 12]. Equation (2.25), the discretized differential equation, defines the dynamic response of the ship structure.

$$[M_s]\{\ddot{x}\}+[C]\{\dot{x}\}+[K]\{x\}=\{f\} \tag{2.25}$$

where $\{x\}$ = the structural displacement vector

$[M_s]$ = the structural mass matrix

$[C]$ = the structural damping matrix

$[K]$ = the structural stiffness matrix

$\{f\}$ = the applied force vector

dots indicate the temporal derivative

As shown in Equation (2.25), the inertial forces, damping forces, internal forces and acoustic fluid pressure forces serve to set up the equilibrium configuration for the system [Ref. 15].

22

For a submerged structure evoked by an acoustic wave, the external forcing function can be expressed as,

$$\{f\} = -[G][A_f](\{p_I\} + \{p_S\}) + \{f_D\} \tag{2.26}$$

where $\{p_I\}$ = the nodal pressure vector for the wetted-surface fluid mesh pertaining to the incident wave

$\{p_S\}$ = the nodal pressure vector for the wetted-surface fluid mesh pertaining to the scattering wave

$\{f_D\}$ = the dry-structure applied force vector

$[G]$ = the transformation matrix relating the nodal surface forces

$[A_f]$ = the diagonal area matrix associated with the elements in the fluid mesh [Ref. 16].

The fluid-structure interaction problem in terms of wet-surface response can be solved by using the DAA. Since it is not applicable in the cavitation region, The First Order Doubly Asymptotic Approximation (DAA₁), which is expressed by Equation (2.27), is used for the long cylindrical shell structures such as surface ships or submarines [Ref. 17]. The DAA₁ is exact if the shell structure is spherical.

$$[M_f]\{\dot{p}_S\} + \rho c[A_f]\{p_S\} = \rho c[M_f]\{\dot{u}_S\} \tag{2.27}$$

where $\{u_s\}$ = the scattered wave fluid particle velocities vector normal to the structure's wetted surface

$[M_f]$ = the fluid mass matrix

ρ = the fluid mass density

c = the acoustic velocity of the fluid.

The fluid mass matrix $[M_f]$ is produced by a boundary-element treatment of Laplace's equation for the irrotational flow that is generated in an infinite, inviscid and incompressible fluid.

For the high frequency response, the Equation (2.27) can be expressed by a plane wave approximation as $p_s = \rho c u_s$. However, for the low frequency response, it can be expressed as $A_f p_s = M_f \dot{u}_s$ by using a virtual mass approximation [Ref. 18].

Since the problem is solved in terms of wet-surface response, the excitation of the wetted surface structure by an incident shock wave, $\{f\}$ is given by Equation (2.28) [Ref. 19].

$$\{f\} = -[G][A_f](\{p_I\} + \{p_S\}) \qquad (2.28)$$

The compatibility relation on the wetted surface of the structure, Equation (2.29) can be used to correlate the scattered wave fluid particle velocities to the structure response

$$[G]^T \{\dot{x}\} = \{u_I\} + \{u_S\} \qquad (2.29)$$

where T represents matrix transpose.

The DAA Interaction Equations are created by combining Equation (2.25) through Equation (2.29).

$$[M_s]\{\ddot{x}\} + [C]\{\dot{x}\} + [K]\{x\} = -[G][A_f](\{p_I\} + \{p_S\}) \qquad (2.30)$$

$$[M_f]\{\dot{p}_S\} + \rho c[A_f]\{p_S\} = \rho c[M_f]([G]^T \{\ddot{x}\} - \{\dot{u}_I\}) \qquad (2.31)$$

The two unknown quantities, x and p_S in Equations (2.30) and (2.31) can be solved by using a staggered solution scheme [Ref. 16].

III. MODELING

A. SEA TENTACLE MODEL
1. Structural Model

The 2005 Naval Postgraduate School Total Ship Systems Engineering (TSSE) interdisciplinary team design, "Sea TENTACLE", which has capabilities of anti-submarine warfare (ASW) and mine warfare (MIW), was used as the structural model basis for the investigation undertaken in this thesis work. Sea TENTACLE has a catamaran hull form that reduces the wave resistance due to the distribution of the displacement between the two hulls and increases stability in the ship's roll response [Ref. 20]. Sea TENTACLE is shown in Figure 11 and the ship hydrostatic characteristics are tabulated in Table 3.
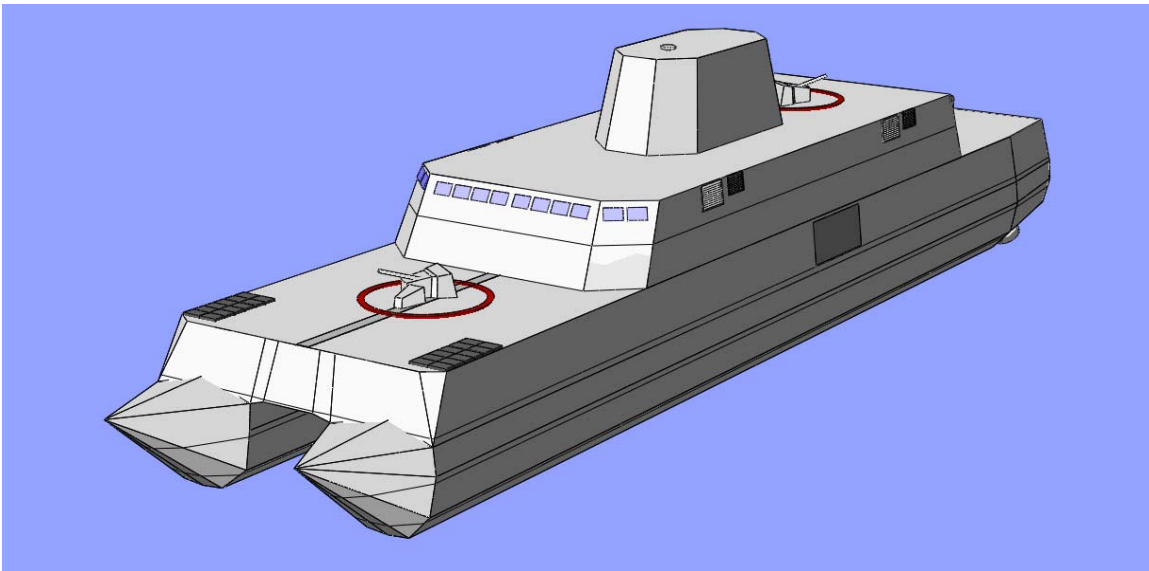
Figure 11.   Sea TENTACLE [Ref. 20]

Table 3. Hydrostatics Characteristics of Sea TENTACLE [Ref. 20]

Draft Amidsh. m	5.198	LCB from Amidsh. (+ve fwd) m	-0.888
Displacement tonne	7023	LCF from Amidsh. (+ve fwd) m	-0.816
Heel to Starboard degrees	-0.51	KB m	2.965
Draft at FP m	5.251	KG fluid m	5.925
Draft at AP m	5.144	BMt m	19.005
Draft at LCF m	5.197	BML m	260.973
Trim (+ve by stern) m	-0.107	GMt m	16.046
WL Length m	117.442	GML m	258.014
WL Beam m	24.553	KMt m	21.969
Wetted Area m^2	3268.975	KML m	263.937
Waterpl. Area m^2	1664.682	Immersion (TPc) tonne/cm	17.066
Prismatic Coeff.	0.925	MTc tonne.m	154.523
Block Coeff.	0.746	RM at 1deg = GMt.Disp.sin(1) tonne.m	1966.81
Midship Area Coeff.	0.806	Max deck inclination deg	0.5
Waterpl. Area Coeff.	0.964	Trim angle (+ve by stern) deg	-0.1

The model of Sea TENTACLE was created by using the Computer Aided Design (CAD) tool RHINO 3.0. The structural model was imported as an IGES file into the finite element mesh generation program TrueGrid [Ref. 21] in order to generate the structural mesh. The mesh generation of the structural model using TrueGrid is explained in Appendix C. The final structural mesh is shown in Figure 12.
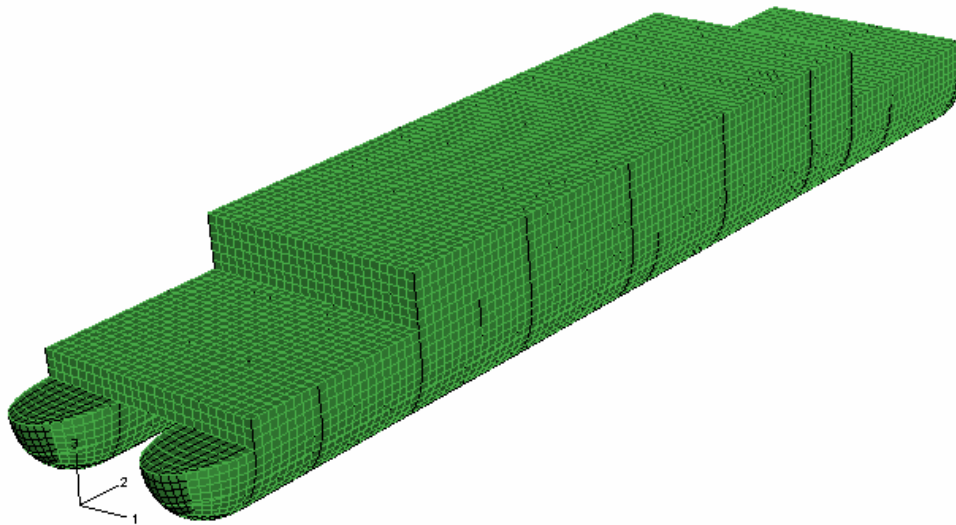
Figure 12. The structural mesh of Sea TENTACLE model

The model is consistent with the dimensions of Sea TENTACLE and hull form. The main dimensions of the structural model are illustrated in Figure 13 and 14.
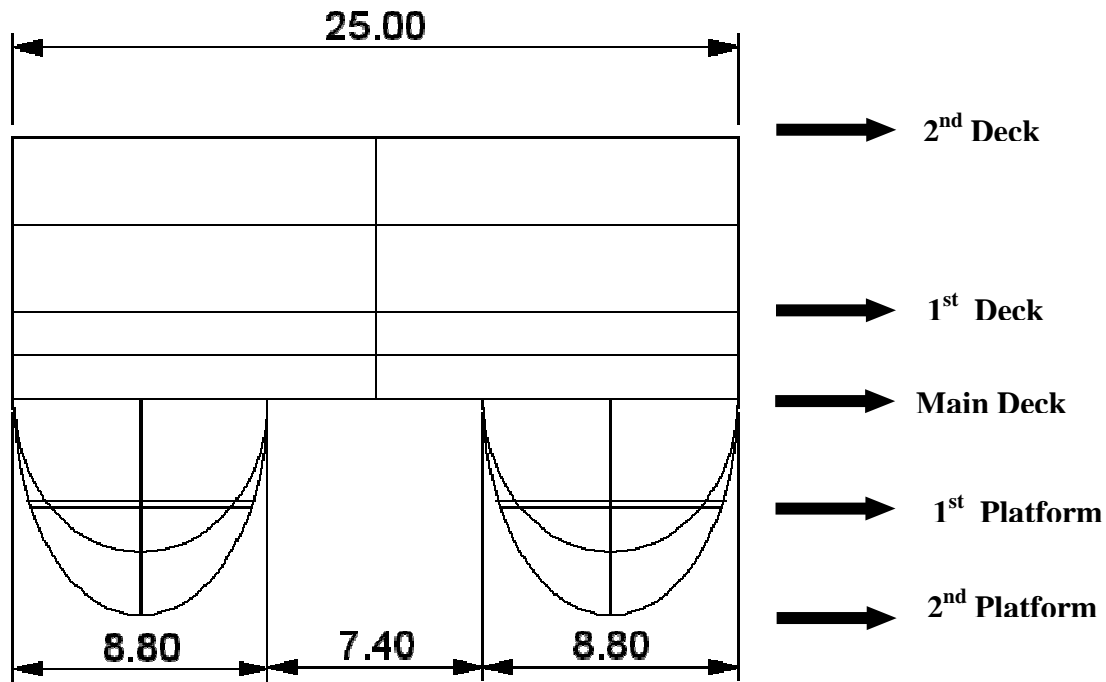
Figure 13. Transverse View of Structural Model (the dimensions are in meters)
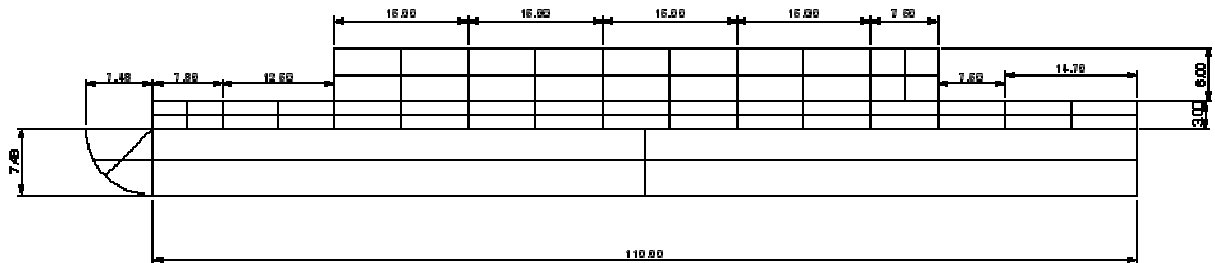
Figure 14. Longitudinal View of Structural Model (the dimensions are in meters)

The model consists of 12 athwartship bulkheads and 50 compartments as shown in Figure 15.

Figure 15. Arrangement of Sea TENTACLE Model

Since the structural model is consistent with the dimensions and hull form of Sea TENTACLE, the displacement of the model is determined as 7,000 tons using the value of 1.025 MTON/m^3 for the seawater weight density whereas the displacement of Sea TENTACLE is 7023 tonnes. The shell plating was constructed of 14 mm high-strength steel SAE 942X having a mass density of 7850 kg/m^3, a Young's Modulus of 200x10^9 Pa, and a Poisson's ratio of 0.33. The shell elements were constructed as square hexagonal elements having a length of 1 m. The same material was also used for the structural beam elements (stiffeners) which are of rectangular cross section. The specifications of the model materials are shown in Table 4.

28

Table 4.   Material Specifications

Material Type	High-Strength Steel SAE 942X
Material Model	Isotropic Material (elastic)
Young's Modulus	200×10^9 Pa
Poisson's Ratio	0.33
Thermal Expansion Coefficient	12.3×10^{-6}
Mass Density	7850 kg/m^3
Mass Damping	19.2
Stiffness Damping	2.09×10^{-6}

The beam elements were used to increase the plating rigidity. In order to make the model realistic, the beams at the hull, having a size of 14 mm wide and 15 cm high, were created thicker than the beams at the superstructure having a size of 12 mm wide and 15 cm high. Figure 16 illustrates the beam cross section while Figure 17 and 18 show the beam elements of the model. The overall finite element mesh of the structural model consists of 11202 nodes, 12300 quadrilateral (4-noded) shell elements, 13870 beam elements and 7774 lumped masses. Table 5 summarizes the model particulars.

The structural mesh of the model was output in ABAQUS input file format after the generation in TrueGrid. The input deck was then read into an ABAQUS database which is a powerful software application for advanced finite element analysis. ABAQUS/CAE is a complete ABAQUS environment that provides a simple, consistent interface for creating, submitting, monitoring, and evaluating results from ABAQUS/Standard and ABAQUS/Explicit simulations. Thus, ABAQUS/CAE was used to create the fluid mesh, couple it with the structural mesh and execute the modal analysis due to an UNDEX pressure wave. ABAQUS also provides a capability for bringing in generalized forces on acoustic and solid media related to the arrival of shock waves [Ref. 22].

Table 5.   Sea TENTACLE Model Specifications

Length	117.48 m
Beam	25 m
Depth	16.48 m
Draft (Design Waterline)	4.73 m
Shell Plating/Beam Element Material	High-Strength Steel SAE 942X
Shell Plating Thickness	14 mm
Beam Element Dimensions (Height x Width)	
- Beam Elements at Hull	$14 \times 150 \ mm^2$
- Beam Elements at Superstructure	$12 \times 150 \ mm^2$
Number of Parts	18
Number of Nodes	22126
Number of Shell Elements	21832
Number of Beam Elements	36056
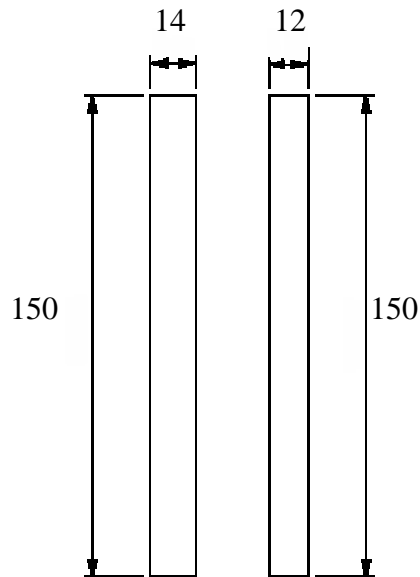
Figure 16.   Beam Cross Section (the dimensions are in millimeters)

30
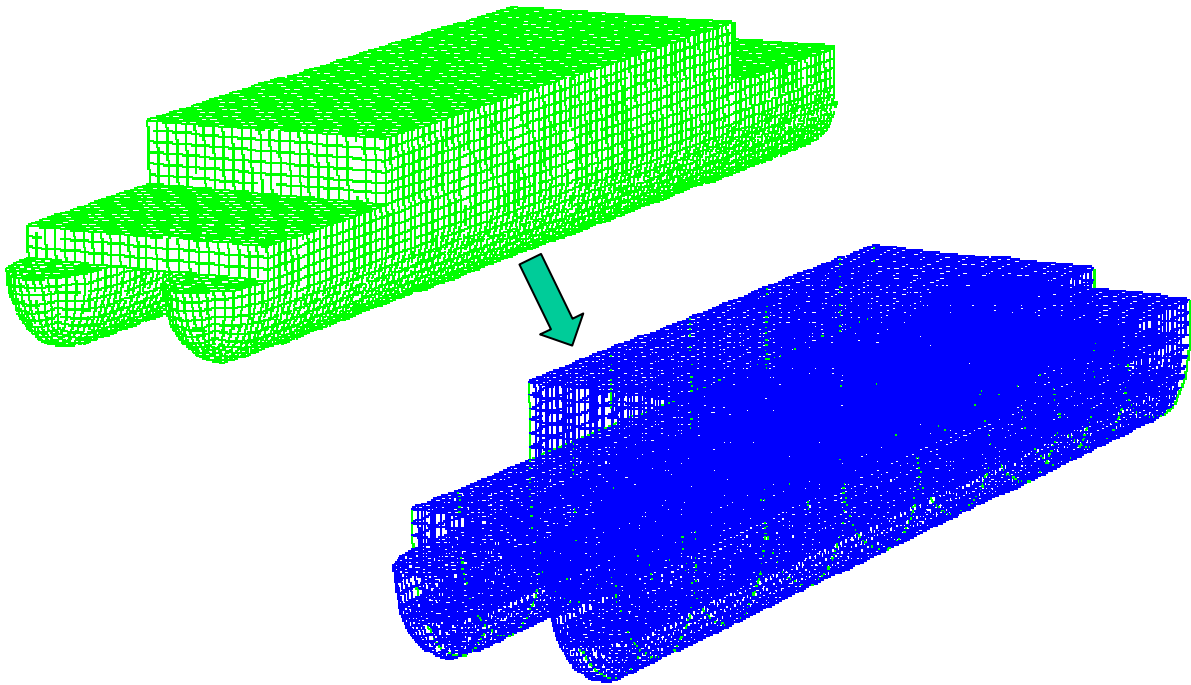
Figure 17. Beam Elements of the Model
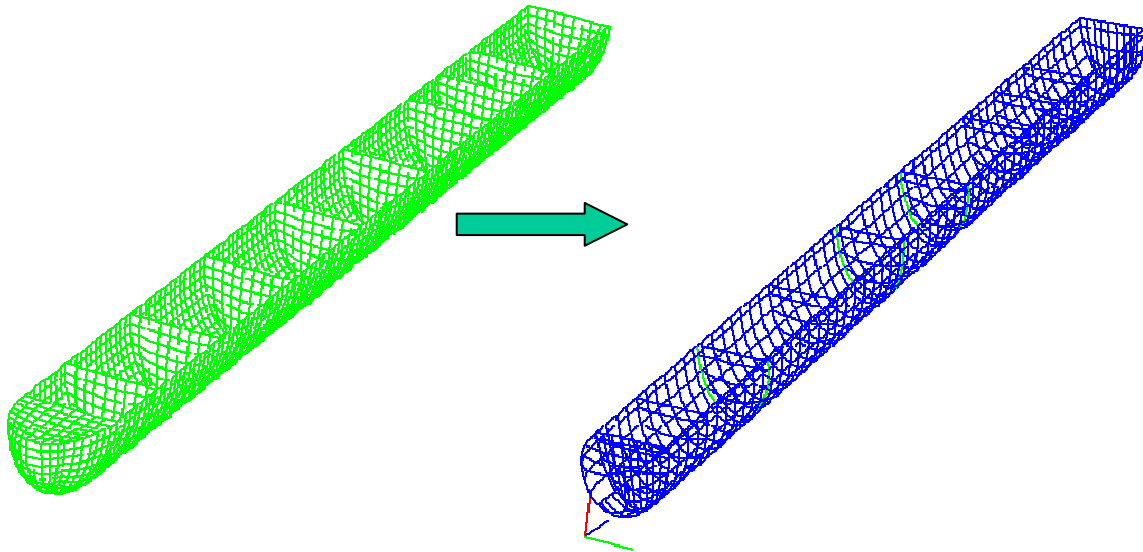
Figure 18. Beam Elements of the Hull

31

After outputting the structural model to ABAQUS, the total 6600 MT point masses were distributed along the deck according to Figure 19. The mass distribution includes the lightship mass, the payload and the fluid mass (fuel, oil, water etc.).

1st Deck : 1044 MT

Main Deck : 1500 MT

Each Hull : 2028 MT
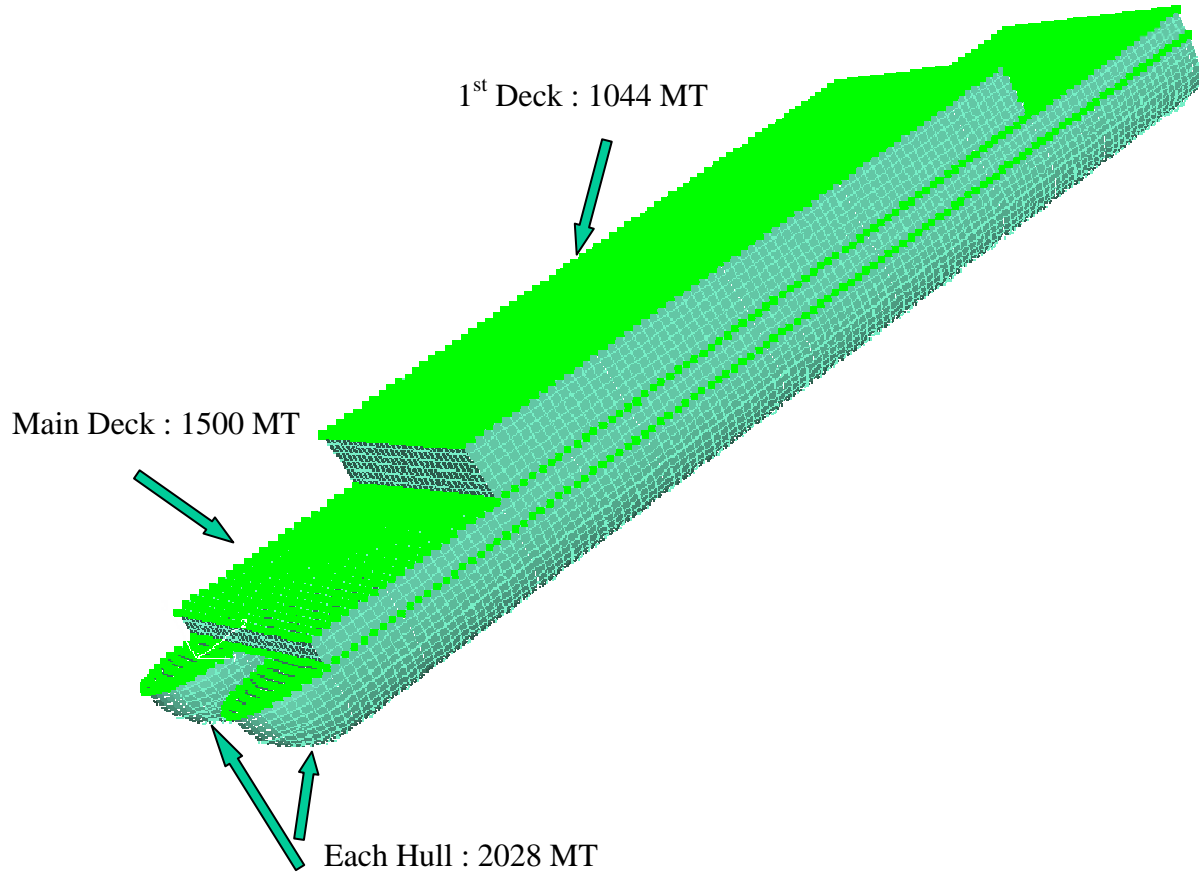
Figure 19.   Mass Distribution of the Model

2.   Fluid Mesh Modeling

Creating the fluid mesh (fluid volume finite element model) was the next step in the Sea TENTACLE model. The fluid part was created by using the CAD tool RHINO 3.0 and imported as an SAT file into ABAQUS in order to generate the fluid mesh. The fluid part was modeled as a closed solid. The Boolean Subtract feature of RHINO 3.0 was used to create the wetted surface in the fluid mesh using the solid hull parts. The fluid part was created as an ellipsoid, because the fluid domain needs to enclose the structure in order to use the infinite elements if needed. The fluid mesh generation using

ABAQUS is explained in Appendix C. The final fluid mesh is shown in Figure 20. The fluid part was meshed with 4-node AC3D4 acoustic tetrahedral elements in ABAQUS. The mass density and the acoustic speed of these solid elements have the values of 1025 kg/m^3 and 1500 m/sec, respectively.
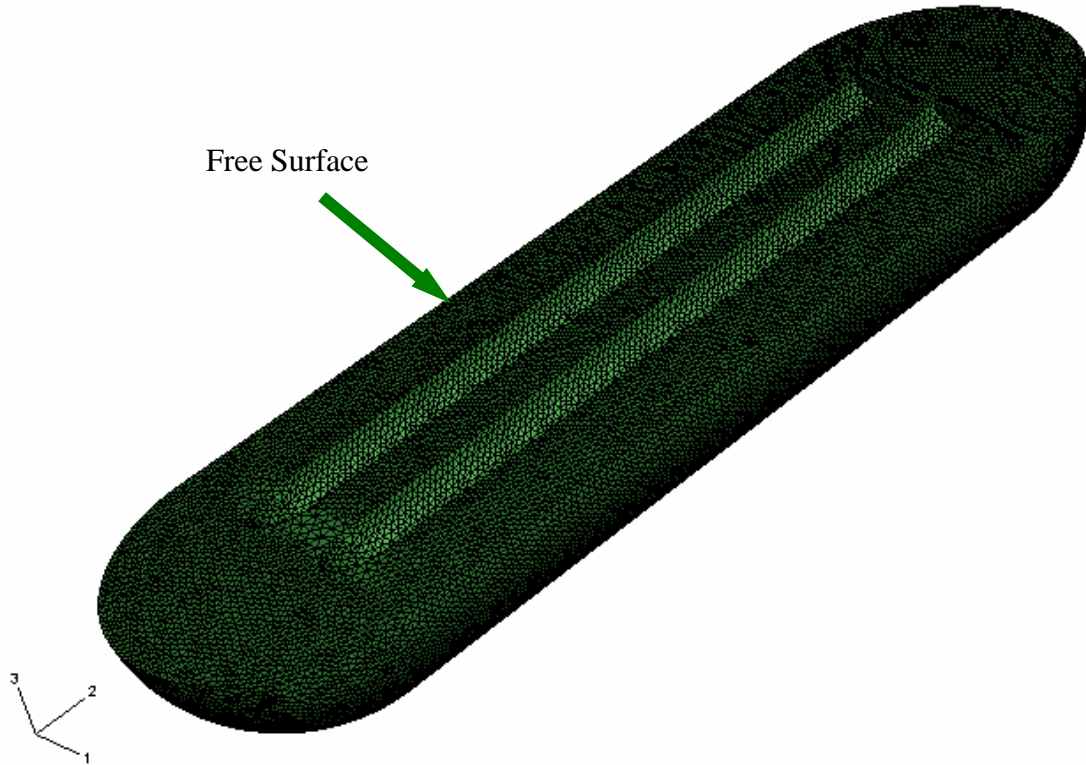
Figure 20. Fluid Mesh in ABAQUS

In order to create the ellipsoid fluid part, two quarter spheres and half cylinder with a radius of 25 m, which is greater than the depth of the computed bulk cavitation zone, were used in RHINO 3.0. Figure 21 illustrates the dimension of the fluid mesh.

The shock analysis in ABAQUS requires a surface-based interaction for coupled acoustic-structural analysis. The acoustic structural coupling between the fluid mesh and the structural mesh at the common wetted interface was achieved by using the *TIE constraint option in ABAQUS. The coupling procedure and *TIE option is described in detail in Appendix D. Figure 22 shows the coupled fluid-ship model.
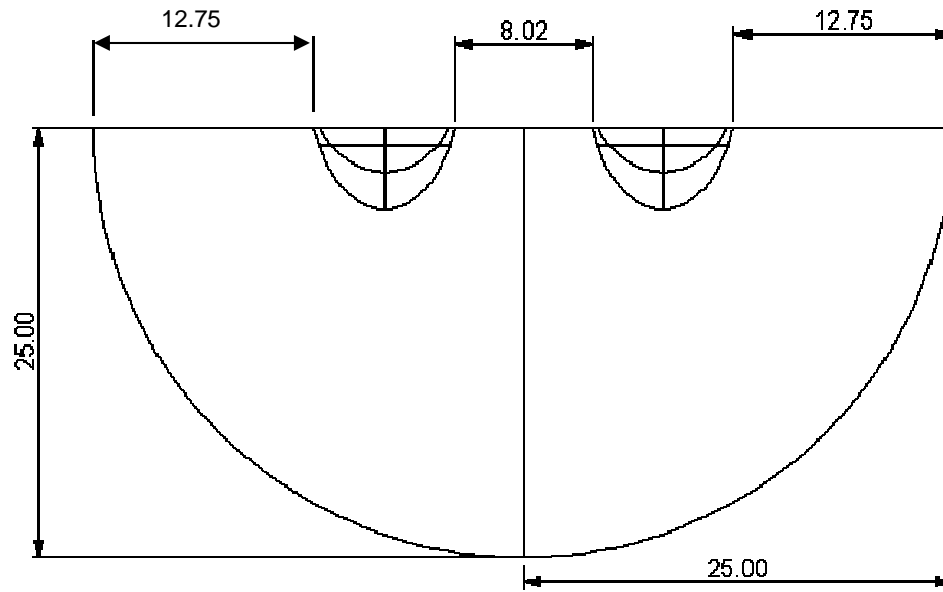
Figure 21. Dimensions of the Fluid Mesh (in meters)
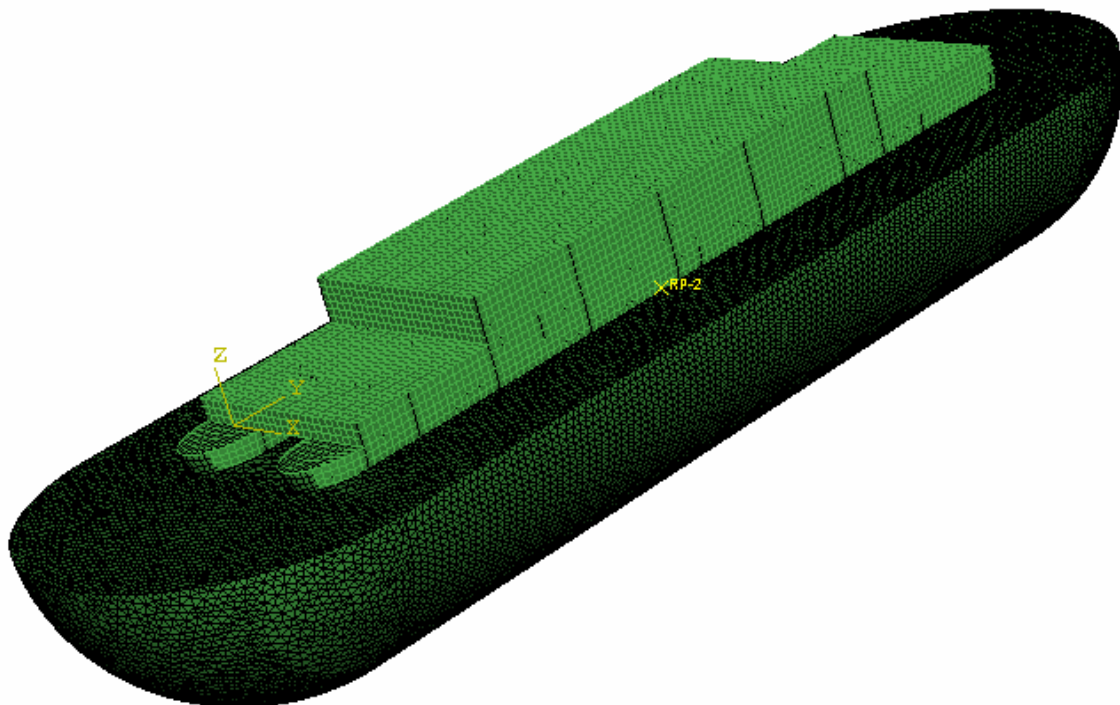
Figure 22. Coupled Fluid-Structural Mesh

34

Table 6 lists the number of elements and element type created for the fluid mesh and structural mesh. As shown from Table 6, the fluid mesh is a large and complex mesh for a relatively small structure due to the cavitation effects. Thus, computational power is required to run a shock simulation involving a fluid mesh.

Table 6.   Coupled Fluid-Structural Mesh Specifications

	Number of Elements	**Element Type**
Fluid Mesh	607496	AC3D4 solid acoustic tetrahedral finite element
Structural Mesh	21832	S4R shell quadrilateral finite element

THIS PAGE INTENTIONALLY LEFT BLANK

IV. SIMULATION

A. MODELING AND SIMULATION PROCESS

The modeling and simulation process involves model construction, pre-processing, analysis and solution, and post-processing of the results. Figure 23 shows a flowchart of the procedure used for the Sea TENTACLE UNDEX simulation.
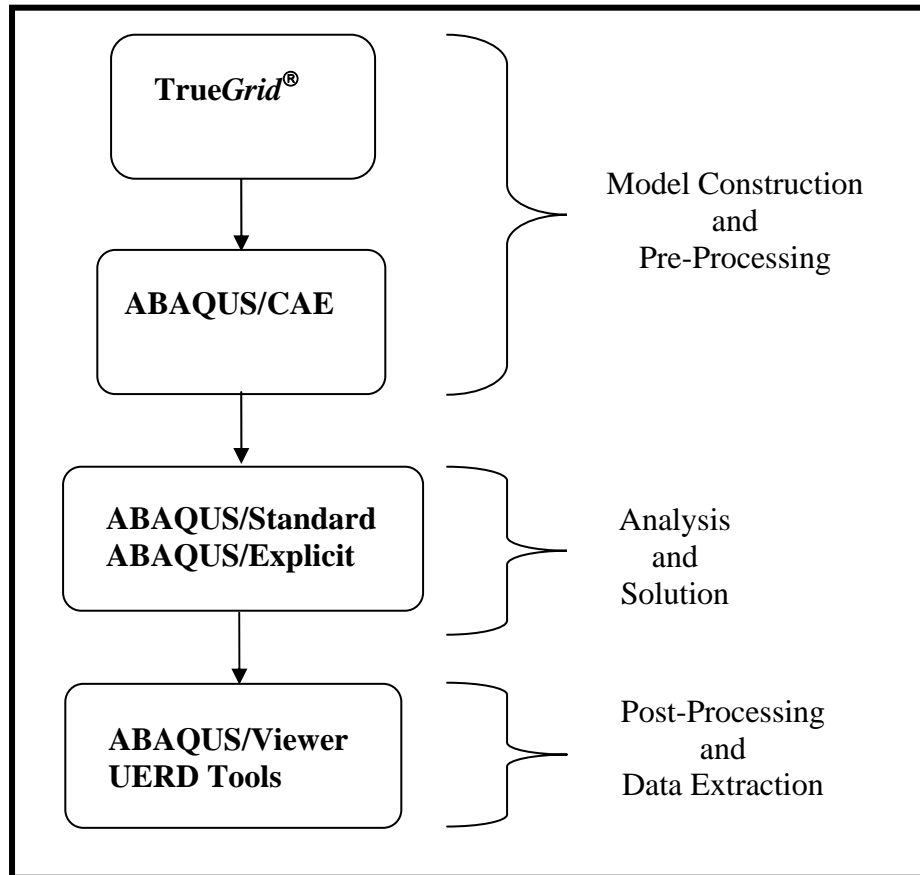
Figure 23. Modeling and Simulation Flow Chart

B. SHOCK SIMULATION WITH ABAQUS

ABAQUS consists of two main analysis products: ABAQUS/Standard and ABAQUS/Explicit. ABAQUS/Standard is a general purpose analysis product that can solve linear and nonlinear problems involving the static, dynamic, thermal and electrical response of components. It solves a system of equations implicitly at each increment

37

whereas ABAQUS/Explicit finds a solution forward through time in small time increments without solving a coupled system of equations at each increment [Ref. 22].

ABAQUS/Explicit is a special purpose analysis product that uses an explicit dynamic finite element formulation. It is convenient for modeling transient dynamic events, such as blast, acoustic and shock problems. It is also very efficient for highly nonlinear problems involving changing contact conditions [Ref. 22].

ABAQUS/CAE (Complete ABAQUS Environment) is an interactive, graphical environment for ABAQUS incorporating the analysis modules into a **C**omplete **A**BAQUS Environment for modeling, managing, and monitoring ABAQUS analyses and visualizing results. It allows the models to be created easily and quickly by producing or importing the geometry of the structure and dividing it into meshable regions. Physical and material properties can be assigned to the model, as can loads and boundary conditions. Once the model is complete, ABAQUS/CAE can submit, monitor and control the analysis jobs. ABAQUS/Viewer is a part of ABAQUS/CAE that contains only post-processing capabilities [Ref. 22].

ABAQUS provides a capability for introducing generalized forces on acoustic and solid media associated with the arrival of dilatational waves. This applies to shock problems. Since the fluid mechanics are assumed to be linear, the wave fields in the fluid can be superimposed in a dynamic problem excited by a propagating wave in the fluid arriving from outside the domain. Therefore, the observed total pressure in the fluid can be divided into two components--the known incident and the wave field--due to the reflections at the fluid boundaries and interactions with the structure. The wave field, referred to as the scattered field, can be calculated by applying loads at the fluid-structure interface [Ref. 22].

In ABAQUS, the shock analysis of a structure includes acoustic finite elements to model the effects of the mass of the fluid and incident wave loading to model UNDEX effects on the structure interacting with fluid. The explosive load is defined with an incident wave load. The load is applied on both the structure and the fluid at the common interface and is similar to a distributed load. These loads are supported only on transient dynamic procedures.

There are two acoustic wave formulations for shock analysis in ABAQUS: total wave formulation and scattered wave formulation. The scattered wave formulation is generated by capitalizing on the fact that the acoustic medium is linear. The model response can be divided into the sum of incident wave and the scattered field and is the response of medium to wave loads, not the wave pulse itself. The pressure in this formulation is the scattered pressure only [Ref. 22].

Total wave is simply the sum of the incident and the scattered waves. The mechanical behavior of the model is nonlinear when the cavitation exists. In this case, with the superposition of the incident wave and the responses of the model due to the boundaries, the cavitating regions are not valid. The total pressure in the total wave formulation includes the effects of the incident wave field and the overall model's response. The total wave formulation presents a complete solution of the acoustic pressure field. When the acoustic medium is capable of cavitation, a total wave formulation must be used. The total wave formulation was used in the Sea TENTACLE model since the cavitation was of considerable interest and cavitation limit was invoked as zero pressure by using the keywords editor. Therefore, the pressure was cut off at zero. In the total wave formulation, the loading must be specified only on the fluid surfaces that have a nonreflecting radiation condition. ABAQUS ensures that the radiation condition is applied only on the scattered response and not on the incident wave [Ref. 22].

ABAQUS also tracks the gas bubble migration and stops the analysis if the bubble reaches the free surface before the end of the analysis. The formulation used for determining the bubble time histories is based on the Geers-Hunter bubble model and exhibits the effects of the radially expanding and upwardly migrating gas bubble. The results were obtained by using ABAQUS/Standard for the Sea TENTACLE model. The parameter value BUBBLE was invoked by using the keywords editor of ABAQUS/CAE.

ABAQUS/Viewer and Underwater Explosions Research Department (UERD) Tools were used as the post-processing and data extraction tools. ABAQUS/Viewer allows the user to view the deformed shape plots, contour plots, animations and X-Y plots. It was especially used for the animation and contour plot purposes in this thesis.

UERD which is a RTD&E organization in the Naval Surface Warfare Center, Carderock Division created the data analysis and plotting program specifically for the analysis of ship shock trial data. UERD Tools was used for X-Y plots and shock spectra since it is capable of importing ASCII history files exported from ABAQUS.

The simulation process using ABAQUS/CAE is described in full detail in Appendix D.

C.   TEST DESCRIPTION OF THE ANALYSIS

The shock trials consist of two different geometries (labeled as SHOT-1 and SHOT-2) for the charge location. These test geometries were based on typical full ship shock tests but adapted to the appropriate size of the Sea TENTACLE model to be investigated. A 7500 lb TNT charge was used for UNDEX analysis of the Sea TENTACLE model. UNDEX analysis is tracked beginning at the stand-off point, so it is desirable to have the stand-off point located as close to the structure as possible in ABAQUS [Ref. 22]. Therefore, the stand-off point was located at the intersection of the midship section of the structural model and the centerline of the port hull for both shots.

1. The Attack Geometry of SHOT-1

The attack (shot) geometry in Figures 24 and 25 was used in the shock simulation of SHOT-1 during the analysis. The offset distance from the stand-off point and the charge depth were set to 100 m and 57 m, respectively. The standoff distance was calculated as 113 m.

Figure 24.   Sea TENTACLE Model Shot-1 Geometry (Transverse View)
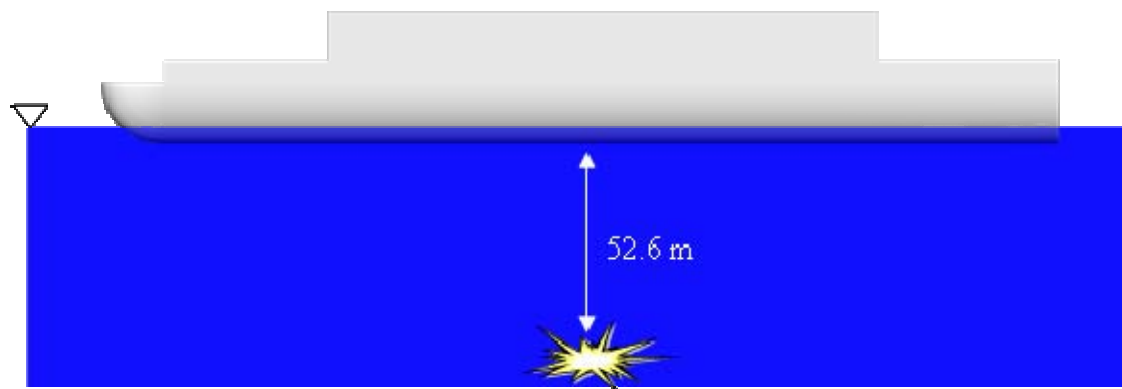
Figure 25.   Sea TENTACLE Model Shot-1 Geometry (Longitudinal View)

The UNDEX parameters with the distances given were calculated and tabulated in Table 7. The bulk cavitation zone for the Sea TENTACLE model was calculated by inputting the computed UNDEX parameters and the shot geometry to the MATLAB

41

program in Appendix A. The largest depth in which the bulk cavitation occurs was determined as 16 m by using the MATLAB program. The bulk cavitation region is illustrated in Figure 26.

Table 7.   UNDEX Parameters for Sea TENTACLE Model SHOT-1 Simulations

P_{max}	700 psi
θ	1.956 msec
T	0.93 sec
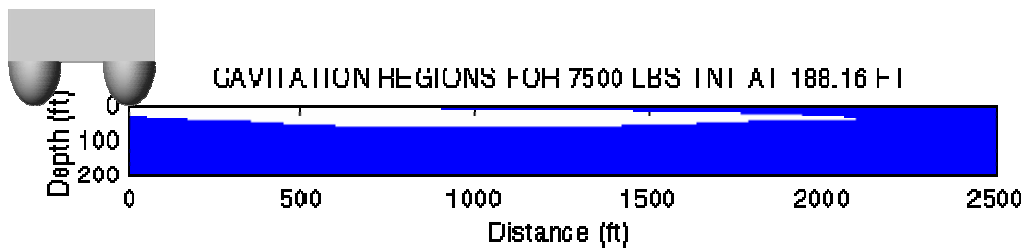
Figure 26.   Bulk Cavitation Zone for SHOT-1

2.   The Attack Geometry of SHOT-2

The attack (shot) geometry in Figures 27 and 28 was used in the shock simulation of SHOT-2 during the analysis. The charge depth was set to 155.25 m and no horizontal offset distance was applied. The standoff distance was calculated as 150.52 m.

The UNDEX parameters with the distances given were calculated and tabulated in Table 8. The bulk cavitation zone for Sea TENTACLE model was also calculated by using the same MATLAB program with the computed UNDEX parameters and the shot geometry. The largest depth in which the bulk cavitation occurs was determined to be 9 m for this shot. The bulk cavitation region is illustrated in Figure 29.
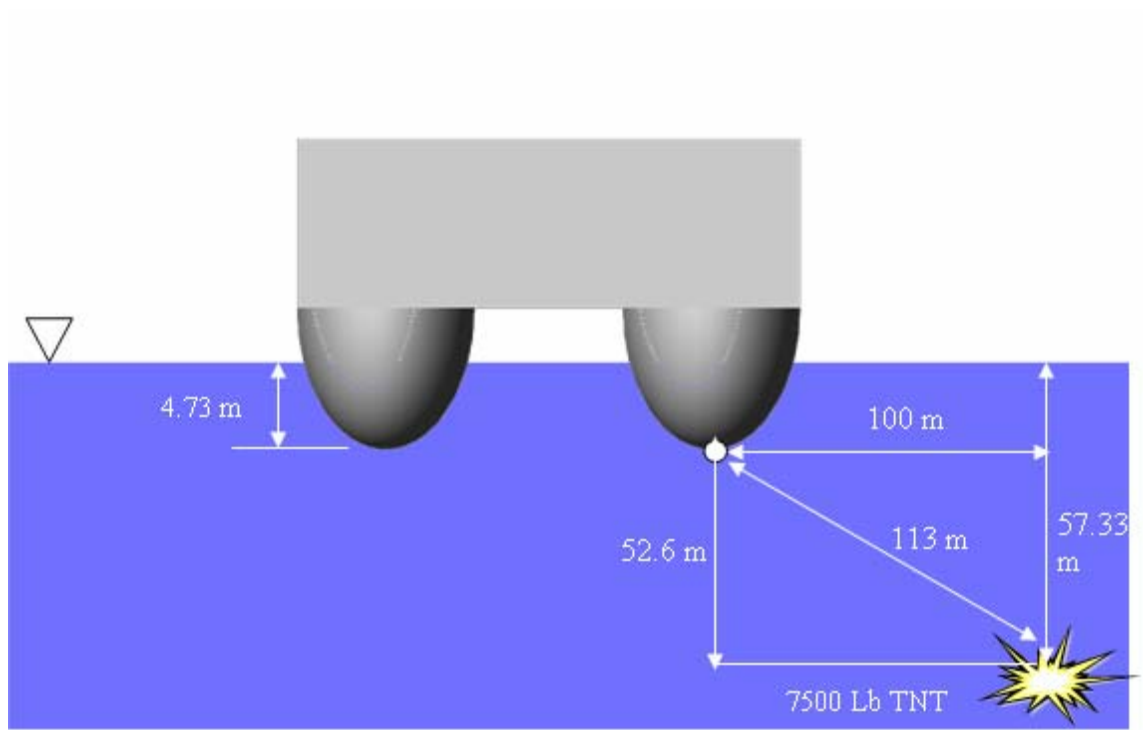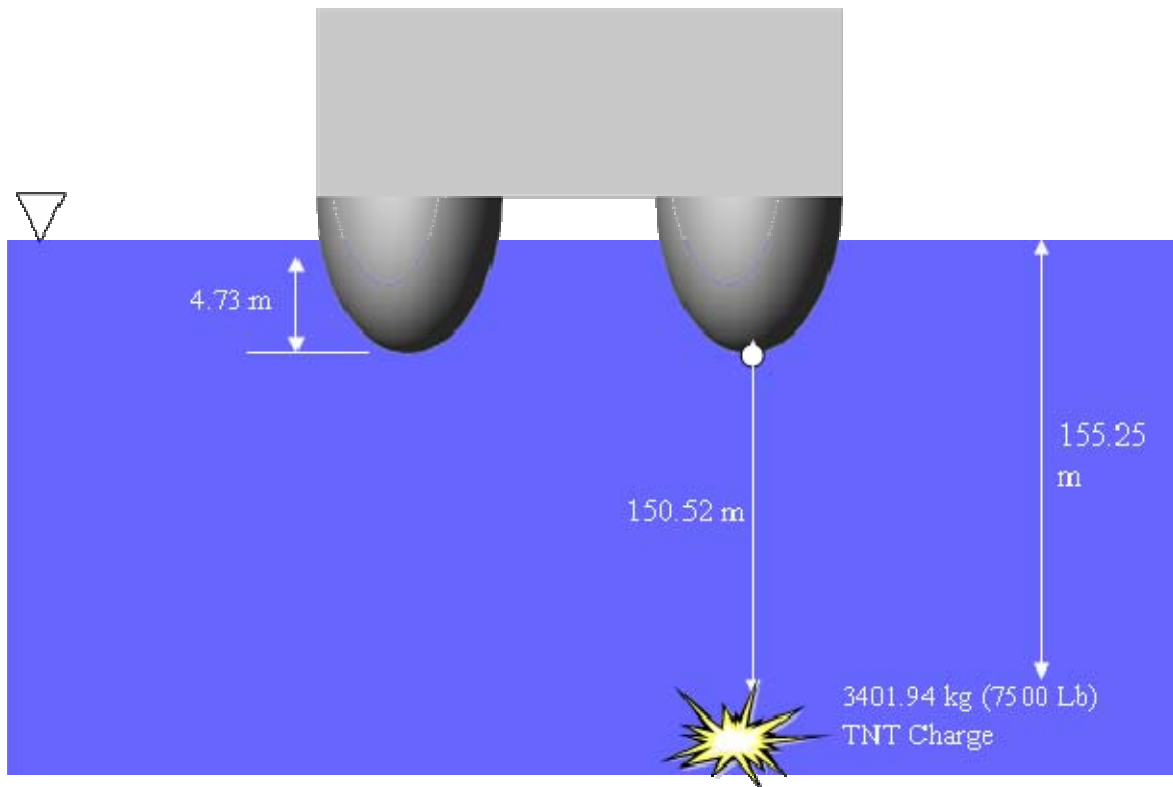
Figure 27.   Sea TENTACLE Model SHOT-2 Geometry (Transverse View)
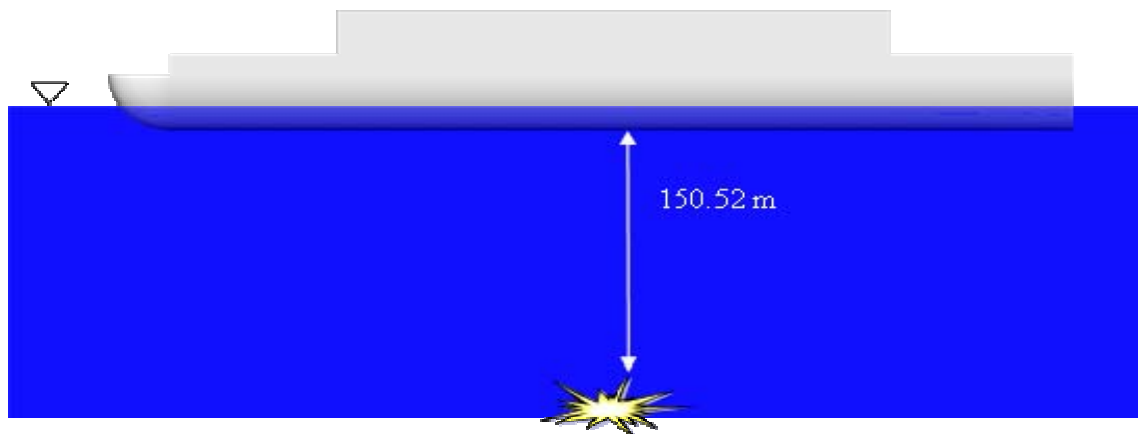
Figure 28.   Sea TENTACLE Model SHOT-2 Geometry (Longitudinal View)

Table 8.   UNDEX Parameters for Sea TENTACLE Model SHOT-2 Simulations

P_{max}	498.94 psi
θ	2.063 msec
T	0.44 sec
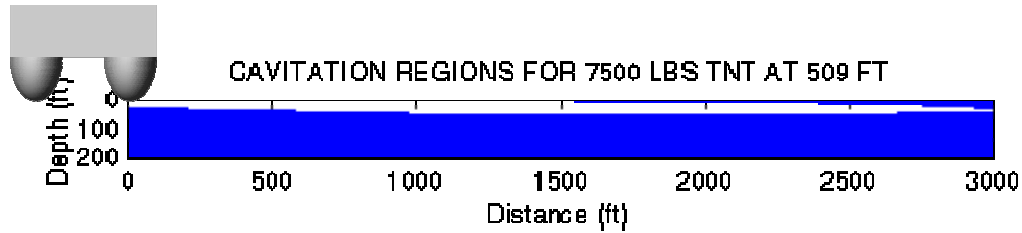
Figure 29.   Bulk Cavitation Zone for SHOT-2

D.   RAYLEIGH DAMPING COEFFICIENTS

Velocity-dependent damping is very difficult to visualize for most real structural systems, such as sea vessels. Only a small number of structures have a finite number of damping elements where real viscous dynamic properties can be measured. In most cases, modal damping ratios are utilized in order to determine the approximate nonlinear frictional energy dissipation.

Most of the inherent damping within a fabricated built-up structure occurs at the mechanical joints due to frictional energy dissipation during the vibration of the structure. When the contact force in bolted connection is reduced, the system vibration amplitudes reduce by increasing joint damping capacity. Nevertheless, the great majority of joints in naval ship structure systems are welded rather than mechanically connected, thus reducing the energy dissipation through the welds. The naval ship systems also have several energy dissipation sources such as long cable trays, hangers, snubbers and the surrounding fluid coupled with the hull [Ref. 23].

Another form of damping, which is often used in the simulation of the dynamic response of a structure, is proportional to the stiffness and mass distribution of the structure. This damping is called Rayleigh damping. A damping matrix based on the

44

physical properties of the structure is avoided by using Rayleigh damping. The damping matrix, $[C]$ is defined in Rayleigh damping as

$$[C] = \alpha[M] + \beta[K] \tag{4.1}$$

in the general expression for the equation of motion.

$$[M]\{\ddot{x}\} + [C]\{\dot{x}\} + [K]\{x\} = \{F\} \tag{4.2}$$

The damping coefficients α and β are pre-defined constants. The orthogonal transformation of the damping matrix reduces the matrix $[C]$ to the form

$$[\phi]^T[C][\phi] = [2\zeta_r\omega_r]_{diag} = \alpha[I] + \beta[\omega_r^2]_{diag} \tag{4.3}$$

Equation (4.3) on simplification reduces to

$$\zeta_i = \frac{1}{2}\left(\frac{\alpha}{\omega_i} + \beta\omega_i\right) \tag{4.4}$$

It can be observed that the damping ratio is proportional to the natural frequencies of the system. When the system has two degrees of freedom, a set of Equation (4.5) is solved easily in order to determine the damping coefficients.

$$\begin{aligned} 2\zeta_1\omega_1 &= \alpha + \beta\omega_1^2 \\ 2\zeta_2\omega_2 &= \alpha + \beta\omega_2^2 \end{aligned} \tag{4.5}$$

However, while solving a system having many degrees of freedom such as a ship, there will be much more of a challenge to obtain the values of Rayleigh damping coefficients, which should be valid for all the n degrees of equation. There is no simple solution to determine the coefficients. An iteration solution is possible and this can be obtained from the best-fit values of α and β in a particular system. Thus, the damping coefficients can be determined by using the measured data and a least squared curve fitting method.

A new set of Rayleigh damping coefficient values was determined by executing a comprehensive study at NPS using the measured data taken from the DDG-53 ship shock

trials for 2000 msec [Ref. 24]. The ship was divided into 67 area groups with 773 sensors for the damping coefficient analysis. Measured modal response over the frequency spectrum of interest, 0 to 250 Hz, was recorded for both the vertical and athwartship responses. A least squares curve fit, as illustrated in Figure 30, was then applied to each area group. Next, weighted averages were given to the area groups based on the number of modes used in the least squares curve fitting process required to determine α and β, which are presented in Table 9.

Table 9. Weighted Mean Values of α and β [Ref. 23]

Rayleigh Damping Parameters	Athwartships Direction	Vertical Direction
α - value	18.4	19.2
β - value	2.82E-06	2.09E-06
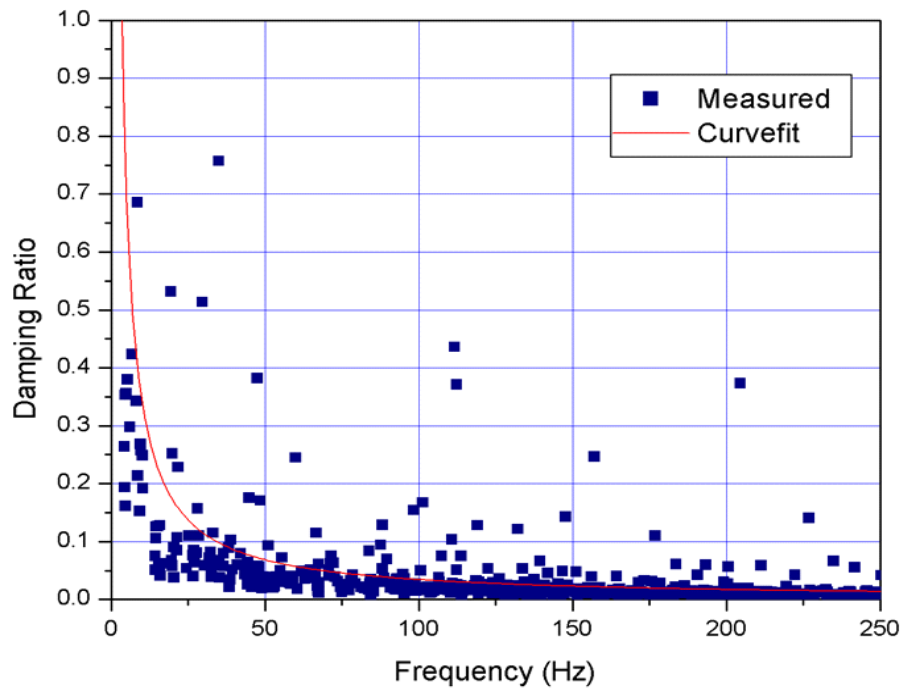
Figure 30. Modal Damping Ratio for Single Area Group, Vertical Direction [Ref. 23]

As a consequence, the NPS damping coefficient values for DDG-53 were defined as $\alpha = 19.2$ and $\beta = 2.09\text{E-}6$ in the vertical direction while they were defined as $\alpha = 18.4$ and $\beta = 2.82\text{E-}6$ in the athwartships direction. The great difference in the two damping coefficients (α and β) implies that the damping within the system is mass-driven. Regarding the similarity of DDG-53 and DDG-81, the resulting damping coefficient values, which were the values in the vertical direction, were used for both since the vertical response is much larger in magnitude than the athwartships response [Ref. 23 and 24]. Since the application of these damping coefficient values to both ships gave very accurate response results close to ship shock trials [Ref. 24], they were used for shock simulations of the Sea TENTACLE model as well. The same damping coefficient values calculated for the vertical direction were assigned to all the structural solid, shell and beam elements in the Sea TENTACLE model in ABAQUS/CAE.

THIS PAGE INTENTIONALLY LEFT BLANK

V.   DATA COLLECTION AND ANALYSIS

The ship shock simulations of the Sea TENTACLE model using ABAQUS were conducted on a workstation with two 3.06 GHz processors and 2.0 Gbytes of RAM. The computational time for each simulation was approximately 3 days.

A spherical incident shock wave propagates gradually toward the structure. Thus, it is apparent that the different portions of the model will exhibit different peak responses depending on the standoff distance from the charge and angle of attack. As a result, several different nodes throughout the model were selected in order to investigate the overall response of the keel, sides, bulkheads and the deck between the two hulls subjected to the UNDEX. The most accurate results were expected at the keel since it interacted with the incident shock wave first. Thus, 8 nodes were selected (as illustrated in Figure 31) in order to determine the response. In order to determine the effect of the gap on the response of the model, the nodes at the main deck between the hulls were selected as shown in Figure 31.
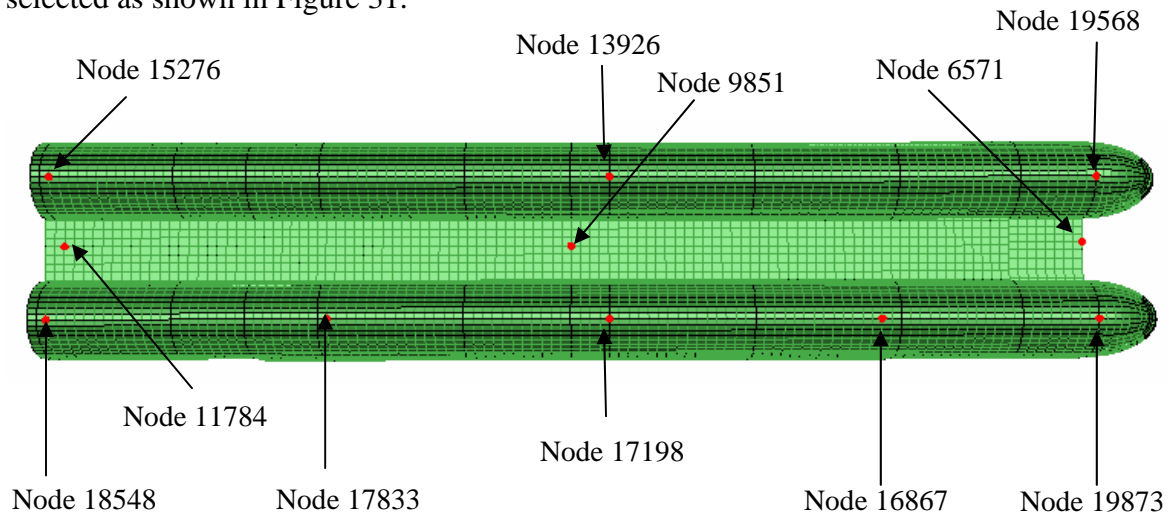
Figure 31.   The location of the nodes at the keel

Equivalent nodes were selected on each hull to study the effect of the gap between the hulls on the response, as shown in Figure 32 and 33. As shown in Figure 34, the bulkheads nodes at the centroid were selected in order to compare the kick-off velocity with the theoretical value.
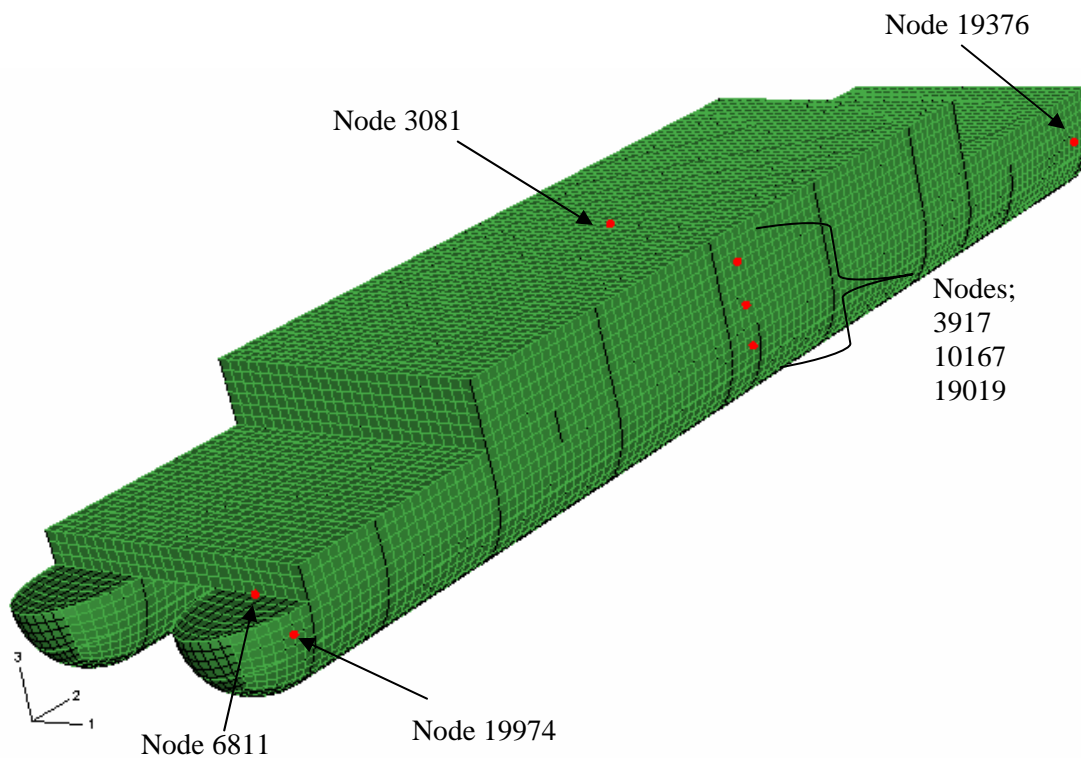
Figure 32.   The Location of the Nodes at the Port Side.
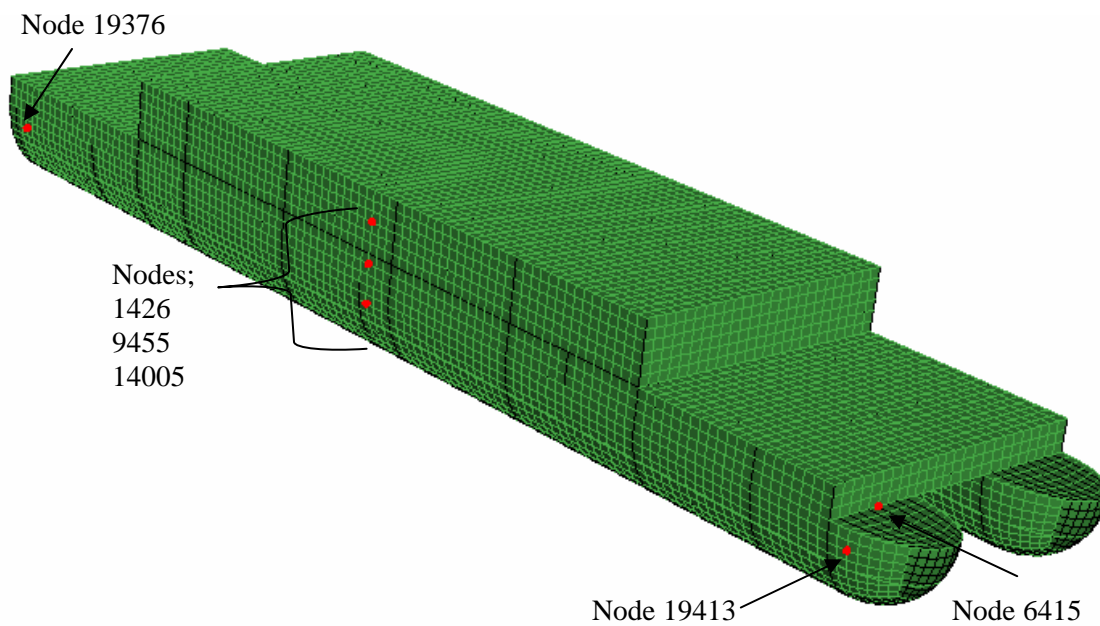
Figure 33.   The Location of the Nodes at the Starboard Side.
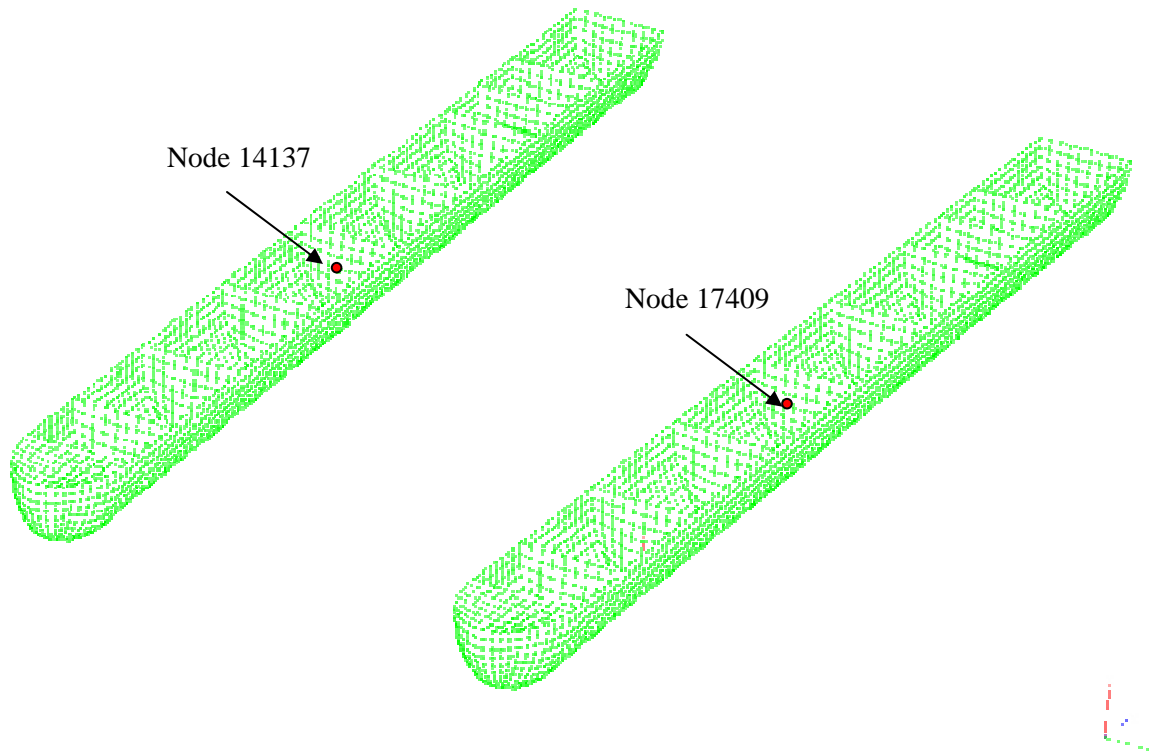
Figure 34. The Location of the Nodes at the Bulkheads

The ABAQUS/Explicit model for the shock simulation had a total of 579020 active degrees of freedom including any Lagrange multiplier variables. The analysis was run for 1.5 seconds with an average 2.818×10^{-6} critical time increment and 544724 solution increments. This time step was computed by ABAQUS/Explicit using element-by-element stable time increment estimator. This element-by-element estimate is determined by using the smallest time increment size due to the dynamic responses in each element.

A.   SHOCK WAVE PROPAGATION AND BUBBLE FORMATION

The shock wave produced by the TNT charge propagates from the source point, impinging on and passing over the model, producing a temporally and spatially varying load on the Sea TENTACLE model. The pressure field is affected by the reflections and emissions from the structure as well as the incident field from the source itself. The locations of the source and standoff points greatly effect the incident shock wave propagation and magnitude. Two output variables were provided for acoustic pressure in

ABAQUS. One of them is acoustic pressure (POR) and the other is absolute acoustic pressure (PABS). POR represents the total dynamic pressure, including additional pressure induced by the incident and scattered waves and the dynamic effects of cavitation whereas PABS is the sum of acoustic pressure and hydrostatic pressure [Ref. 22]. The acoustic pressure magnitudes are in Pascal.

1. Shock Wave Propagation and Bubble Formation for SHOT-1

The shock wave propagation of SHOT-1 is shown in Figure 35. The maximum shock wave pressure was calculated as 4.874×10^6 Pa or 706.9 psi which is close to the theoretical value of 700 psi. The shock wave pressure profiles and cavitation regions are illustrated in Figure 36 and 37 by taking a cross section of the model along the y-axis. The spherical shape of the shock wave and the initial shock wave propagation at time zero can be seen in Figure 35 and 36, respectively.

Figure 35.   Shock Wave Propagation of SHOT-1
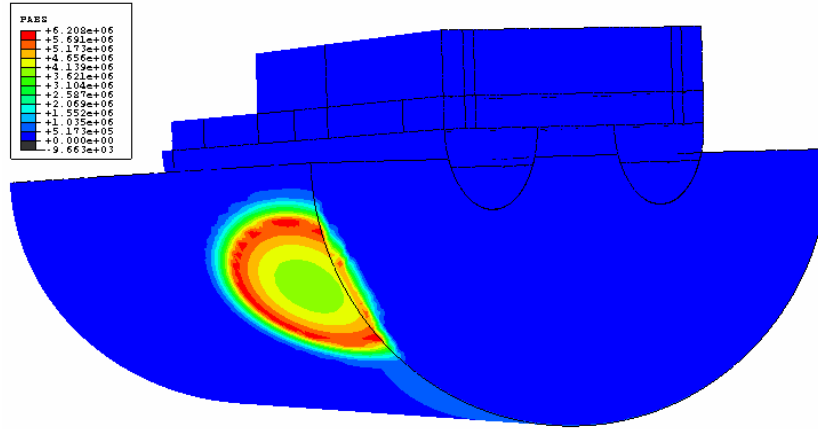
t = 0 sec
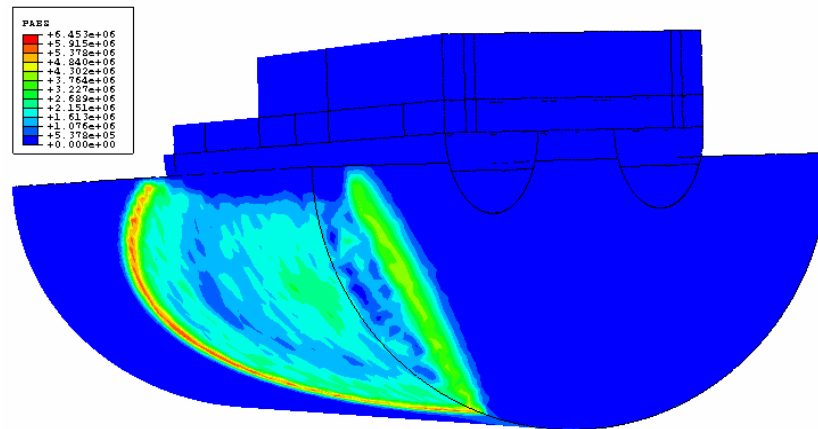
t = 4 msec
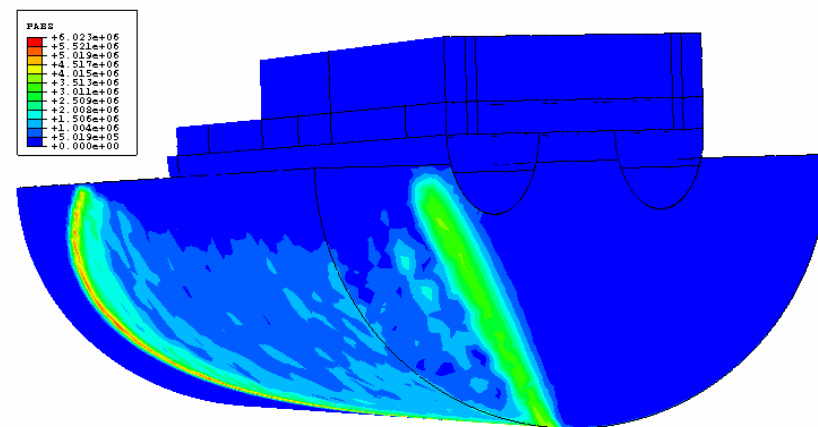
t = 8 msec

Figure 36.   Shock Wave Pressure Profiles and Cavitation Regions
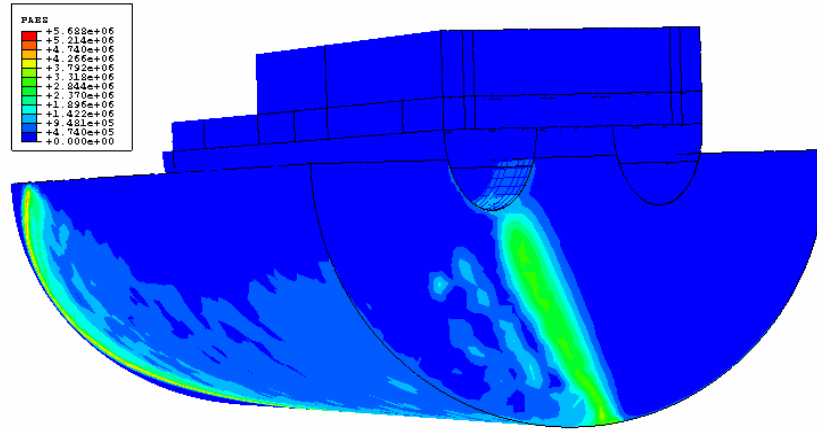
t = 12 msec
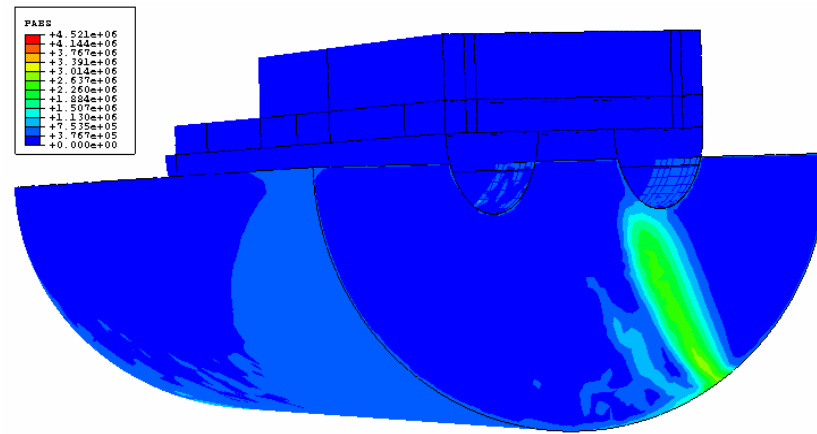
t = 20 msec
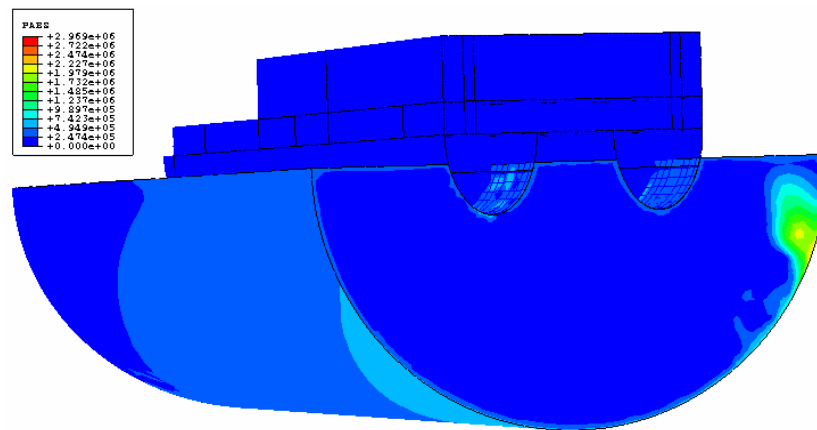
t = 30 msec

Figure 37.   Shock Wave Pressure Profiles and Cavitation Regions (continued)

The regions having zero pressure represent cavitation regions. As shown in Figure 36, the incident shock wave forms at time zero, followed by the initial bulk cavitation formation. As the shock wave reaches the free surface, a tensile reflected wave is generated. This wave decreases the pressure to negative values rapidly. When the pressure drops off to zero, it can be stated that the cavitation is occurring and forms directly under the structure.

The time histories of bubble expansion and migration are shown in Figure 38 and 39 respectively. The bubble oscillation period and the maximum gas bubble radius are functions of the types and the weight of the charge and the ambient pressure [Ref. 10]. From the simulation in ABAQUS, these values were determined as 0.93 sec and 12 m, respectively, which are almost the same as the theoretical values, 0.93 sec and 12.5 m, calculated by using Equation 2.4 and 2.6. As shown from Figure 38 and 39, the gas bubble rises rapidly due to the buoyancy of the bubble. Since the buoyancy force is large, the drag force is also large. After reaching the first maximum, the bubble shrinks due to the energy loss and starts migrating faster due to the smaller drag force. The numbers of these oscillations depend on the bubble's loss of energy by radiation or turbulence.

The gas bubble pressure is also shown in Figure 40. As shown in the figure, the initial high pressure in the gas sphere decreases due to the loss of energy and falls below the equilibrium that is defined by the atmospheric and hydrostatic pressure. When the first bubble pulse forms, the bubble pressure rises again due to the formation of jet stream.

GAS BUBBLE RADIUS
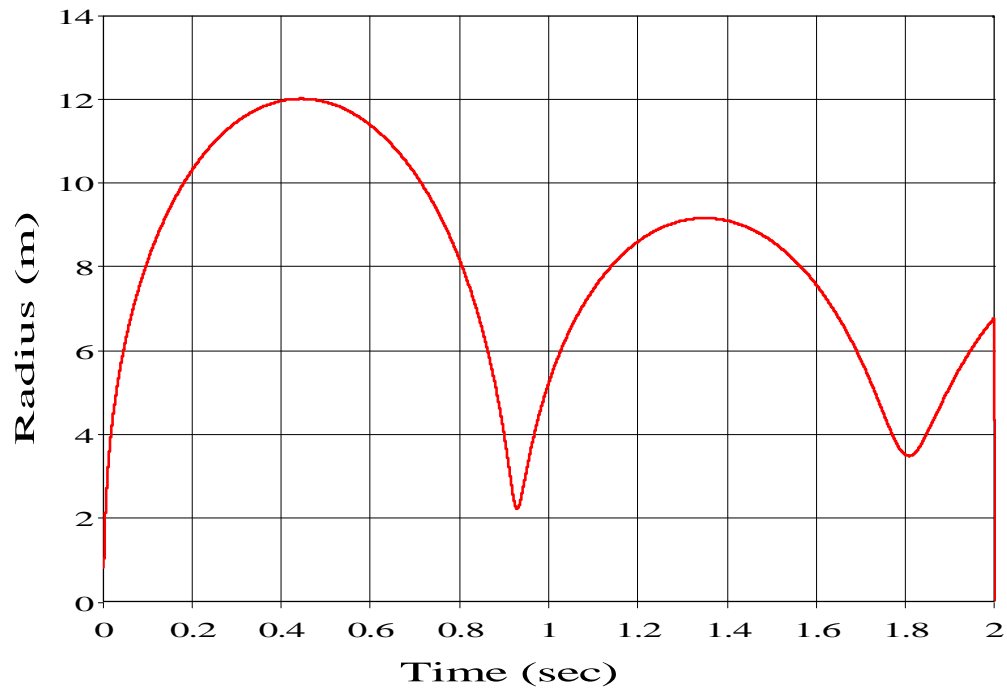
Figure 38. Gas Bubble Expansion for SHOT-1

GAS BUBBLE MIGRATION
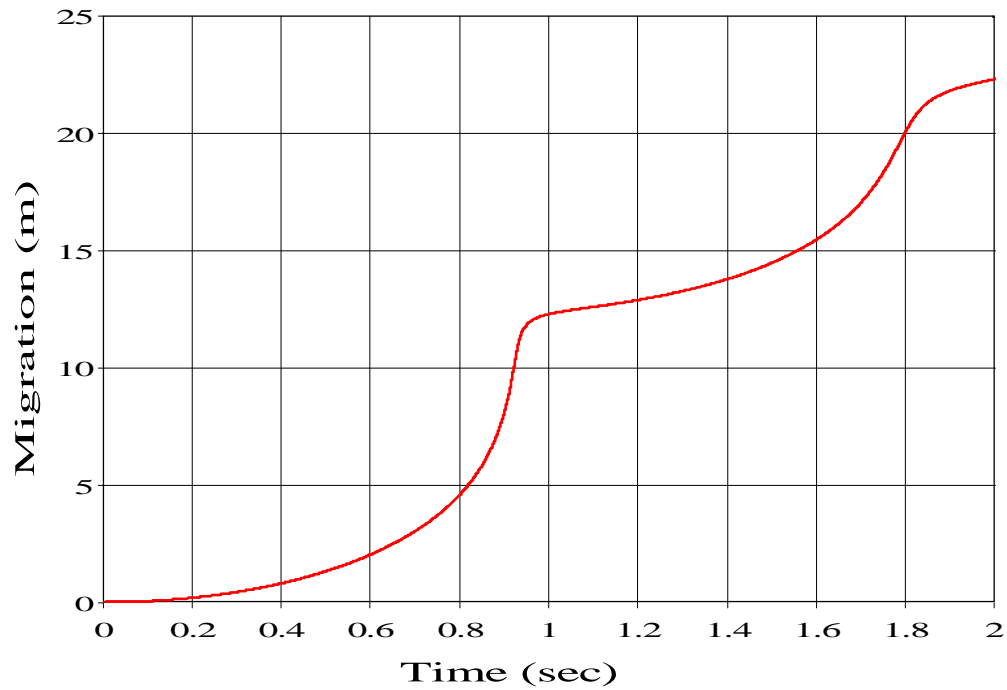
Figure 39. Gas Bubble Migration for SHOT-1

GAS BUBBLE PRESSURE
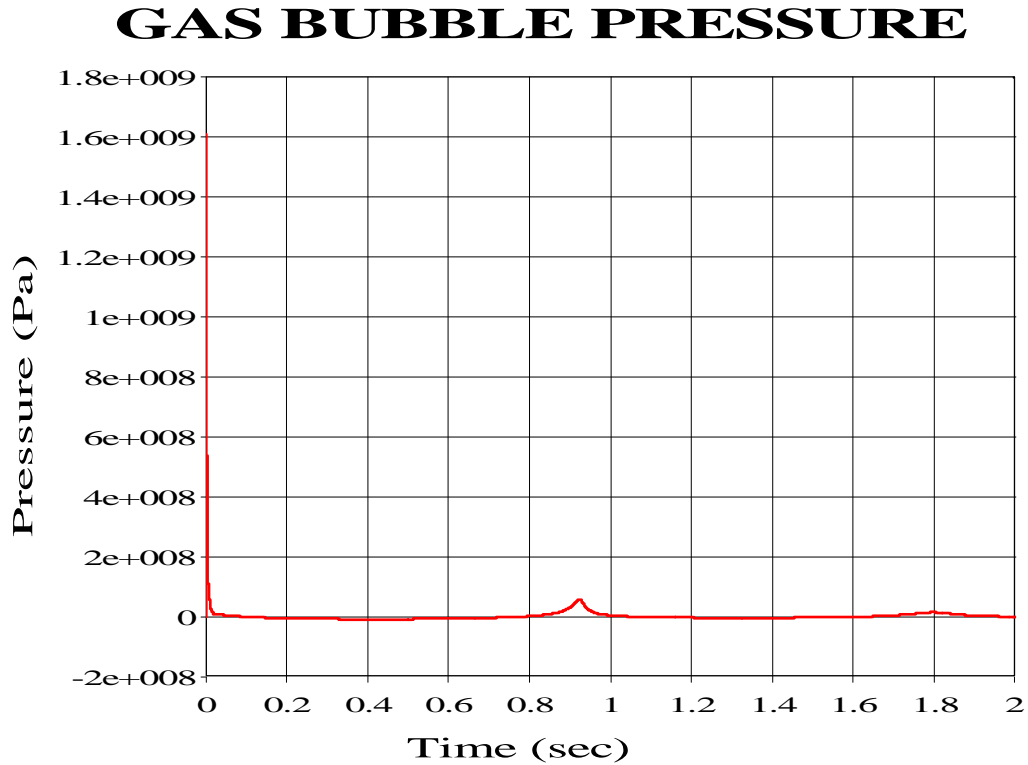
Figure 40.   Gas Bubble Pressure History for SHOT-1

The pressure time history of the fluid node right under the keel is shown in Figure 41. As seen in Figure 41, the pressure rises quickly to a peak value, and then dips. After generation of the tensile reflected wave at the free surface, the pressure drops off to zero representing cavitation, as explained before. The second peak occurs due to the reflection of the incident shock wave off the structural model and the other peaks occur due to the bulk cavitation closure. The cut-off time right under the keel is determined as 3.128 msec, which corresponds well with the theoretical value 3.086 msec calculated by Equation 5.1.

$$t_c \approx \frac{2x}{C} \sin \phi \qquad (5.1)$$

where   x = depth to the point of interest from the surface

C = acoustic velocity in the water

ϕ = angular standoff distance from the charge to the point of interest

57
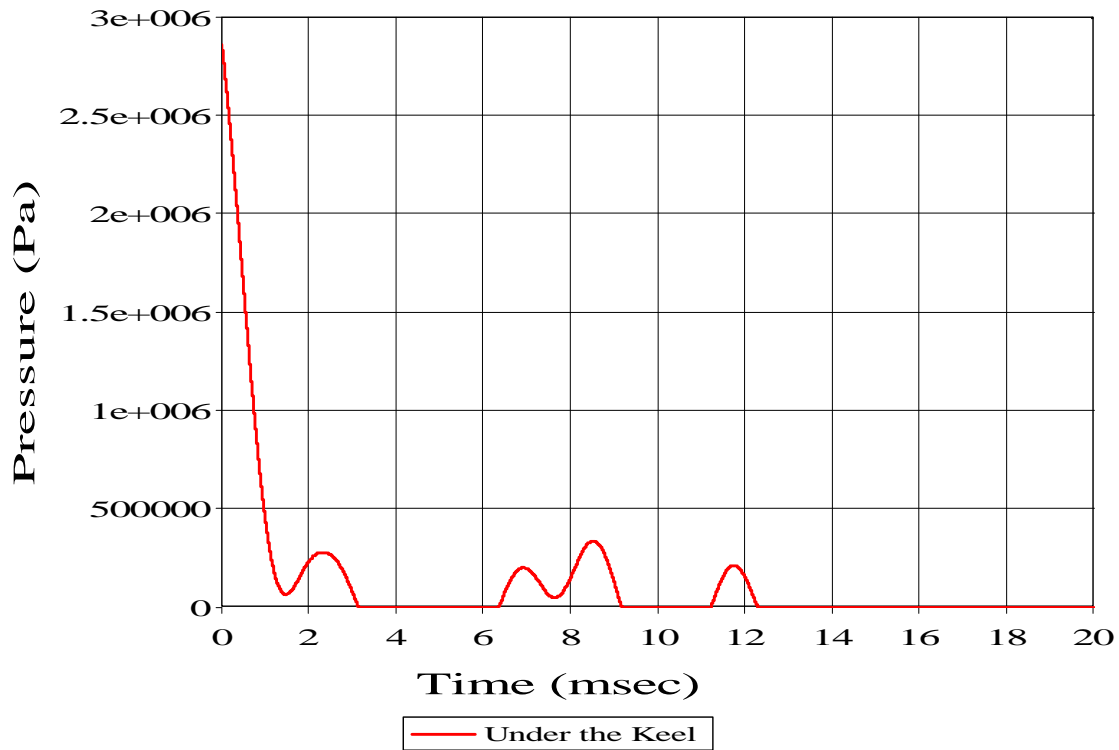
Pressure Profile

Figure 41. Resulting Pressure Profile Under the Keel Subjected to SHOT-1

2. Shock Wave Propagation and Bubble Formation for SHOT-2

The shock wave propagation of SHOT-2 is shown in Figure 42. The maximum shock wave pressure was determined as 3.471×10^6 Pa or 503.4 psi, which is close to the theoretical value, 498.94 psi. The spherical shape of the shock wave and the initial shock wave propagation at time zero can be seen in this figure.
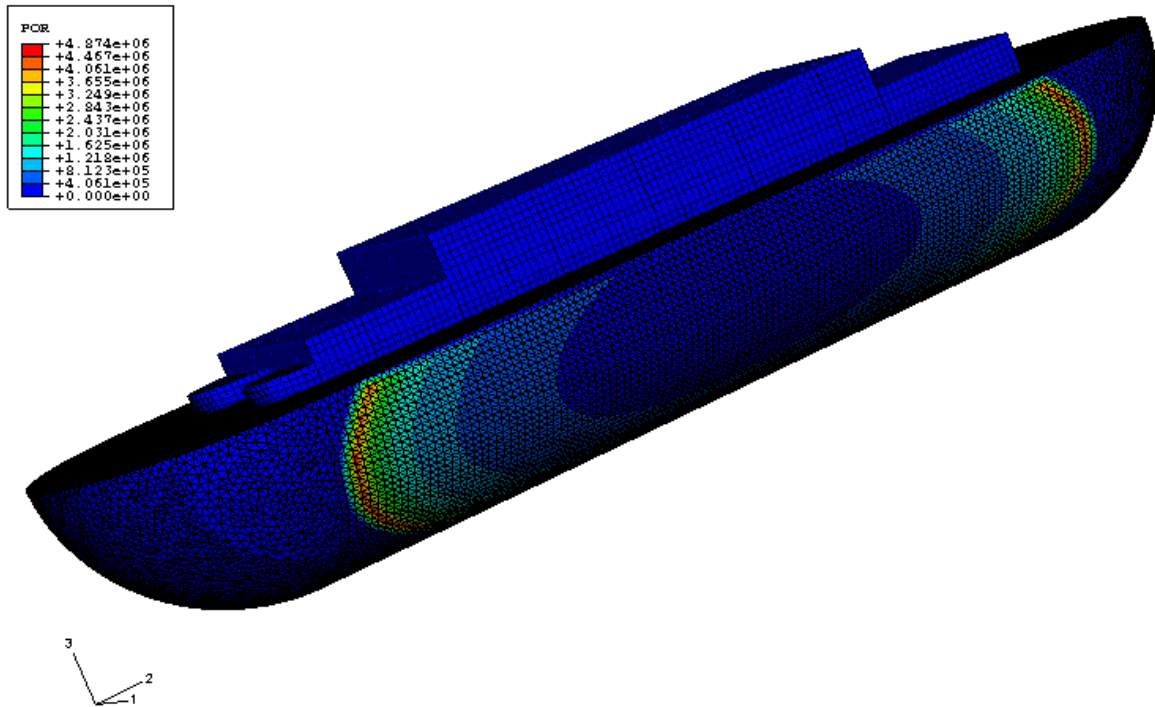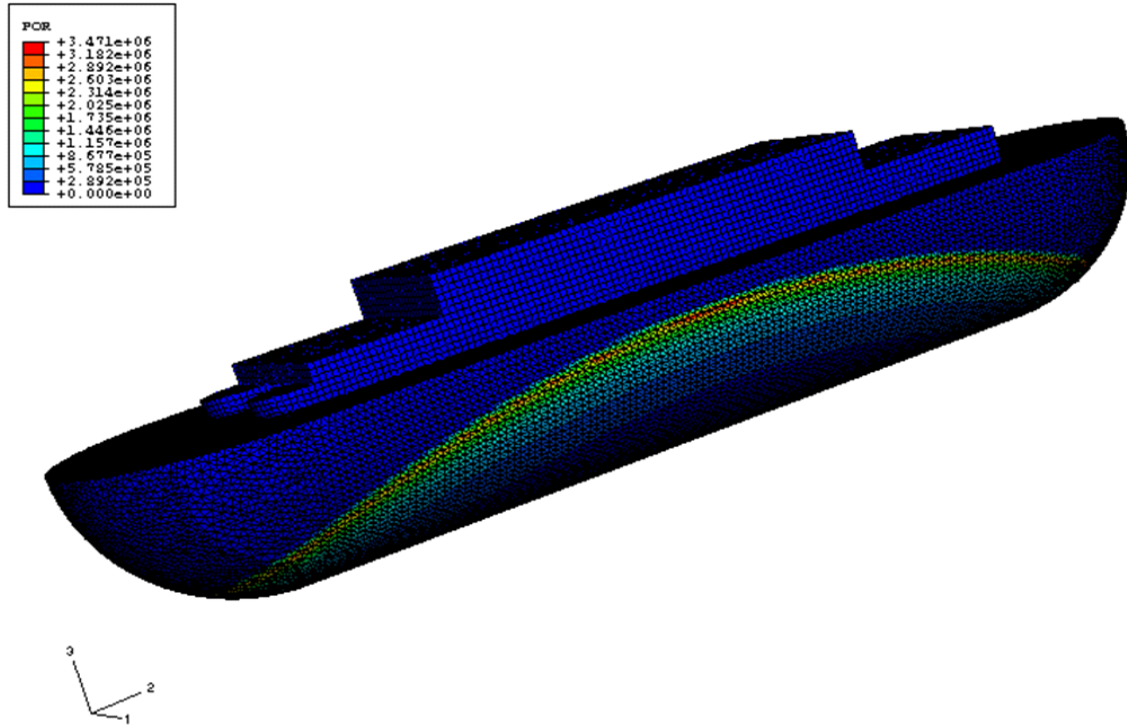
Figure 42. Shock Wave Propagation of SHOT-2

The time histories of bubble expansion and migration are shown in Figure 44 and 45, respectively, while the time history of the gas bubble pressure is shown in Figure 43. From the simulation in ABAQUS, these values were determined as 0.431 sec and 8.825 m, respectively, which are close to the theoretical values, 0.44 sec and 9.27 m, calculated by using Equation 2.4 and 2.6. The second bubble pulse occurs at 0.8 sec and the bubble continues to migrate, losing more energy. The cycle repeats until the total bubble energy is emitted.

GAS BUBBLE PRESSURE
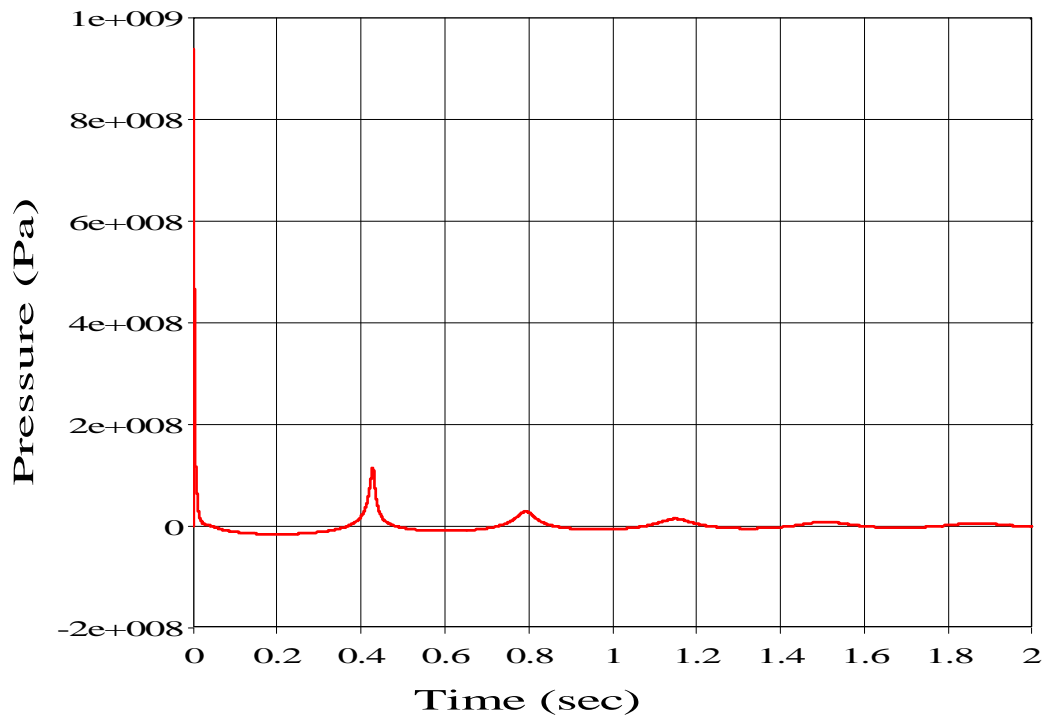
Figure 43. Gas Bubble Pressure History for SHOT-2

GAS BUBBLE RADIUS
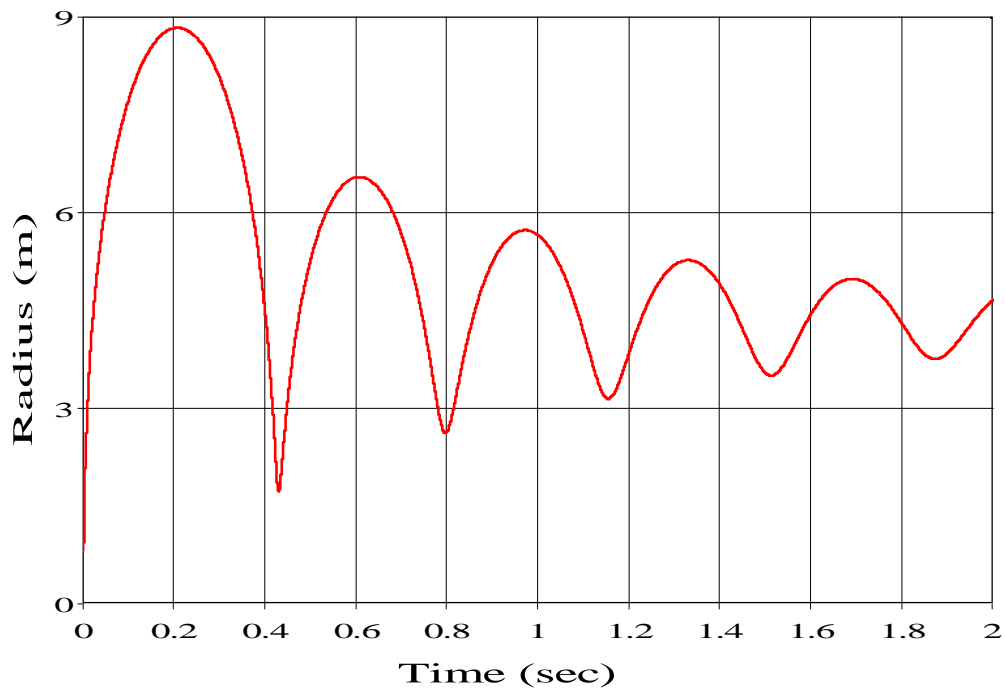
Figure 44. Gas Bubble Expansion for SHOT-2

60
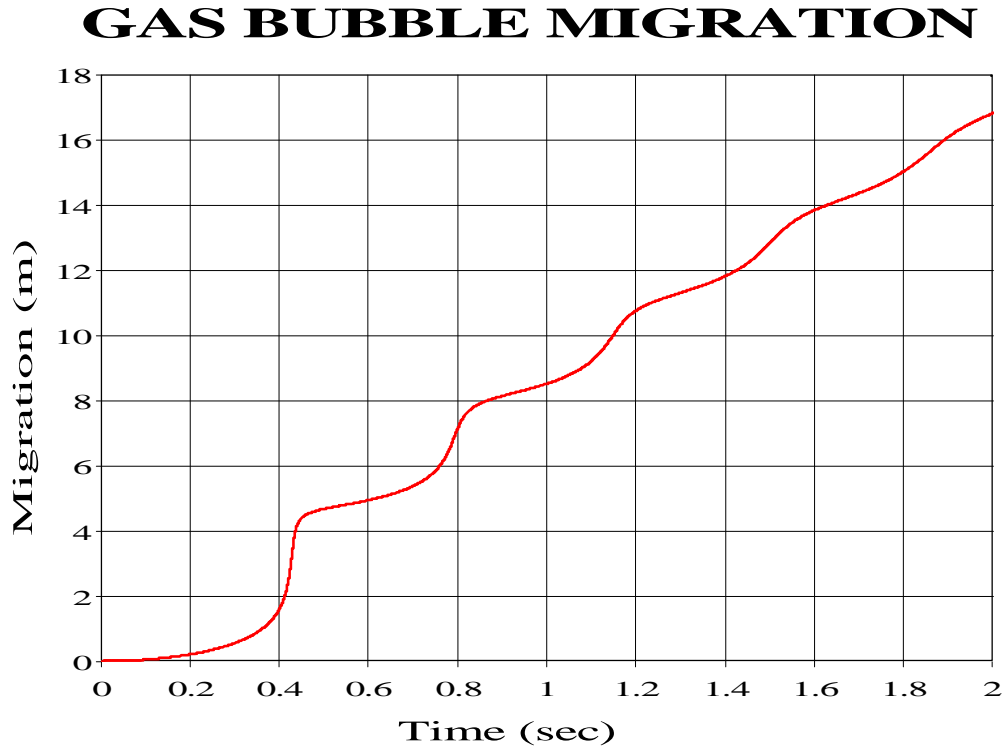
Figure 45.   Gas Bubble Migration for SHOT-2

The pressure time history of the fluid node right under the keel is shown in Figure 46. As seen in Figure 46, the pressure rises quickly to a peak value and then dips. The other peaks occur due to the reflection off of the structure and drops off to zero representing the cavitation or underpressure phase. The cut-off time right under the keel is determined as 7.005 msec whereas the theoretical value is 6.2072 msec calculated by Equation 5.1.

Pressure Profile
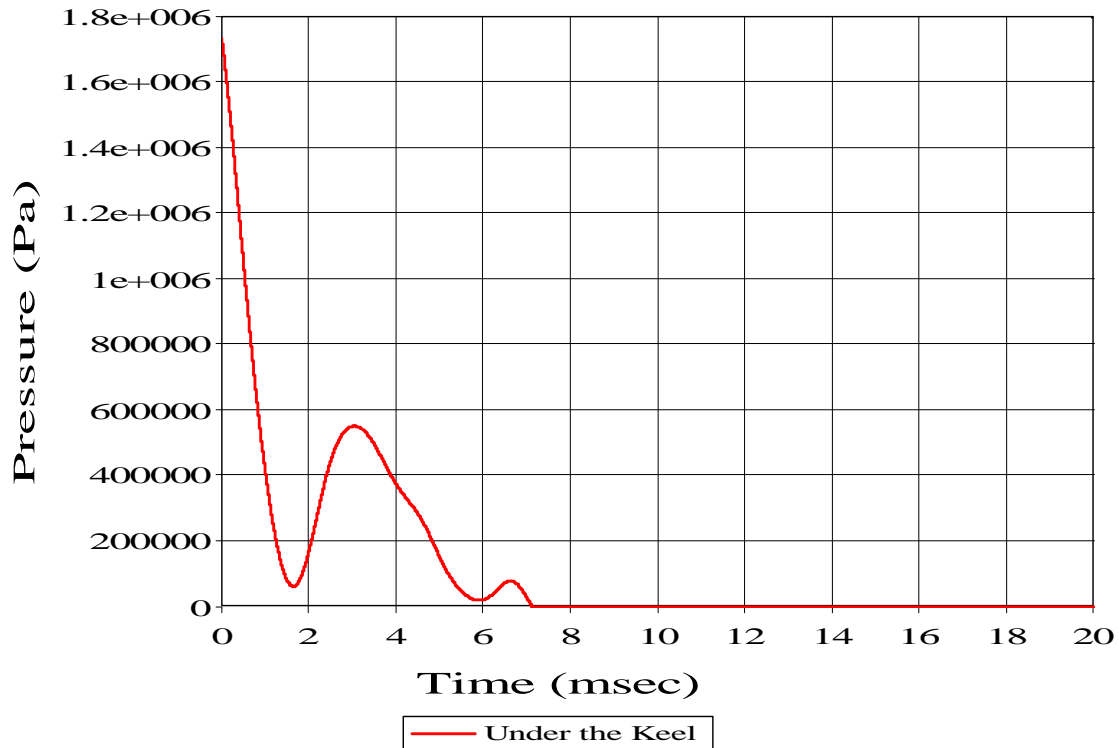
Figure 46. Resulting Pressure Profile Under the Keel Subjected to SHOT-2

B. VERTICAL VELOCITY RESPONSE

During an UNDEX event, the primary structural response is in the vertical direction. The incident shock wave impinges on the structure with extremely high pressure and forces the model to rapidly move upward with respect to the fluid. In Figure 47, the dominance of the velocity in the vertical direction, shown in red, is illustrated by the selected port keel node which was subjected to SHOT-1. The response data for this node is shown in Table 10. The trend in respond of this node was typical of all selected nodes and therefore, the vertical velocity time histories were used primarily for the comparisons discussed in this thesis.

The average vertical kick-off velocity of the model was calculated theoretically for the center of gravity of the submerged part of the hull. The estimated values for both shots are tabulated in Table 11.

VELOCITY HISTORY
NODE 17198
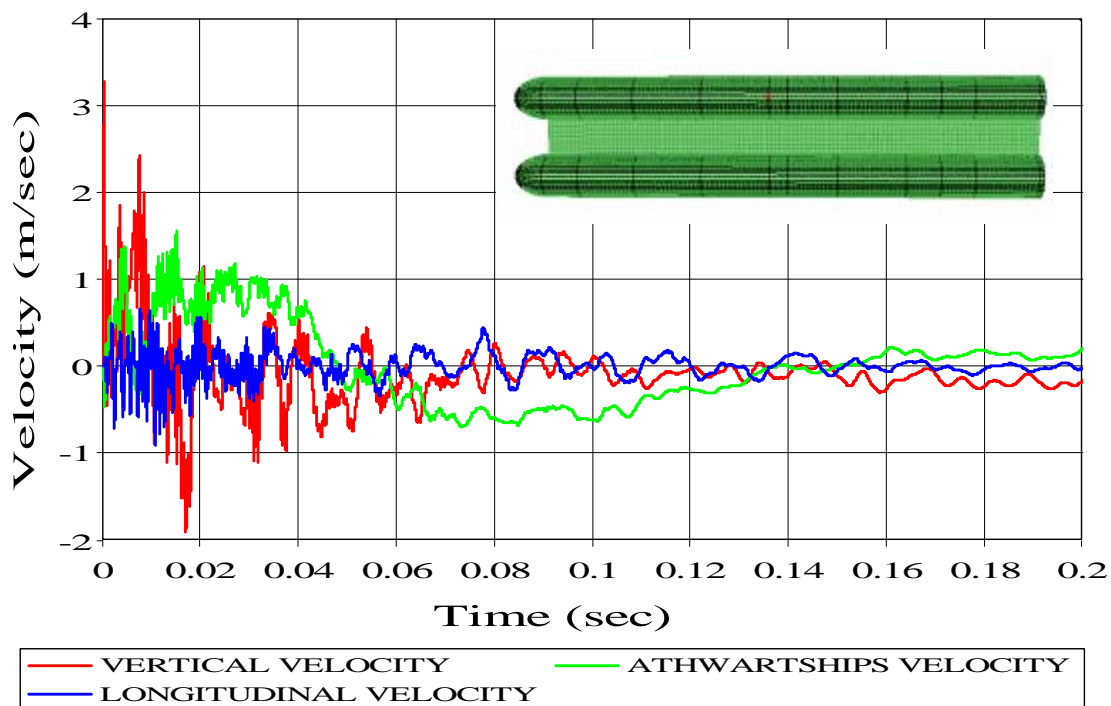
Figure 47. Velocity History of Node 17198 in XYZ-Directions

Table 10. Peak Velocity Values of Node 17198 in XYZ-Directions

	PEAK VELOCITY (m/sec)
Vertical Direction	3.26859
Athwarthships Direction	1.56181
Longitudinal Direction	0.92079

Table 11. Calculated Average Vertical Kick-Off Velocity Values

	SHOT-1	**SHOT-2**
Calculated Average Vertical Kick-Off Velocity (m/sec)	1.51	1.39

1. Vertical Velocity Response of the Model Subjected to SHOT-1

The response of the node at the center of the amidships bulkhead is shown in Figure 48 in order to compare the kick-off velocity with the calculated one. As shown from Figure 48, the initial velocity of Node 17409 is 2.00147 m/sec with corresponding time 7.087 msec, which is closer to the theoretical kickoff velocity 1.51 m/sec
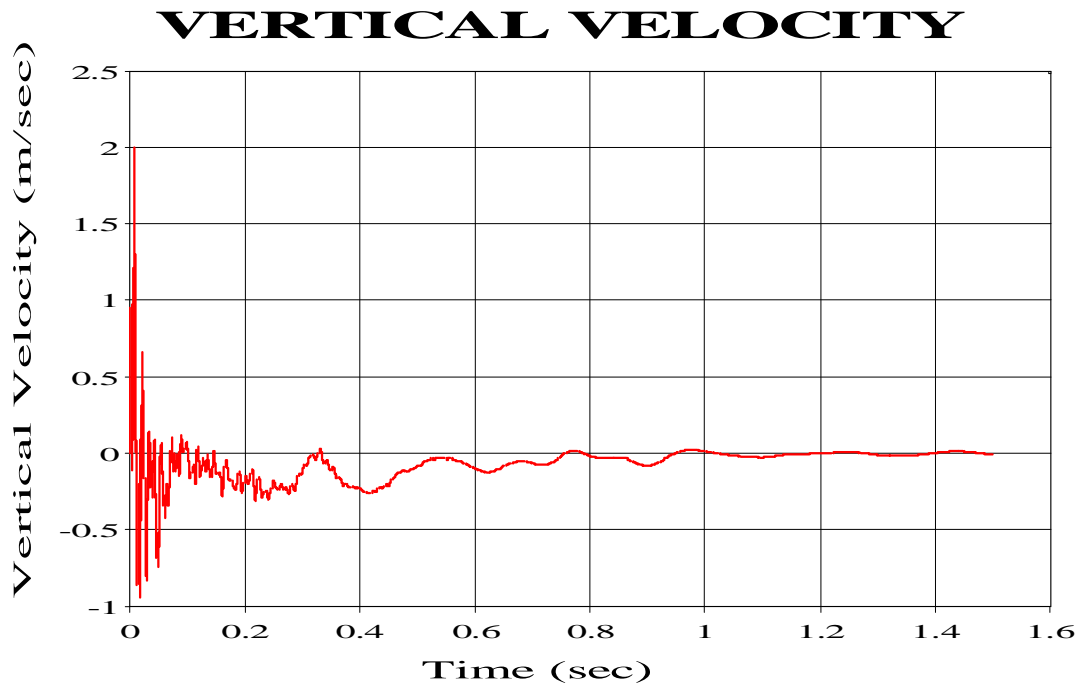
Figure 48. Vertical Velocity History of Node 17409

The responses of the nodes at the port keel up to 1.5 sec are shown in Figure 49. The vertical velocity time history of 0.2 sec is shown in Figure 50 in order to accurately capture the response of the nodes having different radial standoff distance at the early time. The peak vertical velocity values are tabulated in Table 12.

VERTICAL VELOCITY
NODES AT KEEL
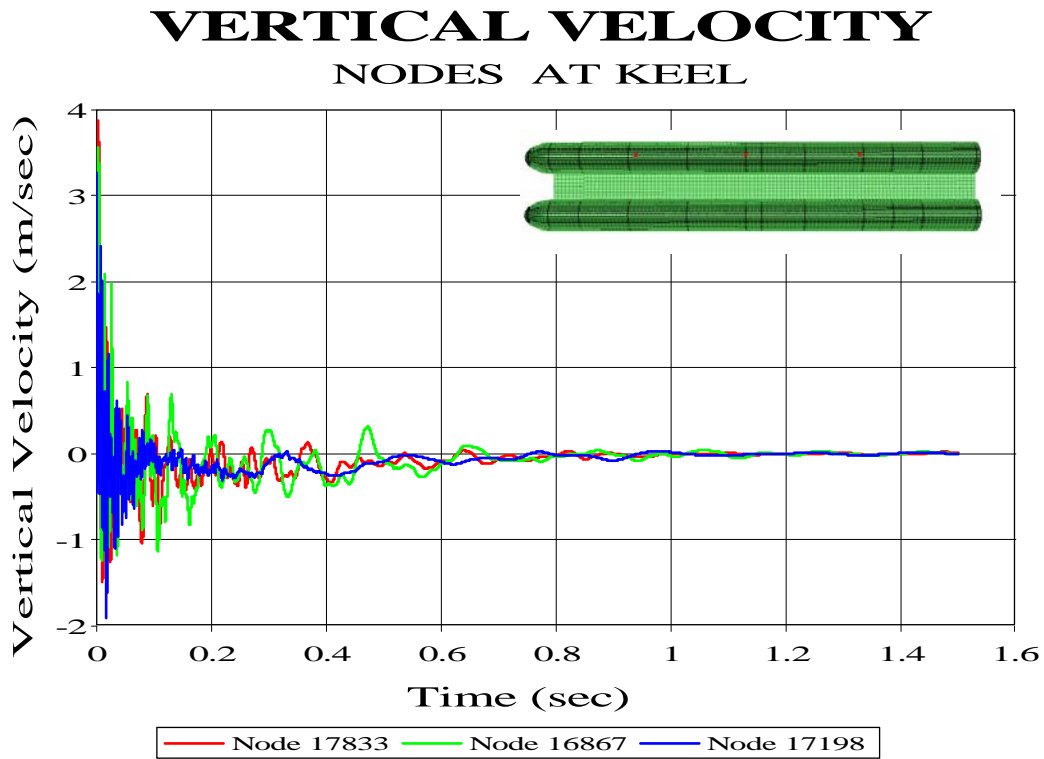
Figure 49.   Vertical Velocity History of Port Keel Nodes

VERTICAL VELOCITY
Nodes At Keel
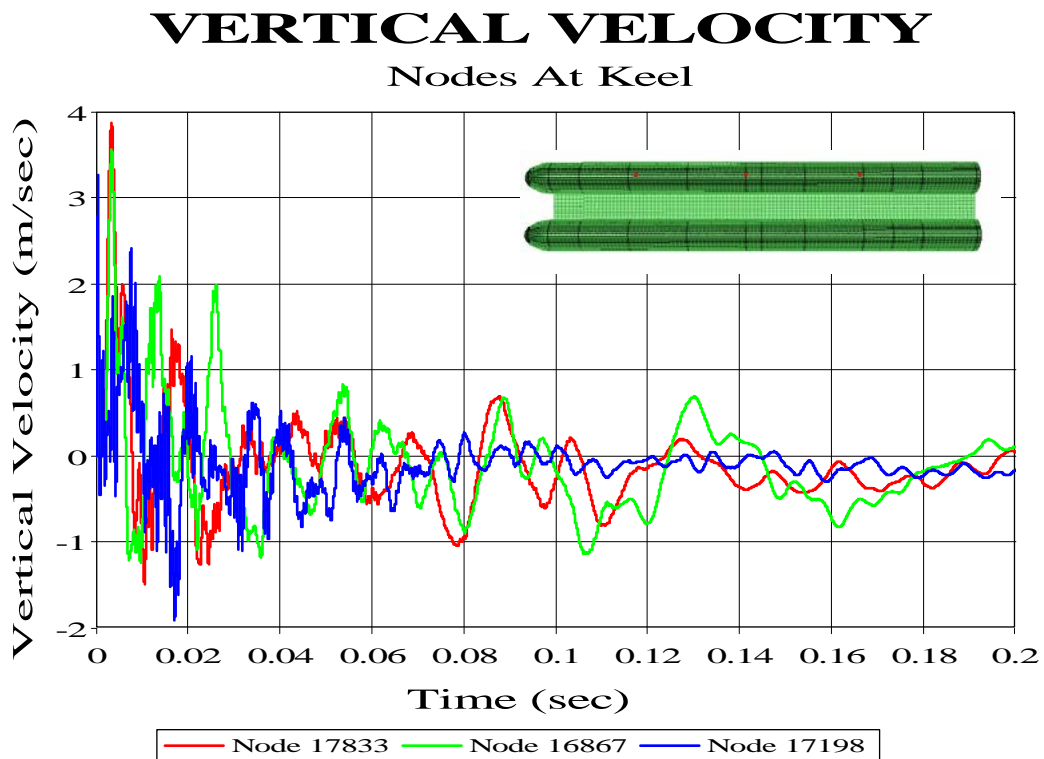
Figure 50.   Trimmed Vertical Velocity History of Port Keel Nodes

Table 12. Peak Vertical Velocity Values for Port Keel Nodes

	Peak Velocity (m/sec)	Time (msec)
Node 17198	3.26859	0.22825
Node 16867	3.55323	3.26838
Node 17833	3.86921	3.22969

The node at amidships, Node 17198 reaches its maximum vertical velocity before the other two nodes since it is closer to the charge. The other nodes at the bow and stern have approximately the same standoff distance, so they exhibit very similar behavior and reach their peak values almost at the same time.

As shown from Figure 51, Node 17198 exhibits high frequency oscillation whereas the other nodes exhibit low frequency oscillation, as expected. Since the incident shock wave pressure gradually increases, it should be expected that the nodes closer to the charge will exhibit high frequency oscillation and take a shorter time to be damped. Nodes 16867 and 17833, having a greater radial standoff distance than Node 17198 show signs of being slightly over damped.

The responses of the nodes at the starboard keel are shown in Figure 51 and the peak vertical velocity values are tabulated in Table 13. As shown from Figure 51, the nodes at the starboard keel respond with a shift in the time and exhibit lower vertical velocity compared to the port keel nodes since the charge is located off the port side. Similarly with the responses of port keel nodes, the node at amidships, Node 13926 reaches its maximum vertical velocity before the other two nodes since the radial standoff distance is smaller than that of the other nodes; Node 19568 and 15276 exhibit very similar behavior and reach their peak values almost at the same time due to the fact that they have approximately same standoff distance.

VERTICAL VELOCITY
Nodes at Starboard Keel

Figure 51. Vertical Velocity History of Starboard Keel Nodes

Table 13. Peak Vertical Velocity Values of Starboard Keel Nodes

	Peak Velocity (m/sec)	Time (msec)
Node 13926	2.35073	14.893
Node 19568	1.53037	19.864
Node 15276	1.72117	20.075

The responses of the nodes at the port side are shown in Figure 52 in order to compare the response of the nodes having the same horizontal standoff distance but different vertical standoff distance. The peak vertical velocity values are tabulated in Table 14.

67

VERTICAL VELOCITY
NODES AT PORT SIDE
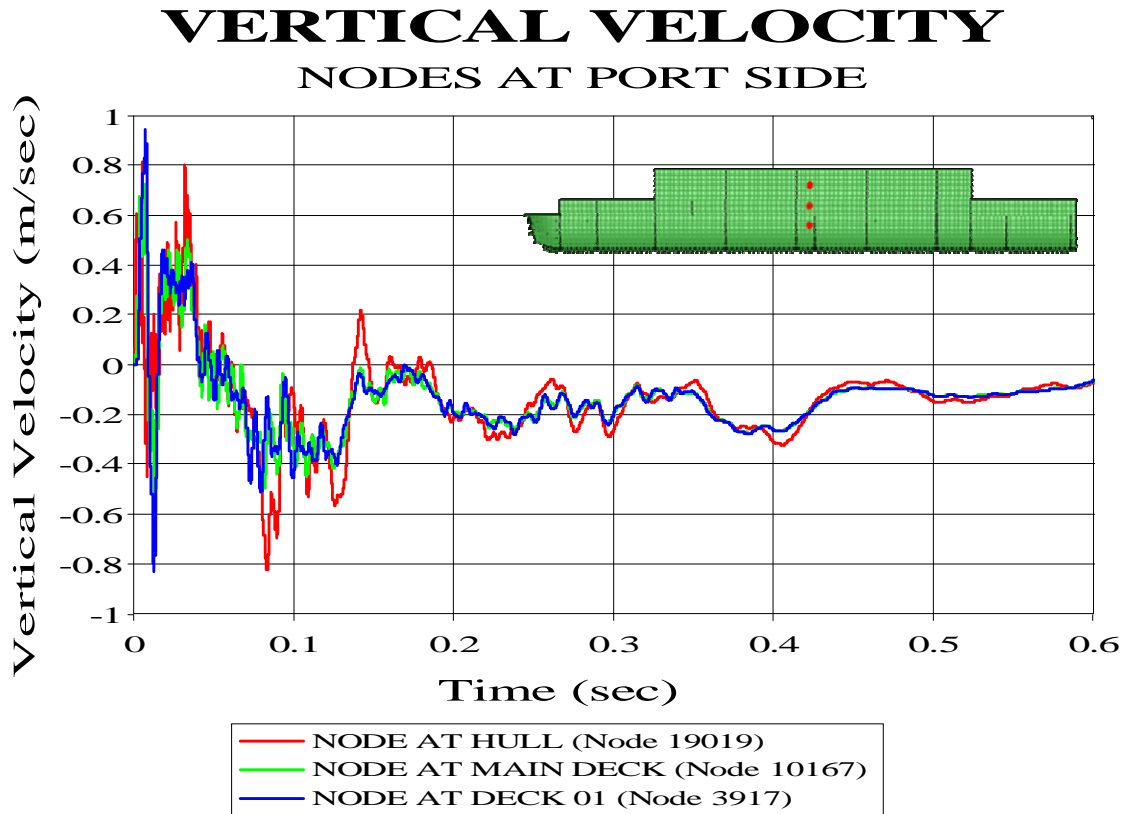
Figure 52.   Vertical Velocity History of Port Side Nodes

Table 14.   Peak Vertical Velocity Values of Port Side Nodes

	Peak Velocity (m/sec)	Time (msec)
Node at Hull (19019)	0.81549	5.4448
Node at Main Deck (10167)	0.724138	7.2190
Node at Deck 01 (3917)	0.943624	7.3323

Node 19019 reaches its maximum vertical velocity first since it is closer to the charge than the other nodes. The nodes located higher in the structure make the prediction of the response more dependent on the structural model and structural damping. Thus, the mass and stiffness distribution must be considered.

As shown from Figure 52, the node closest to the charge exhibits higher frequency oscillations whereas the other nodes exhibit lower frequency oscillations. When the shock wave energy propagates upward to the main deck, higher frequency

68

motion of the model is attenuated by structural damping of the ship and lower frequency oscillations become dominant. Since the nodes are not too far away from each other, the oscillation difference is not so apparent. Thus they exhibit very similar behavior.

As far as the differences in the vertical velocities of nodes are concerned, it can be observed that Node 3917, which is located at deck 01, has the greatest vertical velocity among the other compared nodes due to the fact that the deck 01 is less stiff and lighter in weight than the main deck and the hull.

The responses of the nodes at the starboard side are shown in Figure 53 in order to compare the responses with the responses of the equivalent port side nodes, and the peak vertical velocity values are tabulated in Table 15.

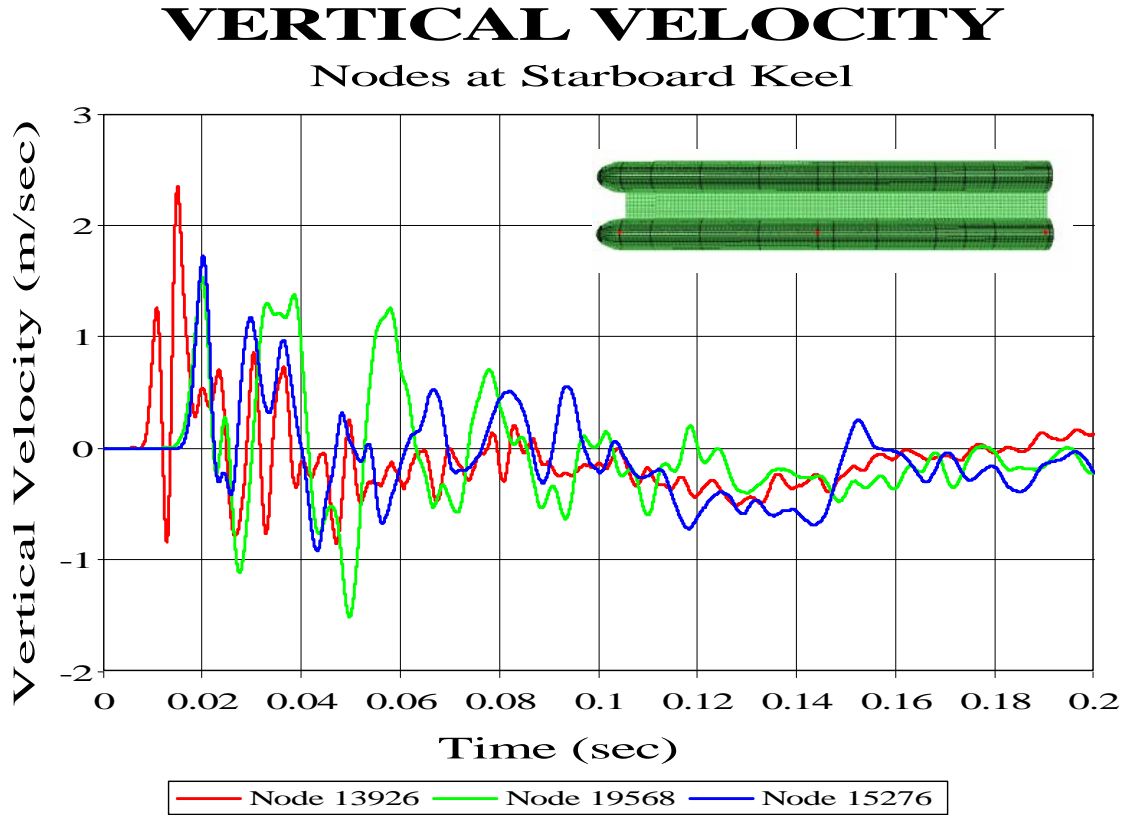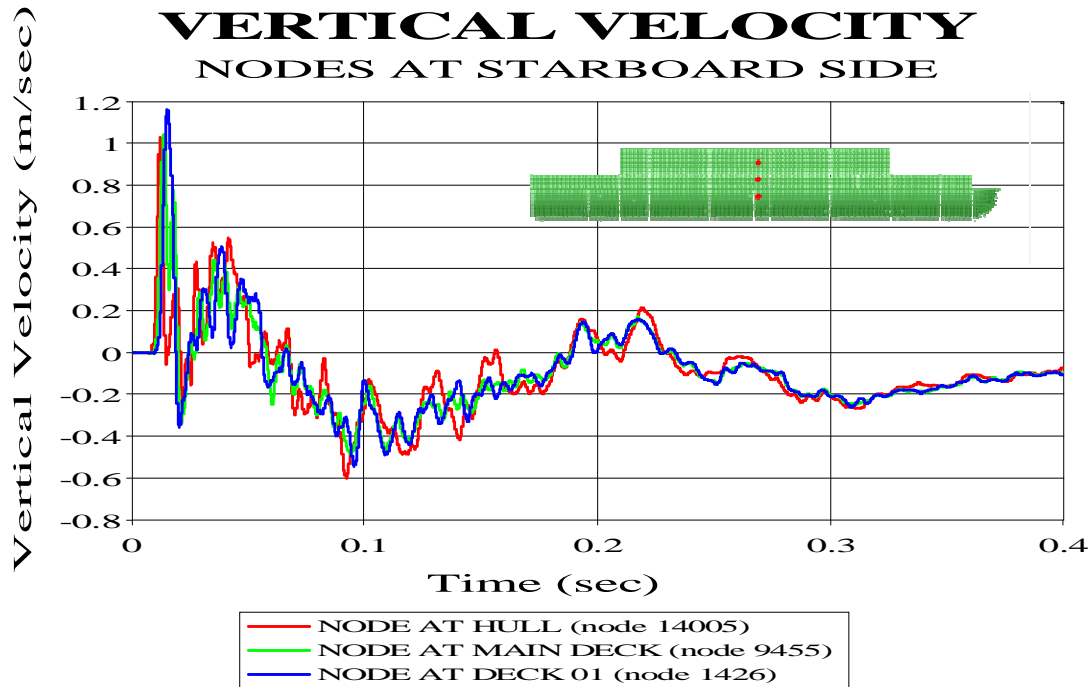**Figure 53.** Vertical Velocity History of Starboard Side Nodes

Table 15. Peak Vertical Velocity Values for Starboard Side Nodes

	Peak Velocity (m/sec)	Time (msec)
Node at Hull (14005)	1.0315	12.1482
Node at Main Deck (9455)	1.04047	13.5689
Node at Deck 01 (1426)	1.16235	15.1471

69

Node 14005 reaches its maximum vertical velocity first since it is closer to the charge than the other nodes, and exhibits higher frequency oscillations whereas the other nodes exhibit a little lower frequency oscillation, as expected.

The starboard side nodes exhibit greater vertical velocities compared to those of the equivalent port side nodes due to the interaction with the deck between the hulls, but need more time to reach the peak values and damp due to the greater standoff distance.

The response of the node at the main deck between the hulls is shown in Figure 54 in order to analyze the effect of the gap between the hulls on the response.
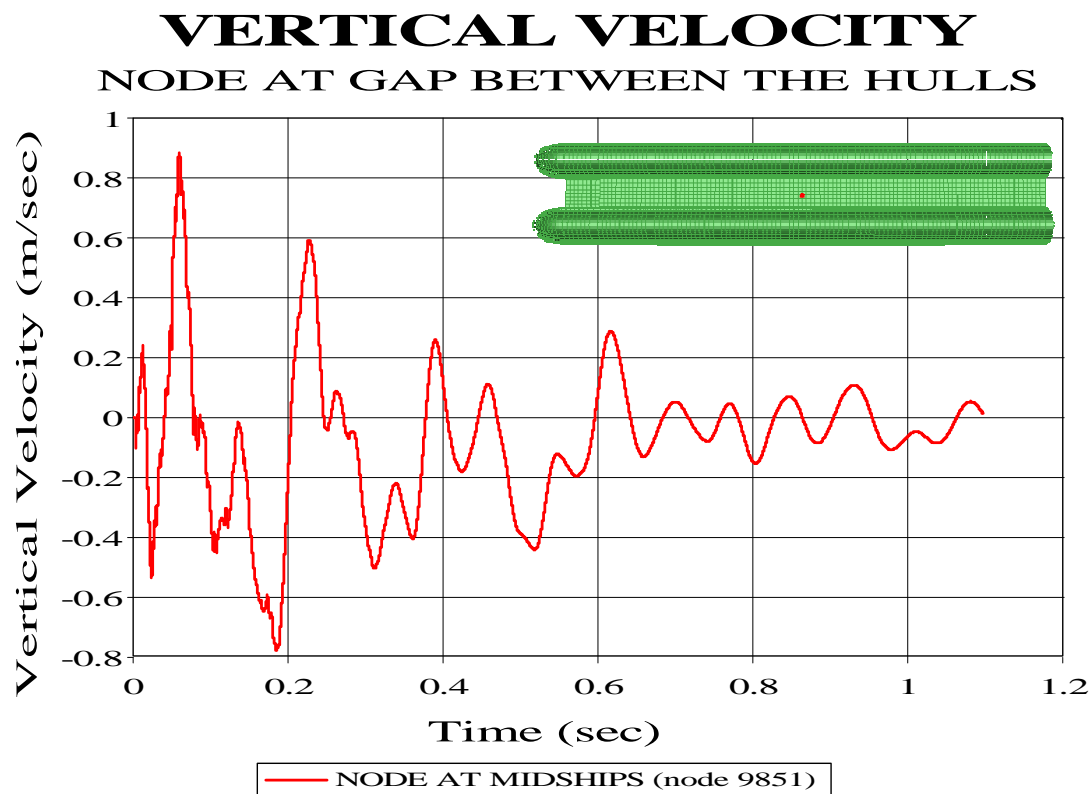
Figure 54.   Vertical Velocity History of Node 9851

Node 9851 of the main deck is located at the intersection of the centerline and the midship line, which does not interact with the fluid mesh but with the air gap. This node is approximately aligned at the same horizontal line as the standoff point. The response shows different behavior from the other responses. The node exhibits several oscillations with low frequency and settles down very slowly compared to other nodes. The incident shock wave propagates gradually until it reaches the free surface. At the free surface, the

70

shock wave pressure drops to zero and atmospheric pressure becomes dominant. Therefore, it can be stated that there is no vertical pressure or impact, generated by the incident shock wave, occurring on the main deck at the gap. Since the node is not connected to any other node at one face, the response just depends on the laterally and longitudinally connected structural nodes, so Node 9851 responds at a later time and generates several low frequency oscillations with a lower peak vertical velocity, 0.8796 m/sec.

The responses of the nodes at the fore of the model are shown in Figure 55 in order to compare the response of the nodes coupled with the fluid mesh and uncoupled with the fluid mesh. The peak vertical velocity values are tabulated in Table 16.
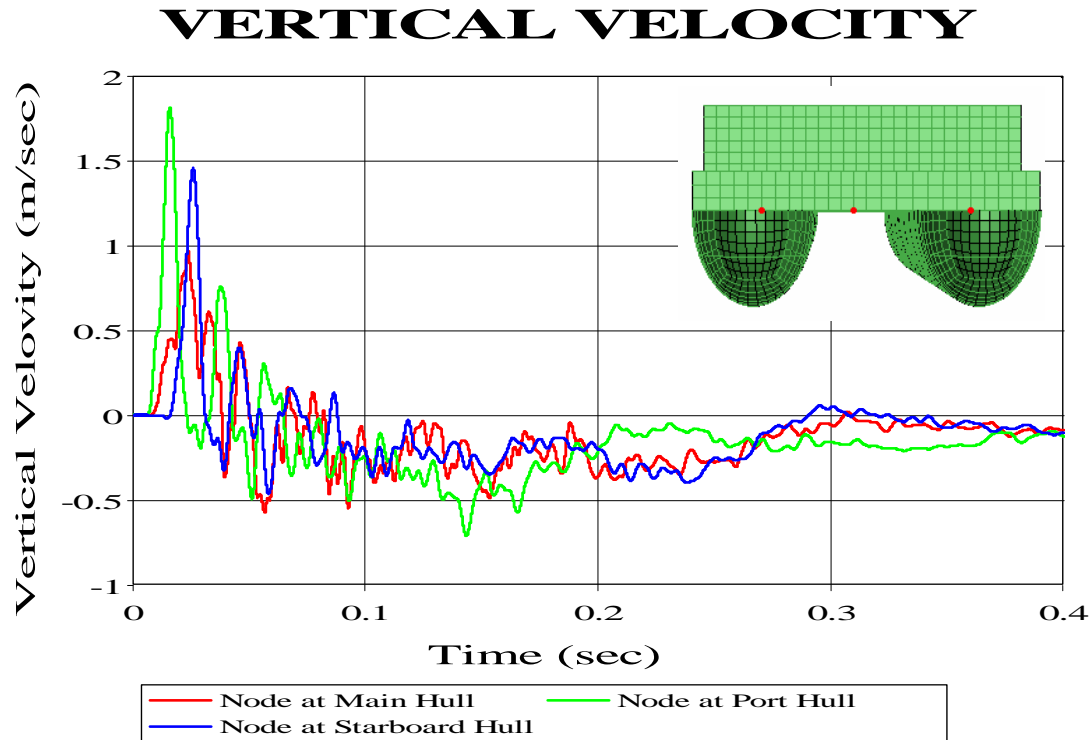
Figure 55. Vertical Velocity History of the Fore Nodes

Table 16. Peak Vertical Velocity Values for the Fore Nodes

	Peak Velocity (m/sec)	**Time (msec)**
Node at Port Hull (6811)	1.8142	15.6947
Node at Main Deck (6571)	0.9633	23.6415
Node at Starboard Hull (6415)	1.45478	25.7870

71

As shown from Figure 55, the node at port hull reaches its maximum vertical velocity before the other two nodes and shows more oscillations than the other nodes due to the fact that it is the closest node to the charge. The responses of the nodes exhibit similar behavior with a small time shift, as expected. The nodes damp almost at the same time because they are close to each other.

Since Node 6571 is not coupled with the fluid mesh and there is no occurrence of vertical incident shock impact on the node, it has the smallest peak velocity among the compared nodes.

2. Vertical Velocity Response of the Model Subjected to SHOT-2

The response of the node at the center of the midships bulkhead of the port hull is shown in Figure 56 in order to compare the kick-off velocity with the calculated one. The initial velocity of Node 17409 is 1.315 m/sec, with corresponding time 1.223 msec, which almost corresponds to the theoretical kickoff velocity 1.392 m/sec.
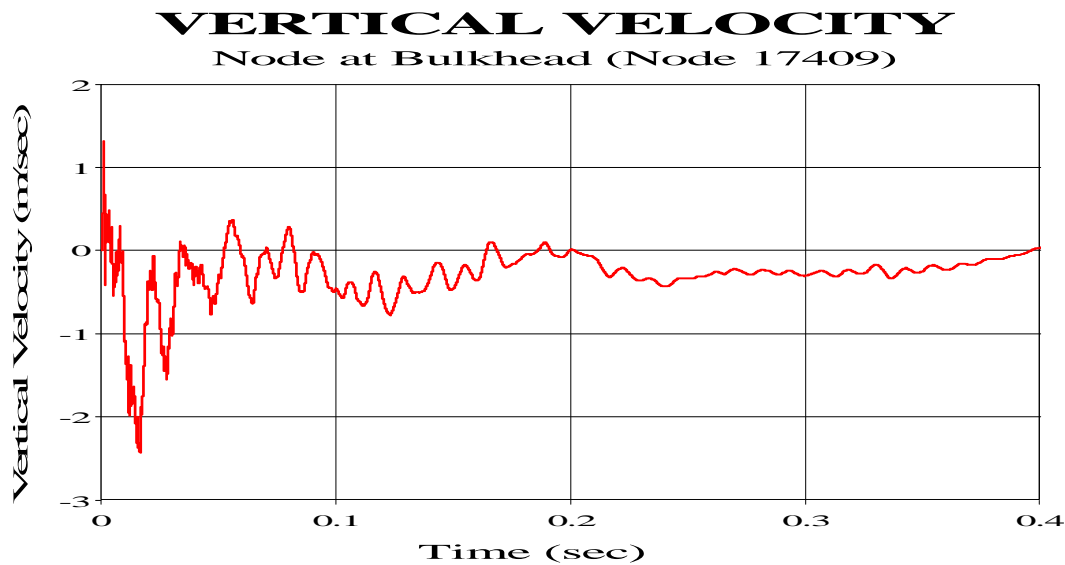
Figure 56.   Vertical Velocity History of Node 17409

The responses of the nodes at the fore of the model are shown in Figure 57 in order to compare the response of the nodes coupled with fluid mesh and uncoupled with the fluid mesh. The peak vertical velocity values are tabulated in Table 17. As shown from the figure, the nodes exhibit a distinctive rise in vertical velocity at the time of the

72

bubble pulse formations, such as time 0.43, 0.8 and 1.18 sec, due to the rise in bubble pressure. In order to analyze the responses accurately, the trimmed vertical velocity time histories are generated as in Figure 58.
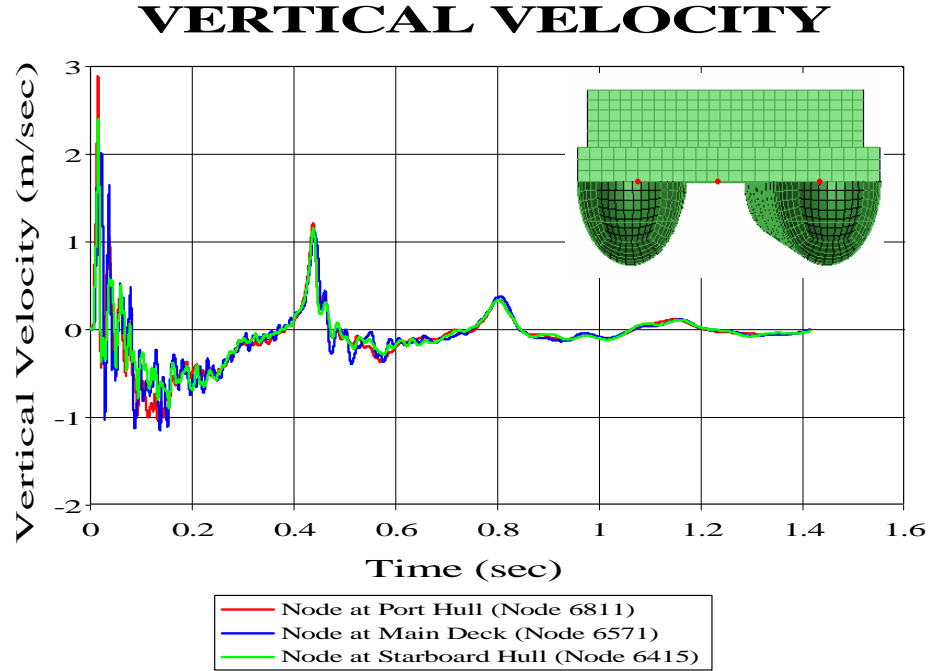
VERTICAL VELOCITY

Figure 57.   Vertical Velocity History of Fore Nodes
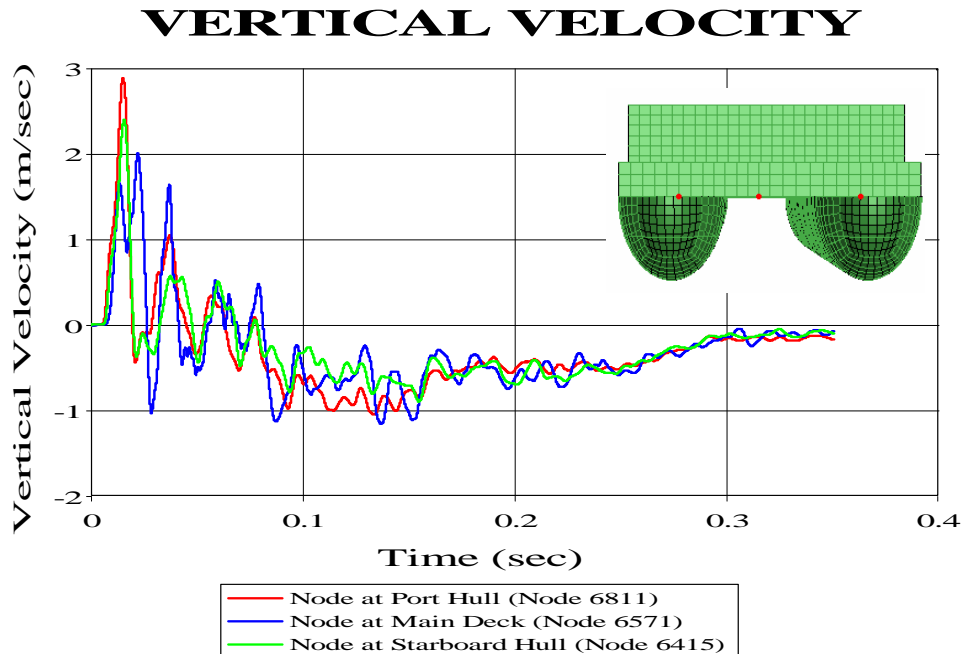
VERTICAL VELOCITY

Figure 58.   Trimmed Vertical Velocity History of Fore Nodes

73

Table 17.　Peak Velocity Values of Fore Nodes

	Peak Velocity (m/sec)	Time (msec)
Node at Port Hull (6811)	2.88399	14.8310
Node at Main Deck (6571)	2.00497	21.8718
Node at Starboard Hull (6415)	2.39654	15.3685

As shown from Figure 58, the node at port hull reaches its maximum vertical velocity before the other two nodes and shows more oscillation than the other nodes due to the fact that it is the closest node to the charge. The nodes damp almost at the same time because they are close to each other.

The behavior of the nodes subjected to SHOT-2 is similar to the behavior subjected to SHOT-1. The difference is that they have higher peak vertical velocities at the fore of the model and need more time to damp when subjected to SHOT-2. Node 6571 exhibits the smallest peak velocity among the compared nodes due to the same reason explained in Section 1.

The responses of the nodes at the port keel are shown in Figure 59 in order to compare the response of the nodes having different radial standoff distance. The peak vertical velocity values are tabulated in Table 18.

As shown from Figure 59, the node at midships, Node 17198 reaches its maximum vertical velocity before the other two nodes since it is closer to the charge. The other nodes at the bow and stern have approximately the same standoff distance, so they exhibit very similar behavior and reach their peak values almost at the same time. Node 17198 exhibits high frequency oscillation whereas the other nodes exhibit low frequency oscillation, as expected.

VERTICAL VELCOITY

Nodes at Port Keel
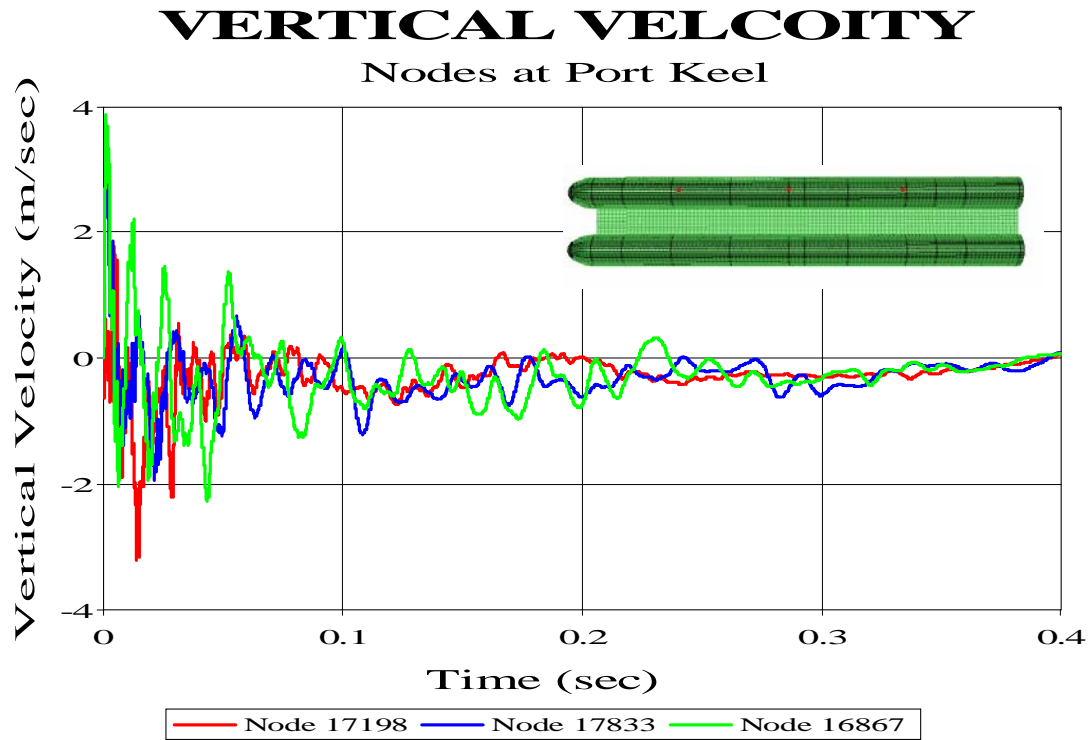
Figure 59. Vertical Velocity History of Port Keel Nodes

Table 18. Peak Vertical Velocity Values of Port Keel Nodes

	Peak Velocity (m/sec)	Time (msec)
Node 17198	1.78315	4.85236
Node 17833	3.74692	1.07925
Node 16867	3.85908	1.29341

The responses of the nodes at the port side are shown in Figure 60 and the peak vertical velocity values are tabulated in Table 19.

VERTICAL VELOCITY
Nodes at Port Side
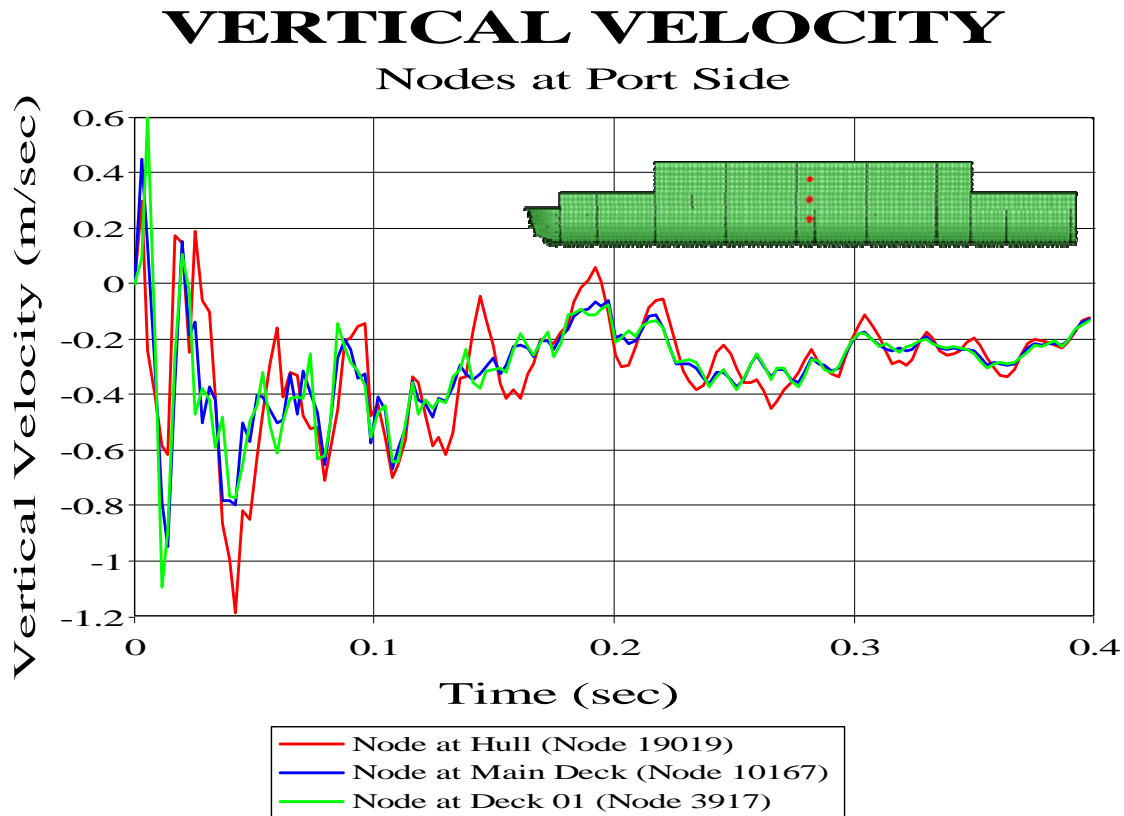
Figure 60. Vertical Velocity History of Port Side Nodes

Table 19. Peak Vertical Velocity Values of Port Side Nodes

	Peak Velocity (m/sec)	Time (msec)
Node 19019	0.5709	1.36949
Node 10167	0.5415	3.22078
Node 3917	0.6037	5.45572

Node 19019 reaches its maximum vertical velocity first since it is closer to the charge than the other nodes and exhibits higher frequency oscillations. The other nodes at the bow and stern have very similar behavior and reach their peak values almost at the same time, as expected. As shown in Table 19 Node 3917, which is located at deck 01, has the greatest vertical velocity among the other compared nodes due to the fact that Node 3917 has more structural support from the bottom and the upper deck is less stiff and lighter in weight than the other decks.

The port side nodes have lower vertical velocity and less time to reach the peak velocity compared to the responses subjected to SHOT-1 due to greater radial standoff distance.

The responses of the nodes at the starboard side are shown in Figure 61 and the peak vertical velocity values are tabulated in Table 20.
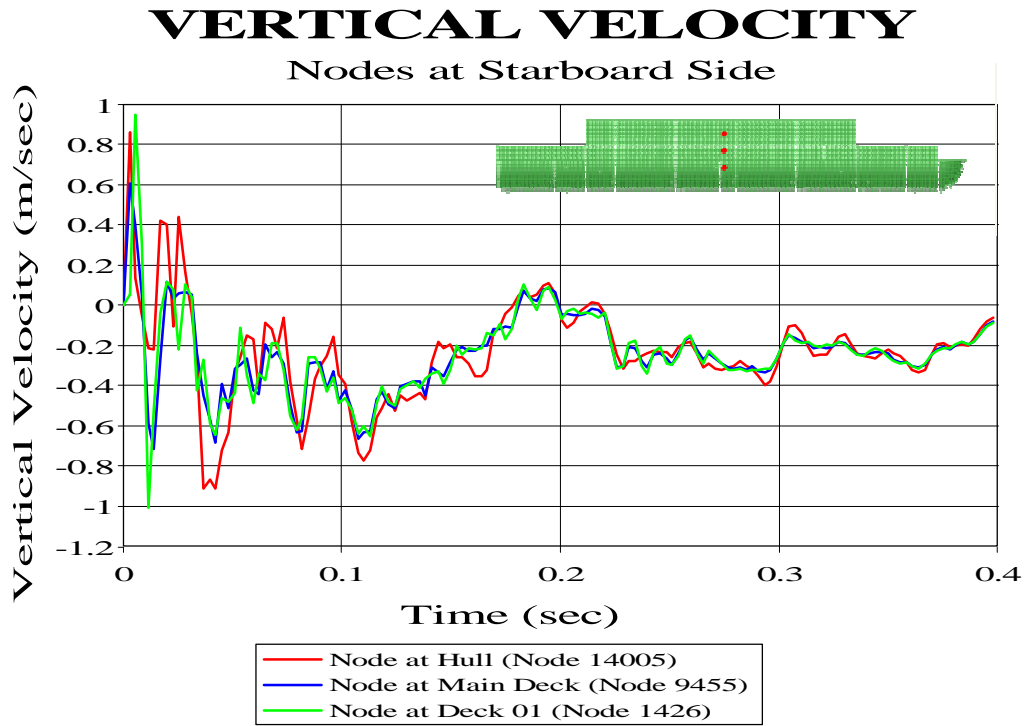
Figure 61. Vertical Velocity History of Starboard Nodes

Table 20. Peak Vertical Velocity Values of Starboard Nodes

	Peak Velocity (m/sec)	Time (msec)
Node 14005	1.07169	1.75554
Node 9455	0.92907	3.83511
Node 1426	0.94686	5.73069

Node 14005 reaches its maximum vertical velocity first since it is closer to the charge than the other nodes, and exhibits higher frequency oscillations whereas the other nodes exhibit a little lower frequency oscillation, as expected.

The starboard side nodes have similar vertical velocity but need more time to reach the peak velocity compared to the responses of the nodes subjected to SHOT-1.

C.   ATHWARTSHIPS AND LONDITUDINAL RESPONSE

Even though the major excitement is in the vertical direction, the athwartships and longitudinal velocity response of several nodes is also included in order to implement the UNDEX analysis of the Sea TENTACLE model. In this section, only SHOT-1 will be considered.

The athwartships velocity time histories of Node 17409, which is located at the midships bulkhead of the port hull are shown in Figure 62 and 63. In Figure 63, the velocity time history is trimmed to 0.6 sec in order to accurately capture the response of the node. The peak athwartships velocity of Node 17409 is determined to be 0.9218 m/sec corresponding to time 13.8819 msec.
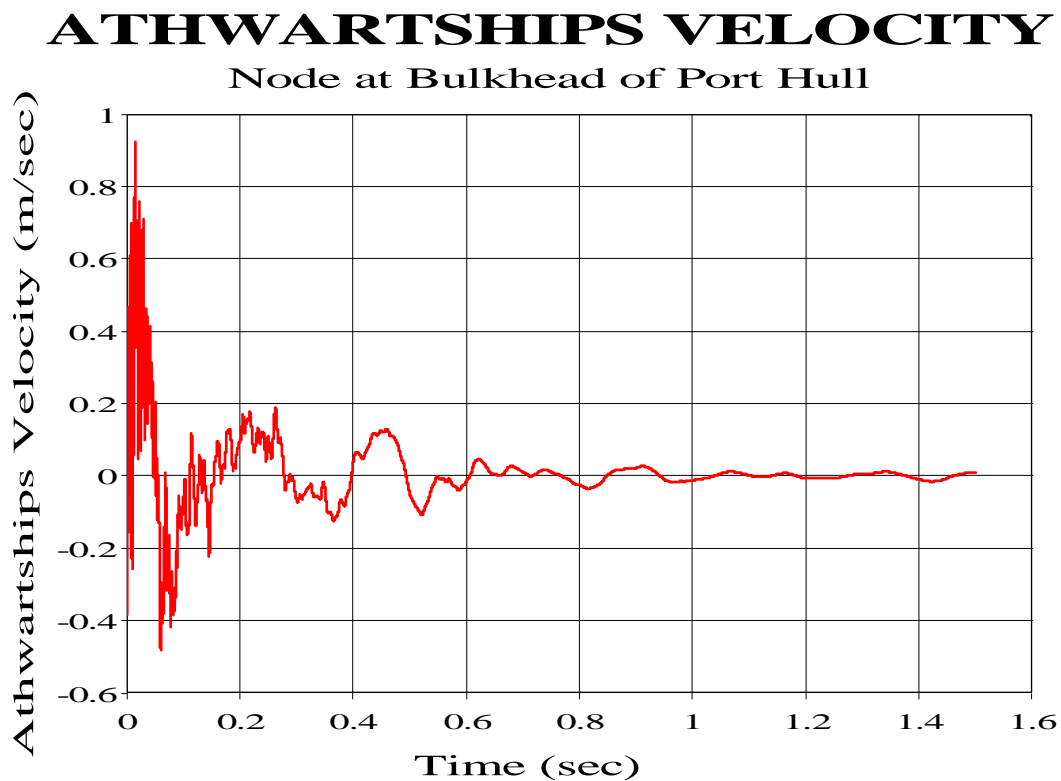
Figure 62.   Athwartships Velocity History of Node 17409

78

Figure 63.   Trimmed Athwartships Velocity History of Node 17409

As shown from Figure 63, the node first gets the negative values that represent the values in the same direction of the shock wave based on the coordinate system of the model, as expected. Then, it reaches the equilibrium point and exhibits positive velocity values that represent the values in the opposite direction of the shock wave.

Node 17409 exhibits very high frequency oscillations at an early time. After time 0.14 msec, the node tends to fluctuate with a lower frequency and damp. The peak athwartships velocity value is 54% lower than that of the peak vertical velocity.

The longitudinal response of Node 17409 is shown in Figure 64. The peak longitudinal velocity of Node 17409 is 0.4133 m/sec corresponding to time 15.9281 msec.
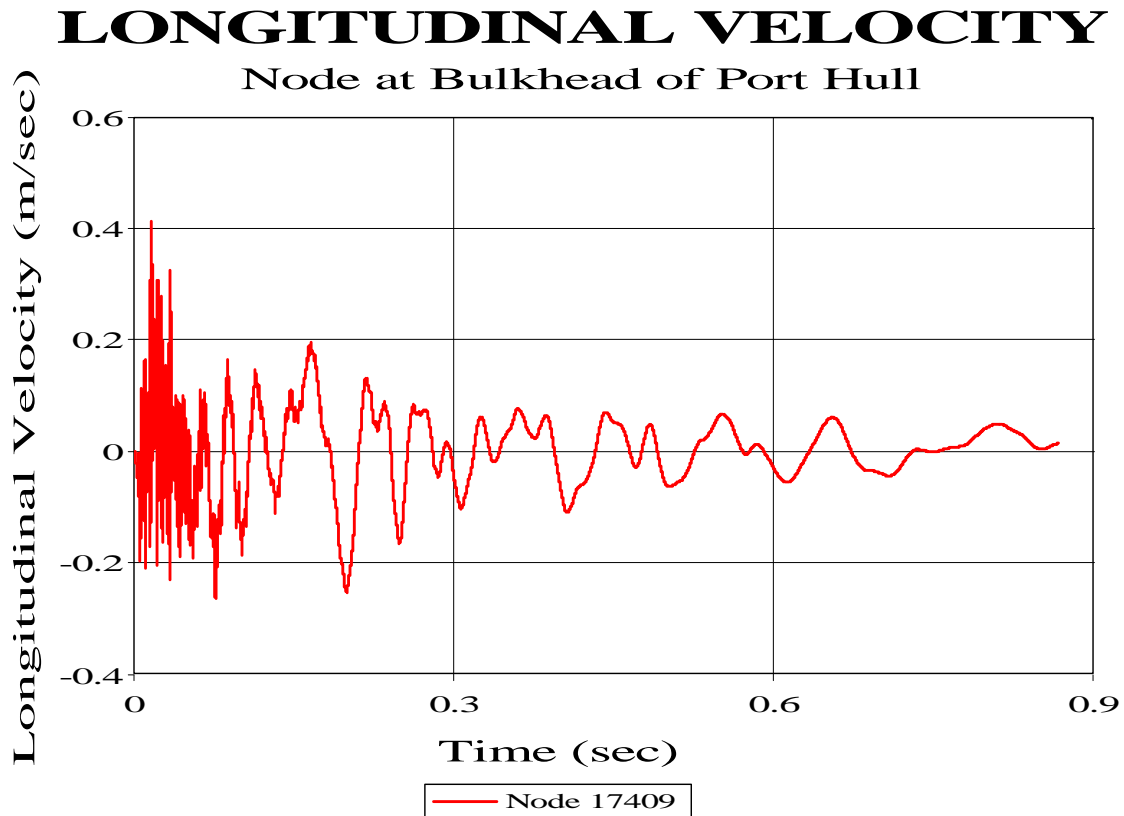
Figure 64.   Longitudinal Velocity History of Node 17409

As shown from Figure 64, the node first gets the negative values that represent the values in the fore direction of the model depending on the coordinate system of the model. Then, it reaches the equilibrium point and exhibits positive velocity values that represent the values in the aft direction of the model.

According to the responses of Node 17409 in all directions, it can be stated that they dampen out almost at the same time and exhibit a similar number of oscillations. The peak longitudinal velocity value is 79% lower than that of the peak vertical velocity.

The athwartships responses of the nodes at the port keel are shown in Figure 65 and the peak athwartships velocity values are tabulated in Table 21.
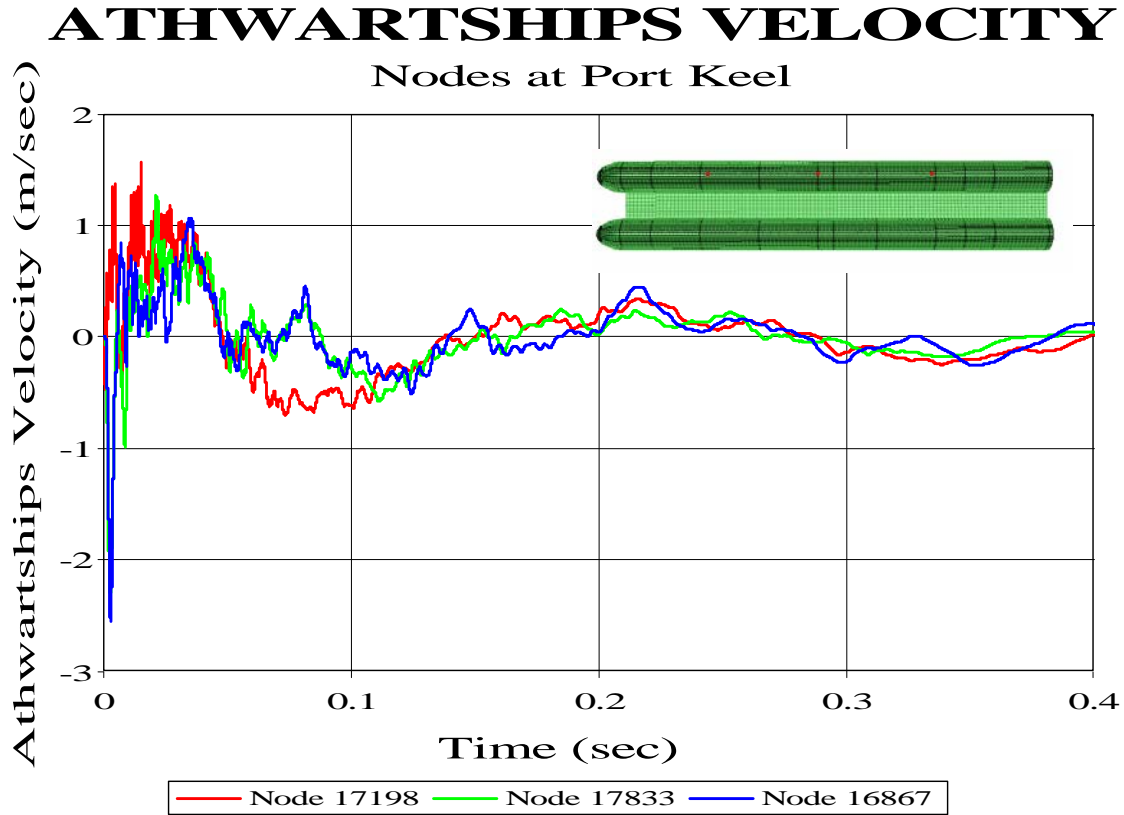
Figure 65.   Athwartships Velocity History of Keel Nodes

Table 21.   Peak Athwartships Velocity Value of Keel Nodes

	Peak Velocity (m/sec)	Time (msec)
Node 17198	1.56181	15.0485
Node 16867	1.06659	34.6506
Node 17833	1.26544	21.1943

Since the node amidships, Node 17198 is closer to the charge, it reaches its maximum vertical velocity before the other two nodes and exhibits high frequency oscillation whereas the other nodes exhibit low frequency oscillation, which is the same as the responses in the vertical direction.

Nodes 16867 and 17833 have approximately the same standoff distance, so they exhibit very similar behavior and dampen out almost at the same time. According to Table 21, the peak athwartships velocity values are approximately 52% lower than those of the peak vertical velocity. The longitudinal responses of the nodes at the port keel are shown in Figure 66 and the peak longitudinal velocity values are tabulated in Table 22.
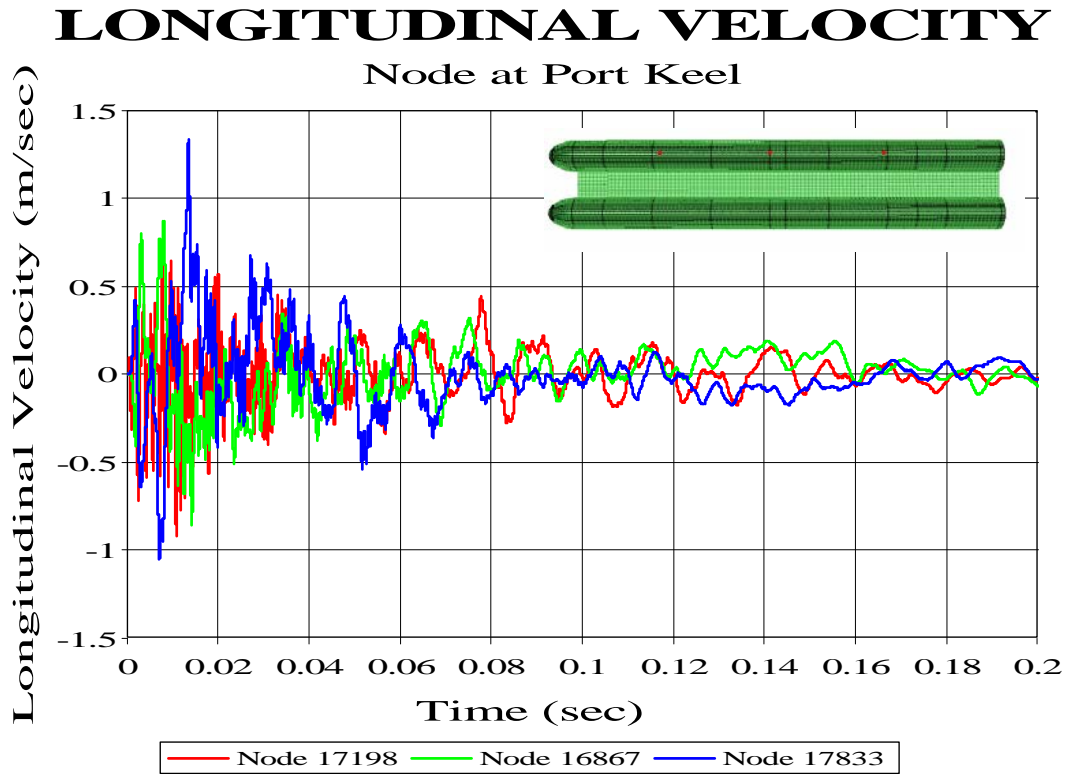
Figure 66. Longitudinal Velocity History of Keel Nodes

Table 22. Peak Longitudinal Velocity Values of Keel Nodes

	Peak Velocity (m/sec)	**Time (msec)**
Node 17198	-0.92106	10.7091
Node 16867	-0.85754	14.1221
Node 17833	1.33261	13.4016

The behavior of the nodes in the longitudinal direction is also similar to the behavior in the vertical and athwartships direction. Node 17198 exhibits the higher frequency oscillation and reaches the peak values first whereas the other nodes exhibit lower frequency oscillation due to the standoff distance. According to Table 22, the peak longitudinal velocity values are approximately 72% lower than those of the peak vertical velocity.

The athwartships response of Node 9851 which is at the main deck between the hulls is shown in Figure 67 and the peak athwartships velocity of Node 9851 was determined to be 0.3838 m/sec corresponding to time 26.3771 msec.

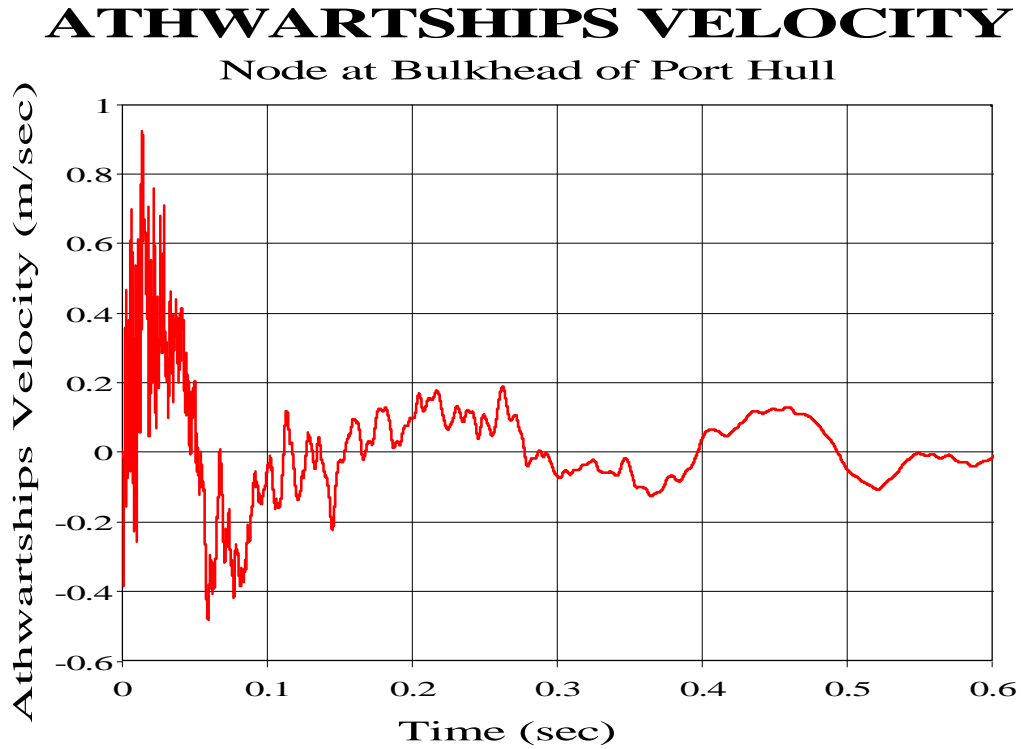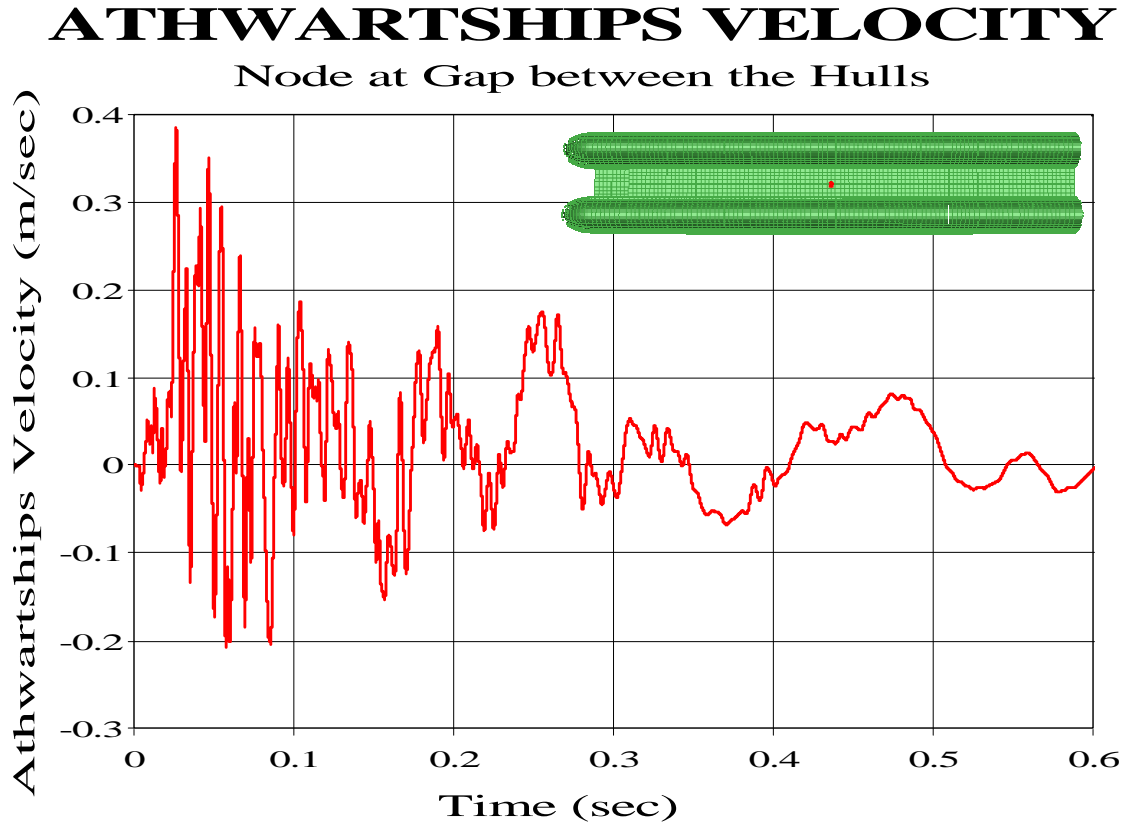**Figure 67.** Athwartships Velocity History of Node 9851

Since Node 9851 does not interact with the fluid mesh directly, it exhibits several oscillations with lower frequency and lower velocity, and settles down very slowly compared to other nodes. As shown from Figure 67, the node fluctuates with very small velocity at an early time. After time 25 msec, the node achieves higher velocity and starts to oscillate. This is due to the fact that the response of Node 9851 depends on the connected structural nodes. Therefore, it exhibits the peak values at a later time.

It can be stated that the behavior in this direction is very similar to the behavior in the vertical direction, but the peak athwartships velocity of Node 9851 was determined to be 0.3838 m/sec corresponding to time 26.3771 msec, which is 56% lower than the peak vertical velocity. The longitudinal response of Node 9851 is shown in Figure 68.

83
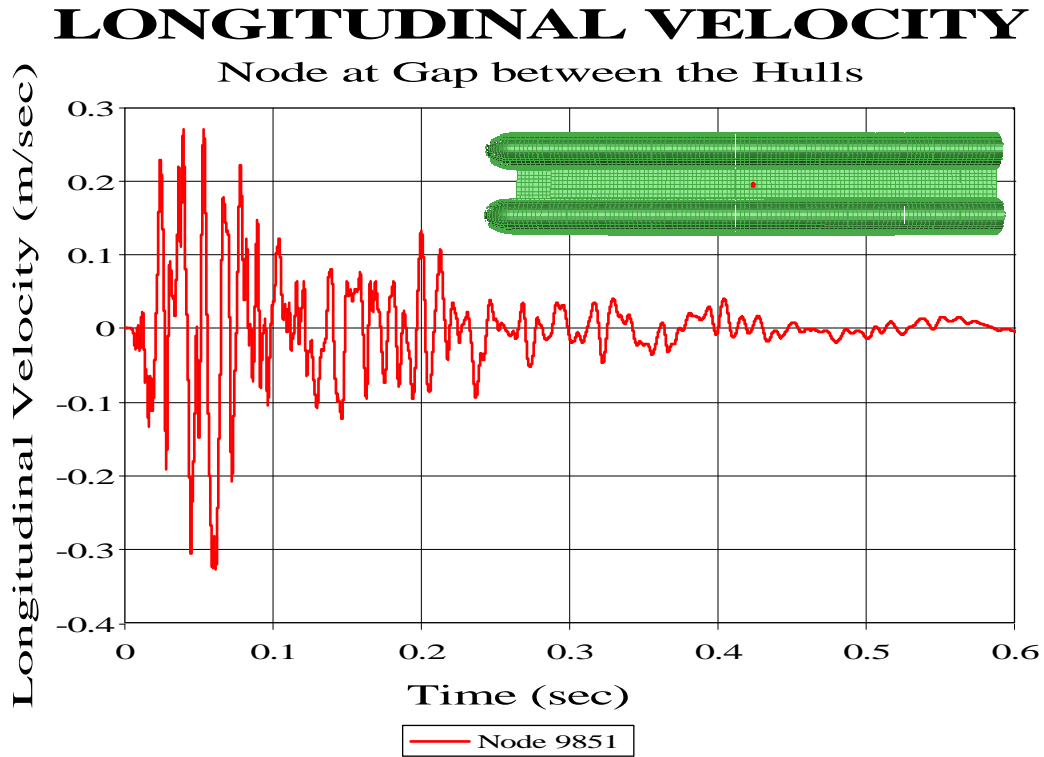
Figure 68. Longitudinal Velocity History of Node 9851

As shown from Figure 68, Node 9851 damps in the longitudinal direction earlier than it does in the other directions and the peak longitudinal velocity value, 0.2722 m/sec, is 69% lower than that of the peak vertical velocity.

According to the velocity history of all 14 nodes, the longitudinal response is 60% and the athwartships response is 48% lower than the vertical response. As a consequence, the vertical response is dominant to the responses in other directions as it was also determined to be the dominant response in previous monohull ship simulations. Because of the determined fact, the vertical response was of considerable interest. Even though the vertical response is dominant, the longitudinal and athwartships responses greatly depend on the geometry of attack.

D.   SHOCK SPECTRA ANALYSIS

The shock spectrum is the peak absolute response of undamped single degree-of-freedom produced by a shock loading with respect to the natural frequency. It is assumed that the shock pulse is applied as a common base input. The peak value of the response is selected from determined response time history. Then, the peak response values over a range of frequencies are determined by varying the natural frequency and shock spectra is formed. [Ref. 10] A shock spectrum is simply a graph of maximum response versus frequency. Since the vertical velocity was dominant as explained in previous sections, then the vertical time history of the nodes was used as the input in this thesis.

Evaluating the data presented in the shock spectra plot is essential for understanding the physical behavior of an UNDEX event. Since the shock spectra reduce the complexity to a simple measure, it is easier to compare the response in the frequency domain than in the time domain, especially at lower natural frequencies of the structure. There is also no need to consider a wide range of velocity values since the shock spectra are generated in terms of velocity and thus, just considering the frequency range will be enough. Consequently, the shock spectrum is a useful tool for easily estimating the damage potential of a shock pulse.

In the shock spectra plot, both axes are in logarithmic scale. The y-axis is called "Pseudo Velocity" instead of vertical velocity because all quantities, determined by using a single degree of freedom system, are exact only if the peak responses occur after the shock pulse has passed. The diagonal and off-diagonal axes indicate the absolute relative displacement and acceleration. In order to read the absolute relative acceleration and displacement response at a desired frequency, the point at the intersection of the curve and frequency should follow the diagonal axis and off–diagonal axis, respectively. The values of the relative displacement and acceleration are shown in logarithmic scale at the top and right sides of the plot.

UERD Tools, which is capable of generating shock spectra practically, was used in order to create the shock spectra plots of the Sea TENTACLE model.

1. Shock Spectra Plots of SHOT-1

Shock spectra of port side nodes subjected to SHOT-1, shown in Figure 69, were generated by averaging the shock spectra of all 15 nodes at the port side of the model. Similarly, shock spectra of starboard side and main deck between the hulls were generated by averaging the response of all 13 and 5 nodes, respectively. The plots are shown in Figure 70 and 71. Maximum pseudo velocity values of the model and corresponding frequencies are tabulated in Table 23.

According to the figures, the frequency range 1-5 Hz can be defined as the fundamental frequency that corresponds to the hull response. The frequency range between 5-50 Hz is essential for mechanical equipment such as engines, pumps, and auxiliary mechanical systems whereas the frequency higher than 100 Hz is essential for electrical equipments such as radar, sonar and control systems.

Shock spectra of all three decks exhibit gradually rise in amplitude without oscillations up to 5 Hz which is defined as the fundamental frequency. As the frequency increases, the shock spectra plots of starboard and port sides display rise in amplitude with some oscillations while the shock spectra of the deck between the hulls exhibit oscillations between 1 and 2 m/sec amplitude. Above 40 Hz, the responses of the starboard and port sides tend to fluctuate much more and the peak pseudo velocity values occur, which was also encountered at the previous simulation of the monohull ships. As far as the shock spectra of the deck between the hulls are concerned, the peak values occur between 10 and 40 Hz. Generally, it can be stated that the peak values occur at the intermediate level of frequency for the deck between the hulls whereas they occur at the high level of frequency for the port and starboard sides.

SHOCK SPECTRA
Port Side
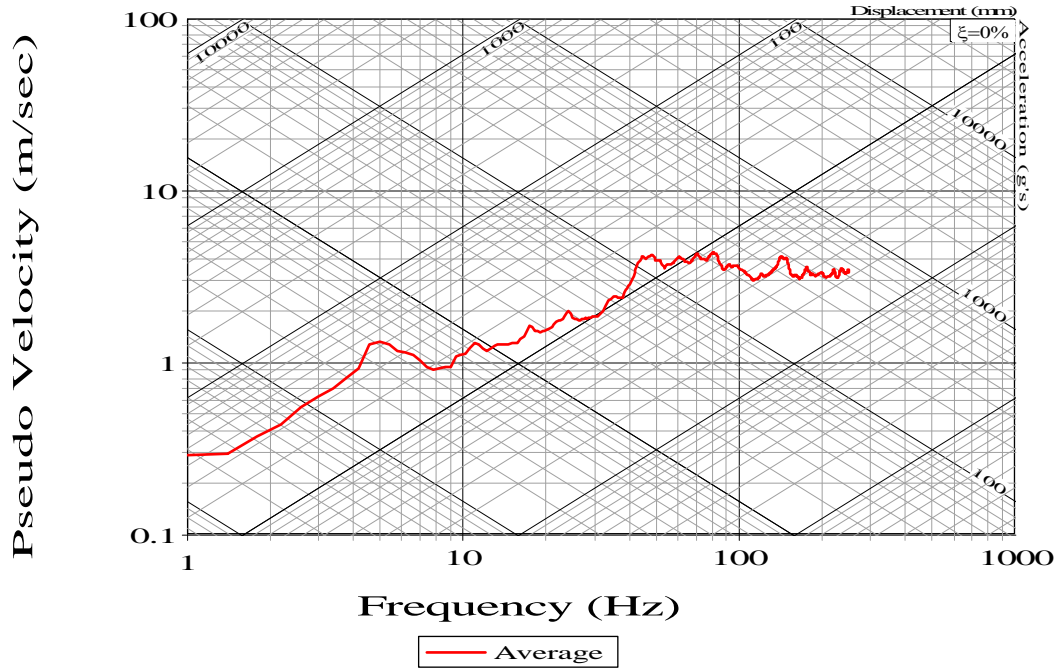
Figure 69. Averaged Shock Spectra of Port Side (SHOT-1)

SHOCK SPECTRA
Starboard Side
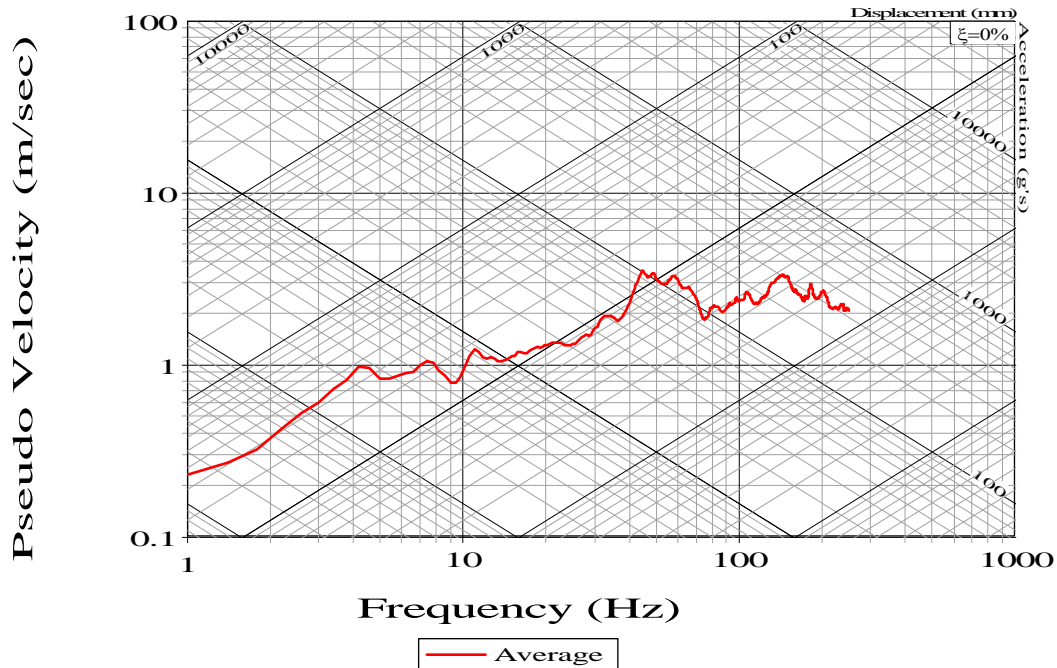
Figure 70. Averaged Shock Spectra of Starboard Side (SHOT-1)

SHOCK SPECTRA

Gap Between the Hulls
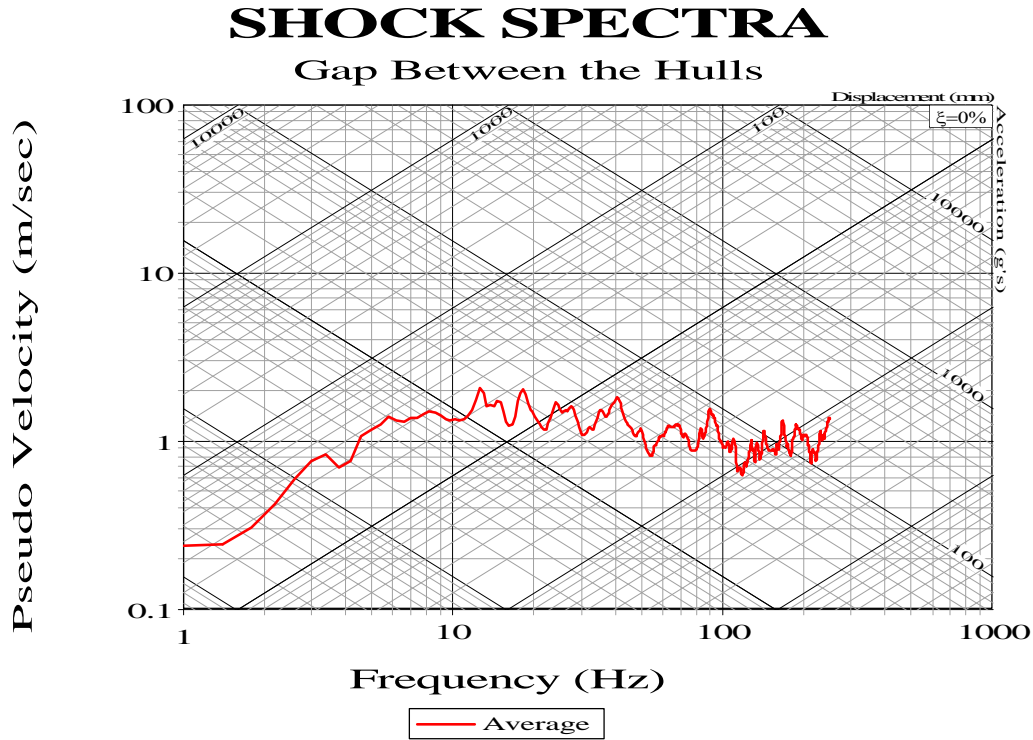
Figure 71. Averaged Shock Spectra of Deck Between the Hulls (SHOT-1)

Table 23. Maximum Pseudo Velocity Values of Model Subjected to SHOT-1

	MAXIMUM PSEUDO VELOCITY (m/sec)	CORRESPONDING FREQUENCY (Hz)
Port Side	4.326	48
Starboard Side	3.541	45
Deck between the Hulls	2.045	18

2.   Shock Spectra Plots of SHOT-2

Shock spectra of port side nodes subjected to SHOT-2, shown in Figure 72, were generated by averaging the shock spectra of all 15 nodes at the port side of the model. Similarly, shock spectra of starboard side and main deck between the hulls were generated by averaging the response of all 13 and 5 nodes, respectively. The plots are shown in Figure 73 and 74. Maximum pseudo velocity values of the model and corresponding frequencies are tabulated in Table 24.

SHOCK SPECTRA
Port Side
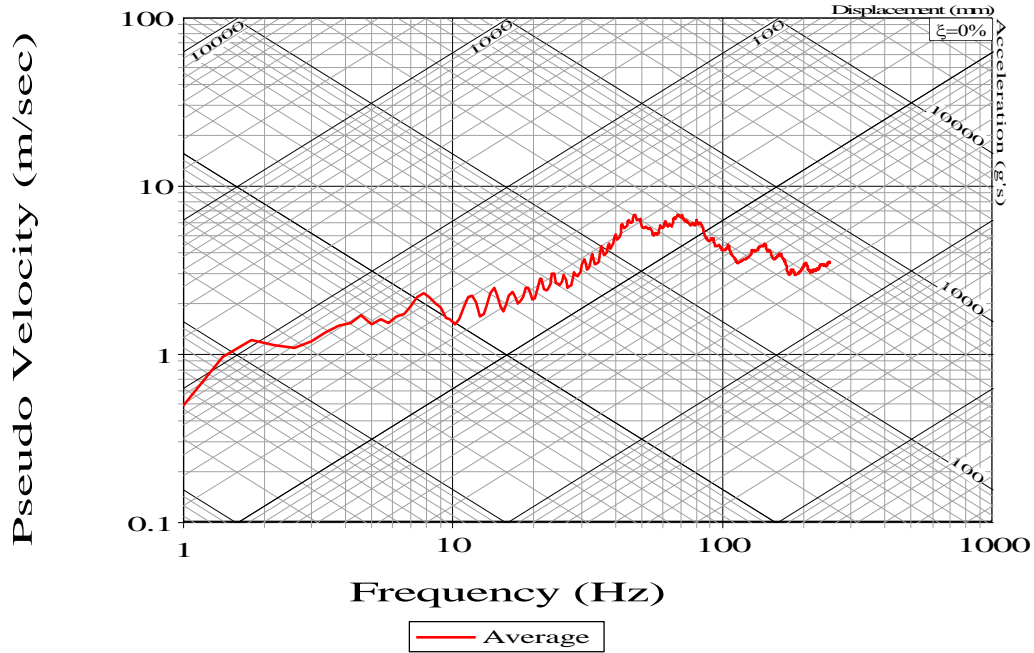
Figure 72. Averaged Shock Spectra of Port Side (SHOT-2)

SHOCK SPECTRA
Starboard Side
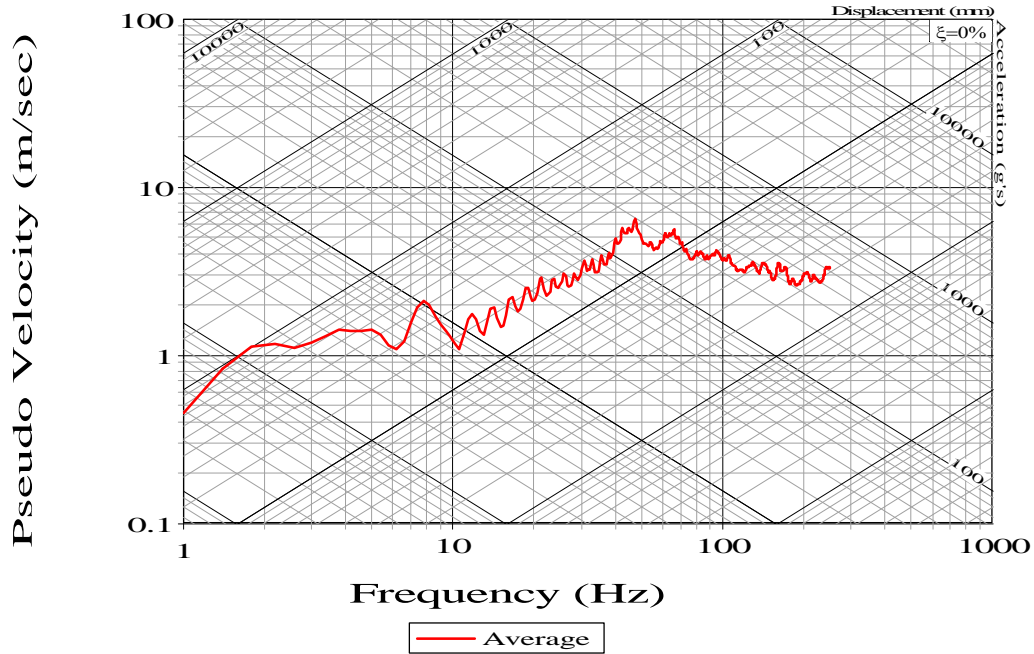
Figure 73. Averaged Shock Spectra of Starboard Side (SHOT-2)

SHOCK SPECTRA

Deck Between the Hulls
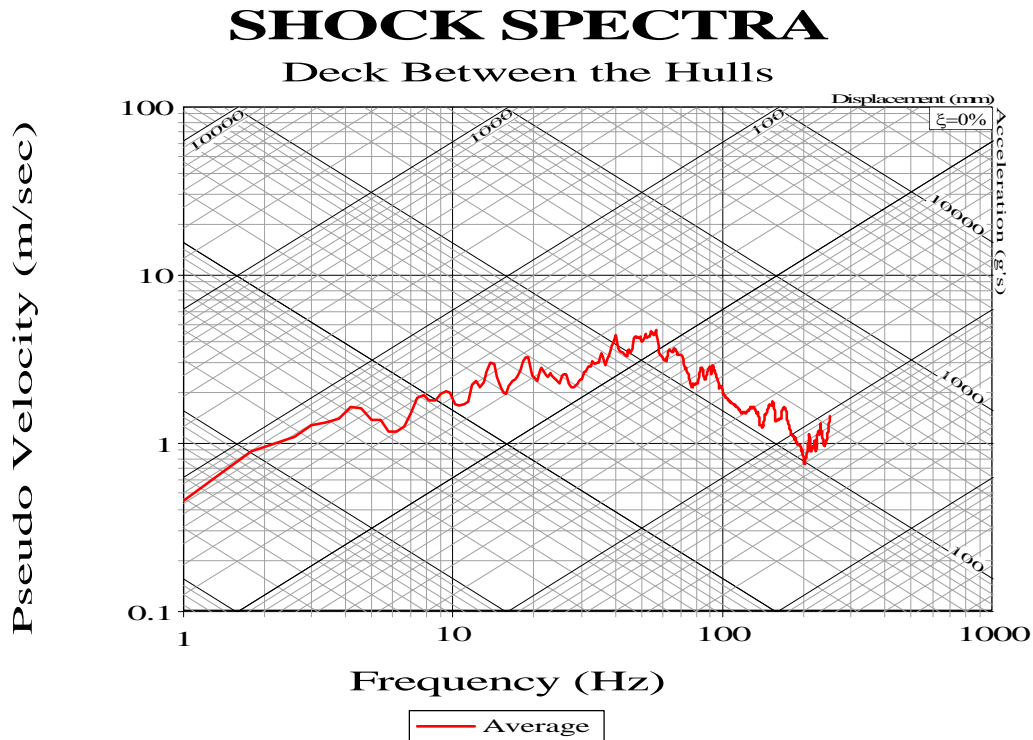
Figure 74. Averaged Shock Spectra of Deck Between the Hulls (SHOT-2)

Table 24. Maximum Pseudo Velocity Values of Model Subjected to SHOT-2

	MAXIMUM PSEUDO VELOCITY (m/sec)	CORRESPONDING FREQUENCY (Hz)
Port Side	6.748	48
Starboard Side	6.405	48
Deck between the Hulls	4.652	56

According to the shock spectra plots of the model subjected to SHOT-2, the peak values occur between 40 Hz and 70 Hz with higher frequency oscillations compared to SHOT-1 results, as expected. Above 70 Hz, the shock spectra plots display a downward trend, which was also encountered during previous simulations of the monohull ships. Generally, it can be stated that the peak values occur at the high level of frequency for the deck between the hulls, the port and starboard sides.

90

VI. CONCLUSION AND RECOMMENDATIONS

This thesis investigated the computer modeling and simulation of a catamaran-hull ship subjected to an underwater explosion. The shock simulation of Sea TENTACLE, the 2005 TSSE interdisciplinary team design, was executed using ABAQUS finite element solver. Of particular concern in this thesis was the effect of the gap between the hulls, which was not coupled with fluid mesh, on the response of the model. Two shots were generated and presented in order to analyze the ship's response to underwater explosions with different attack geometries. Time histories and shock spectra plots of selected nodes were also presented.

From this study, it was determined that the kick-off velocities and cut-off times obtained from the simulation in ABAQUS correspond well with the calculated values. The simulation also introduced a smooth gas bubble time history that matches with the theoretical Geers-Hunter bubble model.

As far as the response of the deck between the hulls is concerned, it was observed that it exhibited several irregular low frequency oscillations and settled down very slowly. Since the incident shock wave did not interact with the deck directly, the response of the deck was dependent on the responses of the connected port and starboard sides.

For both shots the port hull, which was closer to the charge, behaved like the well-studied monohull ship. The starboard hull can be defined as a secondary hull which received an additional impact from the deck in additional to the direct shock from the wetted surface. It showed similar behavior to port hull but with a distinct time shift. The similar response of both hulls was evident in the time history and shock spectra plots.

Additionally, this study examined the role of the responses in different directions. According to the time history of selected nodes, it was determined that the longitudinal response was 60% and the athwartships response was 48% lower than the vertical response. Thus, it can be stated that the vertical response is also dominant in catamaran hull ships' response.

Recommendations for areas of additional study:

1. In order to increase accuracy of the response, modeling the surrounding fluid with a more homogenous hexahedral element mesh is suggested in place of the tetrahedral fluid mesh used herein. In order to achieve this, the fluid geometry should be carefully partitioned before meshing.

2. To fully evaluate the results of the simulation, the simulated responses should be compared with the results from the shock trial of the actual ship. Since the Sea TENTACLE model is not an actual ship, the comparison with the results of the shock trial of a similarly sized catamaran hull ship is recommended.

3. This thesis investigated the far field UNDEX, so the bottom reflection was not taken into consideration. In shallow water reflection of the incident shock wave off the sea bottom cannot be neglected. Therefore, it is recommended that the shock simulation of the Sea TENTACLE model in shallow waters should be conducted.

APPENDIX A. MATLAB PROGRAM CODE FOR BULK CAVITATION ZONE

The following MATLAB code was written using MATLAB® 6.5 Release 13. This code calculates the bulk cavitation zone boundaries and plots a visualization of the bulk cavitation region depending on the user's input. For different aspects of comparison, the user can select the analysis type first, as shown in Figure 75. According to the analysis type, the user has several options to select the charge type, the charge weight, the charge depth, and the vertical and horizontal distances of interest.

This program was used to calculate the bulk cavitation zone for the Sea TENTACLE model.
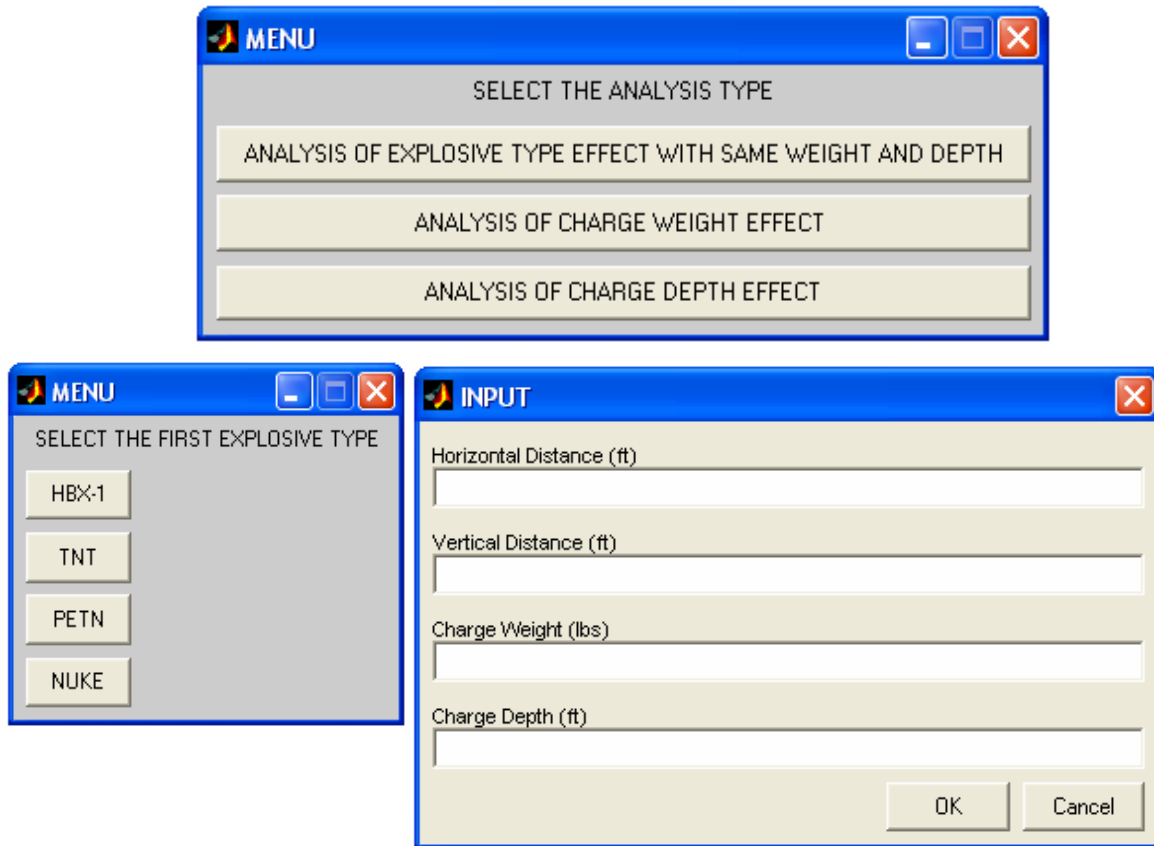
Figure 75.   MATLAB Program Interfaces

```matlab
% cav_zone.m by Hakan UCAR Ltjg., Turkish Navy
% Determining the bulk cavitation
% VARIABLES: W         : Charge weight
%            D         : Charge depth
%            r1        : Radial standoff distance
%            r2        : Image radial standoff distance
%            P1        : Incident pressure at cut-off
%            P2        : Image pressure at cut-off
%            Pa        : Atmospheric pressure
%            Pd        : Hydrostatic pressure
%            theta     : Decay rate constant

clc; clear all;
m=menu(' SELECT THE ANALYSIS TYPE ','ANALYSIS OF EXPLOSIVE TYPE EFFECT
WITH  SAME  WEIGHT  AND  DEPTH','ANALYSIS  OF  CHARGE  WEIGHT  EFFECT
','ANALYSIS OF CHARGE DEPTH EFFECT')
if m == 1;
    n1=menu('     SELECT     THE     FIRST     EXPLOSIVE     TYPE     ','HBX-
1','TNT','PETN','NUKE');
    n2=menu('     SELECT     THE     SECOND     EXPLOSIVE     TYPE     ','HBX-
1','TNT','PETN','NUKE');

    if n1 == 1
        K1 = 22347.6;   % Pmax coefficient
        A1 = 1.144;     % Pmax coefficient
        K2 = 0.056;     % Decay constant coefficient
        A2 = -0.247;    % Decay constant coefficient
        charge='HBX-1';
    end
    if n1 == 2
        K1 = 22505;
        A1 = 1.18;
        K2 = 0.058;
        A2 = -0.185;
        charge='TNT';
    end
    if n1 == 3
        K1 = 24589;
        A1 = 1.194;
        K2 = 0.052;
        A2 = -0.257;
        charge='PETN';
    end
    if n1 == 4
        K1 = 4.38E+06;
        A1 = 1.18;
        K2 = 2.274;
        A2 = -0.22;
        charge='NUKE';
    end
    data   = { 'Horizontal Distance (ft)',...
            'Vertical Distance (ft) ',...
            'Charge Weight (lbs)',...
            'Charge Depth (ft)'};
    input_data = inputdlg(data,'INPUT',1);
```

94

```
    H = str2num(char(input_data(1)));
    V = str2num(char(input_data(2)));
    W = str2num(char(input_data(3)));
    D = str2num(char(input_data(4)));

    depth=zeros(V,H);
    c=5.078;
    i=0;
    for y=1:(V+1)
        for x=1:(H+1)
            r1=sqrt((D - (y-1))^2 + (x-1)^2);
            r2=sqrt((D + (y-1))^2 + (x-1)^2);
            theta = K2*(W^(1/3))*(((W^(1/3))/r1)^(A2));
            P1=(K1*(W^(1/3)/r1)^(A1))*(exp(-(r2 -r1)/(c*theta)));
            Pa=14.7;
            Pd=0.4443680556*(y-1);
            P2=-(K1*((W^(1/3)/r2)^(A1)));
            % Upper boundary
            F = P1 + Pa + Pd + P2;
            g1=-P1/(c*theta)*(1 + (((r2 - 2*D*((D+(y-1))/r2))/r1)
*((A2*r2/r1)-A2-1)));
            g2=-(A1*P1/r1^2)*(r2-2*D*((D+y-1)/r2));
            g3=(0.4443680556*((D+y-1)/r2));
            g4=((A1/r2)*(P1+Pa+Pd));
            % Lower boundary
            G = g1+g2+g3+g4;

            if F < 0 & G < 0;
                depth(y,x)=1;
            end
        end
    end
     figure(1)
     subplot(2,1,1)
     imagesc(depth)
     title(['CAVITATION  REGIONS  FOR  ',num2str(W),'  lb  ',charge,'  AT
',num2str(D),' ft '])
     ylabel('Depth (ft)')
     axis equal
     axis([0 H 0 V])
     hold on;

    if n2 == 1
       K1 = 22347.6;
       A1 = 1.144;
       K2 = 0.056;
       A2 = -0.247;
       charge='HBX-1';
    end
    if n2 == 2
       K1 = 22505;
       A1 = 1.18;
       K2 = 0.058;
       A2 = -0.185;
       charge='TNT';
    end
    if n2 == 3
```

```
      K1 = 24589;
      A1 = 1.194;
      K2 = 0.052;
      A2 = -0.257;
      charge='PETN';
   end
   if n2 == 4
      K1 = 4380000;
      A1 = 1.18;
      K2 = 2.274;
      A2 = -0.22;
      charge='NUKE';
   end

   depth2=zeros(V,H);
   c=5.078;
   for y=1:(V+1)
       for x=1:(H+1)
           r1=sqrt((D - (y-1))^2 + (x-1)^2);
           r2=sqrt((D + (y-1))^2 + (x-1)^2);
           theta = K2*(W^(1/3))*(((W^(1/3))/r1)^(A2));
           P1=(K1*(W^(1/3)/r1)^(A1))*(exp(-(r2 -r1)/(c*theta)));
           Pa=14.7;
           Pd=0.4443680556*(y-1);
           P2=-(K1*((W^(1/3)/r2)^(A1)));
           F = P1 + Pa + Pd + P2;
           g1=-P1/(c*theta)*(1 + (((r2-2*D*((D+(y-1))/r2))/r1)* ((A2*
r2/r1)-A2-1)));
           g2=-(A1*P1/r1^2)*(r2-2*D*((D+y-1)/r2));
           g3=(0.4443680556*((D+y-1)/r2));
           g4=((A1/r2)*(P1+Pa+Pd));
           G = g1+g2+g3+g4;

           if F < 0 & G < 0;
               depth2(y,x)=1;
           end
       end
   end

    figure(1)
    subplot(2,1,2)
    imagesc(depth2)
    title(['CAVITATION  REGIONS  FOR  ',num2str(W),'  lb  ',charge,'  AT
',num2str(D),' ft '])
    xlabel(' RED REGION IS CAVITATION REGION ')
    ylabel('Depth (ft)')
    axis equal
    axis([0 H 0 V])
    hold on;
end

if m == 2;
n=menu(' SELECT THE EXPLOSIVE TYPE ','HBX-1','TNT','PETN','NUKE');
if n == 1
    K1 = 22347.6;
    A1 = 1.144;
    K2 = 0.056;
```

```
    A2 = -0.247;
    charge='HBX-1';
end
if n == 2
    K1 = 22505;
    A1 = 1.18;
    K2 = 0.058;
    A2 = -0.185;
    charge='TNT';
end
if n == 3
    K1 = 24589;
    A1 = 1.194;
    K2 = 0.052;
    A2 = -0.257;
    charge='PETN';
end
if n == 4
    K1 = 4.38E+06;
    A1 = 1.18;
    K2 = 2.274;
    A2 = -0.22;
    charge='NUKE';
end
data  = { 'Horizontal Distance (ft)',...
          'Vertical Distance (ft) ',...
          'Charge Weight-I (lbs)',...
          'Charge Weight-II (lbs)',...
          'Charge Weight-III (lbs)',...
          'Charge Depth (ft)'};
input_data = inputdlg(data,'INPUT',1);
H = str2num(char(input_data(1)));
V = str2num(char(input_data(2)));
W1 = str2num(char(input_data(3)));
W2 = str2num(char(input_data(4)));
W3 = str2num(char(input_data(5)));
D = str2num(char(input_data(6)));

depth=zeros(V,H);
c=5.078;
i=0;
j=0;
Gamma = 63.989/144;
    for W=[W1 W2 W3]
        i=i+1;
        for y=1:(V+1)
            for x=1:(H+1)
                r1=sqrt((D - (y-1))^2 + (x-1)^2);
                r2=sqrt((D + (y-1))^2 + (x-1)^2);
                theta = K2*(W^(1/3))*(((W^(1/3))/r1)^(A2));
                P1=(K1*(W^(1/3)/r1)^(A1))*(exp(-(r2 -r1)/(c*theta)));
                Pa=14.7;
                Pd=0.4443680556*(y-1);
                P2=-(K1*((W^(1/3)/r2)^(A1)));
                F = P1 + Pa + Pd + P2;
                g1=-P1/(c*theta)*(1 + (((r2 - 2*D*((D+(y-1))/r2))/r1)
*((A2*r2/r1)-A2-1)));
```

```matlab
                g2=-(A1*P1/r1^2)*(r2-2*D*((D+y-1)/r2));
                g3=(0.4443680556*((D+y-1)/r2));
                g4=((A1/r2)*(P1+Pa+Pd));
                G = g1+g2+g3+g4;

                if F < 0 & G < 0;
                    depth(y,x)=1;
                end
            end
        end
        temp(:,:,i)=depth;
 end
     figure(1)
     subplot(3,1,1)
     imagesc(temp(:,:,1))
     title(['CAVITATION REGIONS FOR ',num2str(W1),' lb ',charge,' AT
',num2str(D),' ft '])
     ylabel('Depth (ft)')
     axis equal
     axis([0 H 0 V])

     subplot(3,1,2)
     imagesc(temp(:,:,2))
     title(['CAVITATION REGIONS FOR ',num2str(W2),' lb ',charge,' AT
',num2str(D),' ft '])
     ylabel('Depth (ft)')
     axis equal
     axis([0 H 0 V])

     subplot(3,1,3)
     imagesc(temp(:,:,3))
     title(['CAVITATION REGIONS FOR ',num2str(W3),' lb ',charge,' AT
',num2str(D),' ft '])
     ylabel('Depth (ft)')
     xlabel(' RED REGION IS CAVITATION REGION ')
     axis equal
     axis([0 H 0 V])
end

if m == 3;
    n=menu(' SELECT THE EXPLOSIVE TYPE ','HBX-1','TNT','PETN','NUKE');

    if n == 1
       K1 = 22347.6;
       A1 = 1.144;
       K2 = 0.056;
       A2 = -0.247;
       charge='HBX-1';
    end
    if n == 2
       K1 = 22505;
       A1 = 1.18;
       K2 = 0.058;
       A2 = -0.185;
       charge='TNT';
    end
    if n == 3
```

```matlab
    K1 = 24589;
    A1 = 1.194;
    K2 = 0.052;
    A2 = -0.257;
    charge='PETN';
end
if n == 4
    K1 = 4.38E+06;
    A1 = 1.18;
    K2 = 2.274;
    A2 = -0.22;
    charge='NUKE';
end
data    = { 'Horizontal Distance (ft)',...
            'Vertical Distance (ft) ',...
            'Charge Depth-I (ft)',...
            'Charge Depth-II (ft)',...
            'Charge Depth-III (ft)',...
            'Charge Weight (lbs)'};
input_data = inputdlg(data,'INPUT',1);
H = str2num(char(input_data(1)));
V = str2num(char(input_data(2)));
D1 = str2num(char(input_data(3)));
D2 = str2num(char(input_data(4)));
D3 = str2num(char(input_data(5)));
W = str2num(char(input_data(6)));
depth=zeros(V,H);
c=5.078;
i=0;

for D=[D1 D2 D3]
    i=i+1;
    for y=1:(V+1)
        for x=1:(H+1)
            r1=sqrt((D - (y-1))^2 + (x-1)^2);
            r2=sqrt((D + (y-1))^2 + (x-1)^2);
            theta = K2*(W^(1/3))*(((W^(1/3))/r1)^(A2));
            P1=(K1*(W^(1/3)/r1)^(A1))*(exp(-(r2 -r1)/(c*theta)));
            Pa=14.7;
            Pd=0.4443680556*(y-1);
            P2=-(K1*((W^(1/3)/r2)^(A1)));
            F = P1 + Pa + Pd + P2;
            g1=-P1/(c*theta)*(1 + (((r2 - 2*D*((D+(y-1))/r2))/r1)
*((A2*r2/r1)-A2-1)));
            g2=-(A1*P1/r1^2)*(r2-2*D*((D+y-1)/r2));
            g3=(0.4443680556*((D+y-1)/r2));
            g4=((A1/r2)*(P1+Pa+Pd));
            G = g1+g2+g3+g4;

            if F < 0 & G < 0;
                depth(y,x)=1;
            end
        end
    end
    temp(:,:,i)=depth;
end
figure(1)
```
99

```
    subplot(3,1,1)
    imagesc(temp(:,:,1))
    title(['CAVITATION  REGIONS  FOR  ',num2str(W),'  lb  ',charge,'  AT
',num2str(D1),' ft '])
    ylabel('Depth (ft)')
    axis equal
    axis([0 H 0 V])

    subplot(3,1,2)
    imagesc(temp(:,:,2))
    title(['CAVITATION  REGIONS  FOR  ',num2str(W),'  lb  ',charge,'  AT
',num2str(D2),' ft '])
    ylabel('Depth (ft)')
    axis equal
    axis([0 H 0 V])

    subplot(3,1,3)
    imagesc(temp(:,:,3))
    title(['CAVITATION  REGIONS  FOR  ',num2str(W),'  lb  ',charge,'  AT
',num2str(D3),' ft '])
    ylabel('Depth (ft)')
    xlabel(' RED REGION IS CAVITATION REGION ')
    axis equal
    axis([0 H 0 V])
end
```

APPENDIX B.   STRUCTURAL MODELING OF SEA TENTACLE MODEL USING TRUEGRID

This appendix covers the detailed process for creating the structural finite element mesh of the Sea TENTACLE model by using TrueGrid's part feature **BLOCK** command and **PROJECTION** method that projects the nodes onto the surface.

The **BLOCK** command, which is used in part phase, is the standard way to generate parts in TrueGrid. By using the **PROJECTION** command, TrueGrid automatically places the edges of the block along intersections of the surfaces and the corners at the intersection of the surfaces. The intent of this appendix is not to serve as a tutorial since the familiarity of the code is assumed. Additional information can be found in the TrueGrid user manual [Ref. 21].

The part generation procedure is described as follows. The important commands and menu selections are denoted in bold and in all capital letters for emphasis.

1. The **IGES** command is used to import the geometry in the ASCII IGES file. The structural geometry that was created in RHINO 3.0 was imported as an IGES file (CatHakanWithNewFront2.igs) by using this command.

2. The **ABAQMATS** command is used to specify the material model in TrueGrid. This command can be used in the TrueGrid code file before each element type --such as beam, shell and solid elements-- has been created. Two ABAQUS material were defined in the model, one for the beam elements and the other for the shell elements. The specifications of the elements --such as the density, the modulus of the elasticity and Poisson's ratio-- were entered by using this command.

3. In the **PARTS** phase, the **BLOCK** command is used to create the parts. These blocks are the main parts of the structural mesh. The block part is defined by a list of integers (logical mesh) and coordinates (physical mesh). Six lists of numbers follow the **BLOCK** command. The first three lists are lists of indices (i, j and k). The first list of integers must start with 1 or -1. The integers that follow must be zero or have an absolute value greater than the absolute values of the integers that preceded them in that list. These numbers tell TrueGrid the number of nodes to be created in the first dimension of the computational mesh. A positive integer indicates that there will be a partition at that nodal index in the first dimension of the computational mesh. These partitions are used to break the part into multiple structured blocks. When positive integers are used, solid elements are created. A negative integer in the list also produces a partition in the mesh with a nodal index corresponding to the absolute value of the

integer, with shell elements created along that partition in the computational mesh. The second list is the lists of values of physical coordinates (x, y, and z coordinate) which indicate the location of the part. 18 blocks were created with shell elements in the Sea TENTACLE model.

4. The **MATE** command is used to assign the material number, which is defined by **ABAQMATS** command, for the whole part or the beam elements. The material assignment can be overwritten by other commands (**MT**, **MTI**) for any combination of the regions of the part. The **MT** and **MTI** commands assign a material number to a region, overriding any previous material specifications.

5. The **THIC** command is used to set the thickness of a shell element. This command can be overwritten by another command, **THI** which is used to set the thickness of a shell element in a region of the part.

6. The **EDGE** command is used to distribute the nodes along an edge of a surface. An edge of the mesh and an edge of the surface must be selected before executing this command. This can be done interactively in TrueGrid. The edge identifier of the surfaces in the window can be viewed by clicking on the **Labels** and **Surf Edge** buttons in the environment window. By selecting the edge of the mesh and the surface edge identifier from the window, the command can be issued. In the Sea TENTACLE model, this command was used for the mesh generation of the hull, the bow and the platforms.

7. The **SFI** command, which is a projection command, is used to project the regions of the mesh onto a surface by index progression. Projection method is a powerful technique in TrueGrid. This method allows faces, edges and nodes of the mesh to be directly placed on surfaces. This method can be used interactively. A face of the mesh and a surface must be selected prior to the execution of the command. The surface identifier in the window can be viewed by clicking on the **Labels** and **Surface** buttons in the environment window. The projection can be executed by selecting the face of the mesh and the surface identifier from the window, and clicking the **PROJECT** button. In the Sea TENTACLE model, this command was used for the mesh generation of the hull, the bow and the platforms. Figure 76 shows the mesh of the hull of the model before the projection onto the surface and after the projection.
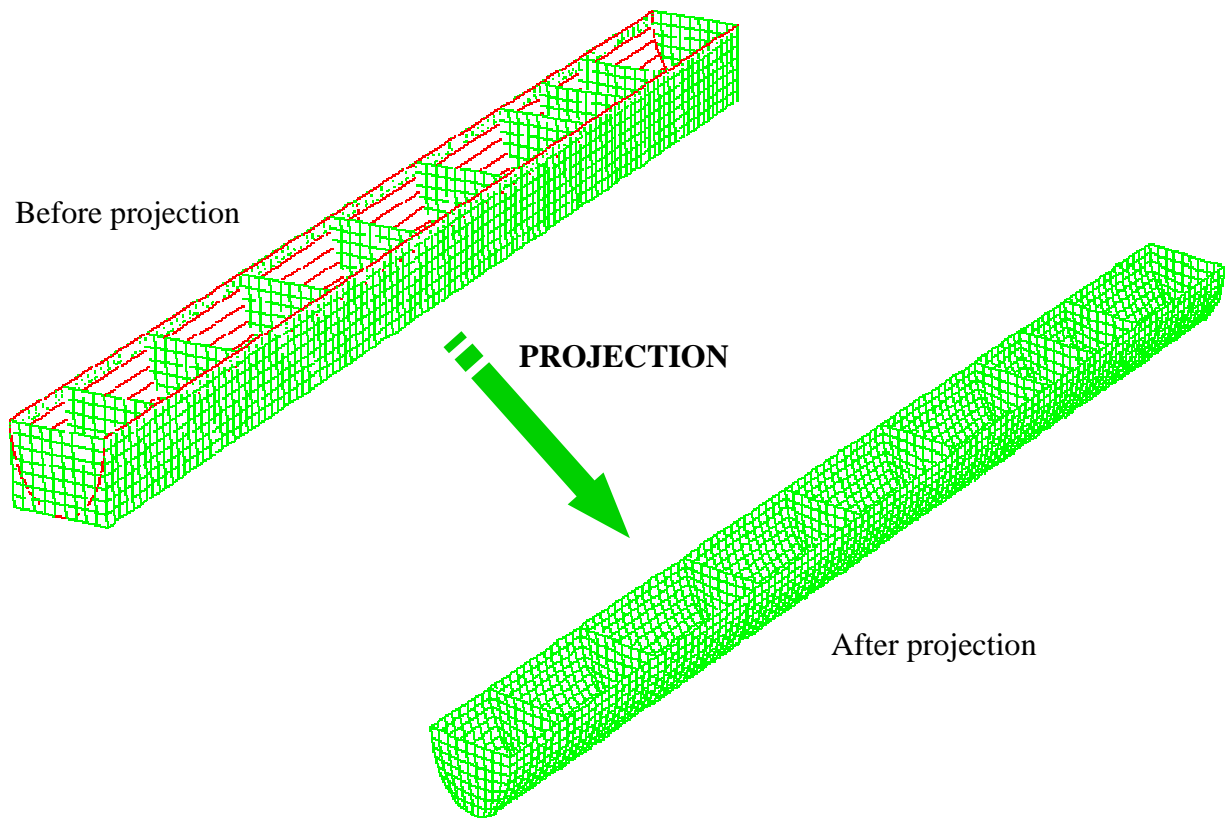
Before projection

PROJECTION

After projection

Figure 76.   The mesh generation of the hull by projection method

8.   The global beam cross-section definition **BSD** is used to define the specifications of the cross-section of the beam elements to be created. This command has several option lists. For the Sea TENTACLE model, the ABAQUS beams option having a rectangular cross-section was selected.

9.   **IBMI, JBMI** and **KBMI** are used to create the beam elements in the corresponding direction by index progression. This method of beam element generation extracts the needed nodes from an existing shell part and is a way to embed beam elements within a shell. This is only available in part phase. The orientation of the cross section axis is very important in the model. It is ensured by orienting the second axis of the cross-section. This can be accomplished in three different ways. The first way is orienting the second axis in the coordinate axis (i, j or k). The second way is orienting the second axis by an orientation vector and the last way is orienting the second axis in the normal to a desired surface. In the Sea TENTACLE model, the orientation of the beam elements is ensured by using orientation vectors. After the MERGE command, which will be explained later, the local axes of the beam elements can be displayed by using the **co or rst** command. During the generation of the beam elements, the orientation of the beam elements was ensured by using this command in the Sea TENTACLE model.

10. The **ZTOL** command causes each coordinate of each node, whose absolute value is less than given tolerance, to be set to zero prior to merging and prior to the generation of output. The value 0.0001 was used to tolerate the coordinate of each node.

11. The **MERGE** command causes the part to end, switches to the merge (assembly) phase and merges the individual parts together.

12. The **DELEM LBM** command is used to delete the beam elements in the mesh. In the Sea TENTACLE model, the beam elements at the intersection of the bulkheads and decks were deleted since the corners were not stiffened but welded.

13. The **FSET** command is used to create a face set. This can be created interactively by selecting the **SETS** button under the **PICK** option in the environment window. After selecting the **FACES** button, the face of the hull under the waterline can be picked interactively. The **HIDE** drawing mode should be used in order to pick only visible elements of the wetted surface and the four-node selection option should also be picked for easiness since it selects the four nodes of an element and groups as a set. If some elements that are not desired in the faceset are selected, they can be removed by selecting the **REMOVE** button and using the one-node selection option. After selecting the faces, the set must be named and saved. The wetted surface of the ship was grouped into a **FACESET** which was named as "hull". Creating a set for wetted surface of the ship is an important process for coupling the fluid and structural mesh. The coupling process will be explained in Appendix D.

14. The **OUTPUT** command is used to output the file to a desired format such as **ABAQUS, LS DYNA, NASTRAN**, etc. For the Sea TENTACLE model, first the **ABAQUS** output option and then the **WRITE** command was selected in order to output the file in ABAQUS format.

According to the procedure described above, the structural mesh was created. The TrueGrid code file for the construction of the structural mesh is shown as follows.

```
iges CatHakanWithNewFront2.igs 1 1 ;

c defining the ABAQUS material for beam elements
abaqmats 1 aqeltyp b3 aqdens 7850 aqelas aqelis 2.0684e+11 0.3 ; ; ;

c defining the ABAQUS material for shell elements
abaqmats 2 aqeltyp s aqdens 7850 aqelas aqelis 2.0684e+11 0.3 ; ; ;

bsd 1 cstype 11 abcs1 12e-3 abcs2 0.15;;
bsd 2 cstype 11 abcs1 14e-3 abcs2 0.15;;
c bridge

block -1 -26;
      -1 -16;
      -1 -7;
```

```
        -4.40 20.6
         20.3 35.3
         3 9
thic 0.014;
mate 2;
c along x-axis
 jbmi 1 2;1 2;1 2;26 2 1 v 1 0 0 1
c along z-axis
 jbmi 1 1;1 2;1 2;1 7 1 v 0 0 1 1;
 jbmi 2 2;1 2;1 2;1 7 1 v 0 0 1 1;
c along y-axis
 kbmi 1 2;1 2;1 2;2 16 1 v 0 1 0 1;
c along x-axis
 kbmi 1 2;1 2;1 2;26 2 1 v 1 0 0 1;
c along y-axis
 ibmi 1 2;1 2;1 2;16 2 1 v 0 1 0 1;
c along z-axis
 ibmi 1 2;1 1;1 2;1 7 1 v 0 0 1 1;
 ibmi 1 2;2 2;1 2;1 7 1 v 0 0 1 1;


c deck 1 (cic / radio)

block -1 -3 -4 -23 -24 -26;
      1 -16 -31;
      -1 -7;
      -4.4 -2.4 -1.4 17.6 18.6 20.6
      35.3 50.3 65.3
      3 9
thic 0.014;
mate 2;
c along x-axis
jbmi 1 6;1 3;1 2;26 2 1 v 1 0 0 1;
c along z-axis
jbmi 1 1;1 3;1 2;1 7 1 v 0 0 1 1;
jbmi 6 6;1 3;1 2;1 7 1 v 0 0 1 1;
c along y-axis
kbmi 1 6;1 3;1 2;2 31 1 v 0 1 0 1;
c along x-axis
kbmi 1 6;2 3;1 2;26 2 1 v 1 0 0 1;
c along y-axis
ibmi 1 6;1 3;1 2;31 2 1 v 0 1 0 1;
c along z-axis
ibmi 1 6;3 3;1 2;1 7 1 v 0 0 1 1;


c deck 1 (wr/cardio/helo)

block -1 -3 -4 -12 -15 -23 -24 -26;
      1 -16 -24;
      -1 -7;
      -4.4 -2.4 -1.4 6.6 9.6 17.6 18.6 20.6
      65.3 80.3 87.8
      3 9
thic 0.014;
mate 2;
c along x-axis
 jbmi 1 8;1 3;1 2;26 2 1 v 1 0 0 1;
c along z-axis
```

```
 jbmi 1 1;1 3;1 2;1 7 1 v 0 0 1 1;
 jbmi 8 8;1 3;1 2;1 7 1 v 0 0 1 1;
c along y-axis
 kbmi 1 8;1 3;1 2;2 24 1 v 0 1 0 1;
c along x-axis
 kbmi 1 8;2 3;1 2;26 2 1 v 1 0 0 1;
c along y-axis
 ibmi 1 8;1 3;1 2;24 2 1 v 0 1 0 1;
c along z-axis
 ibmi 1 8;3 3;1 2;1 7 1 v 0 0 1 1;

c main deck (anchor/chain)

block -1 -8 -14 -19 -26;
      -1 9;
      -1 -4;
      -4.4 2.6 8.1 13.6 20.6
       0 7.8
       0 3
thic 0.014;
mate 2;
c along x-axis
 jbmi 1 5;1 2;1 2;26 2 1 v 1 0 0 1;
c along z-axis
 jbmi 1 1;1 2;1 2;1 4 1 v 0 0 1 1;
 jbmi 5 5;1 2;1 2;1 4 1 v 0 0 1 1;
c along y-axis
 kbmi 1 5;1 2;1 2;2 9 1 v 0 1 0 1;
c along x-axis
 kbmi 1 5;1 1;1 2;26 1 1 v 1 0 0 1;
c along y-axis
 ibmi 1 5;1 2;1 2;9 2 1 v 0 1 0 1;
c along z-axis
 ibmi 1 5;1 1;1 2;1 4 1 v 0 0 1 1;
 ibmi 1 5;2 2;1 2;1 4 1 v 0 0 1 1;

c main deck (berthing)

block -1 -8 -10 -17 -19 -26;
      -1 14;
      -1 -4;
      -4.4 2.6 4.6 11.6 13.6 20.6
       7.8 20.3
       0 3
thic 0.014;
mate 2;
c along x-axis
 jbmi 1 6;1 2;1 2;26 2 1 v 1 0 0 1;
c along z-axis
 jbmi 1 1;1 2;1 2;1 4 1 v 0 0 1 1;
 jbmi 6 6;1 2;1 2;1 4 1 v 0 0 1 1;
c along y-axis
 kbmi 1 6;1 2;1 2;2 14 1 v 0 1 0 1;
c along x-axis
 kbmi 1 6;1 1;1 2;26 1 1 v 1 0 0 1;
c along y-axis
 ibmi 1 6;1 2;1 2;14 2 1 v 0 1 0 1;
```

```
c along z-axis
 ibmi 1 6;1 1;1 2;1 4 1 v 0 0 1 1;

c main deck (ship off/of.berth./repair)

block -1 -8 -10 -17 -19 -26;
      -1 9;
      -1 4;
      -4.4 2.6 4.6 11.6 13.6 20.6
       20.3 28.3
       0 3
thic 0.014;
mate 2;
c along x-axis
 jbmi 1 6;1 2;1 1;26 2 1 v 1 0 0 1;
c along z-axis
 jbmi 1 1;1 2;1 2;1 4 1 v 0 0 1 1;
 jbmi 6 6;1 2;1 2;1 4 1 v 0 0 1 1;
c along y-axis
 kbmi 1 6;1 2;1 2;2 9 1 v 0 1 0 1;
c along x-axis
 kbmi 1 6;1 1;1 2;26 1 1 v 1 0 0 1;
c along y-axis
 ibmi 1 6;1 2;1 1;9 1 1 v 0 1 0 1;
c along z-axis
 ibmi 1 6;1 1;1 2;1 4 1 v 0 0 1 1;

c main deck (med./gym/storage)

block -1 -8 -10 -17 -19 -26;
      -1 8;
      -1 4;
      -4.4 2.6 4.6 11.6 13.6 20.6
       28.3 35.3
       0 3
thic 0.014;
mate 2;
c along x-axis
 jbmi 1 6;1 2;1 1;26 2 1 v 1 0 0 1;
c along z-axis
 jbmi 1 1;1 2;1 2;1 4 1 v 0 0 1 1;
 jbmi 6 6;1 2;1 2;1 4 1 v 0 0 1 1;
c along y-axis
 kbmi 1 6;1 2;1 2;2 8 1 v 0 1 0 1;
c along x-axis
 kbmi 1 6;1 1;1 2;26 1 1 v 1 0 0 1;
c along y-axis
 ibmi 1 6;1 2;1 1;8 1 1 v 0 1 0 1;
c along z-axis
 ibmi 1 6;1 1;1 2;1 4 1 v 0 0 1 1;

c main deck (uuvs 1)

block -1 -3 -24 -26;
      -1 16;
      -1 4;
      -4.4 -2.4 18.6 20.6
```

```
       35.3 50.3
       0 3
thic 0.014;
mate 2;
c along x-axis
 jbmi 1 4;1 2;1 1;26 2 1 v 1 0 0 1;
c along z-axis
 jbmi 1 1;1 2;1 2;1 4 1 v 0 0 1 1;
 jbmi 4 4;1 2;1 2;1 4 1 v 0 0 1 1;
c along y-axis
 kbmi 1 4;1 2;1 2;2 16 1 v 0 1 0 1;
c along x-axis
 kbmi 1 4;1 1;1 2;26 1 1 v 1 0 0 1;
c along y-axis
 ibmi 1 4;1 2;1 1;16 1 1 v 0 1 0 1;
c along z-axis
 ibmi 1 4;1 1;1 2;1 4 1 v 0 0 1 1;


c main deck (ramp)

block -1 -3 -4 -23 -24 -26;
      -1 16;
      -1 4;
      -4.4 -2.4 -1.4 17.6 18.6 20.6
       50.3 65.3
       0 3
thic 0.014;
mate 2;
c along x-axis
 jbmi 1 6;1 2;1 1;26 2 1 v 1 0 0 1;
c along z-axis
 jbmi 1 1;1 2;1 2;1 4 1 v 0 0 1 1;
 jbmi 6 6;1 2;1 2;1 4 1 v 0 0 1 1;
c along y-axis
 kbmi 1 6;1 2;1 2;2 16 1 v 0 1 0 1;
c along x-axis
 kbmi 1 6;1 1;1 2;26 1 1 v 1 0 0 1;
c along y-axis
 ibmi 1 6;1 2;1 1;16 1 1 v 0 1 0 1;
c along z-axis
 ibmi 1 6;1 1;1 2;1 4 1 v 0 0 1 1;


c main deck (uuvs 2)

block -1 -13 -14 -26;
      -1 16;
      -1 4;
      -4.4 7.6 8.6 20.6
       65.3 80.3
       0 3
thic 0.014;
mate 2;
c along x-axis
 jbmi 1 4;1 2;1 1;26 2 1 v 1 0 0 1;
c along z-axis
 jbmi 1 1;1 2;1 2;1 4 1 v 0 0 1 1;
 jbmi 4 4;1 2;1 2;1 4 1 v 0 0 1 1;
```

108

```
c along y-axis
 kbmi 1 4;1 2;1 2;2 16 1 v 0 1 0 1;
c along x-axis
 kbmi 1 4;1 1;1 2;26 1 1 v 1 0 0 1;
c along y-axis
 ibmi 1 4;1 2;1 1;16 1 1 v 0 1 0 1;
c along z-axis
 ibmi 1 4;1 1;1 2;1 4 1 v 0 0 1 1;


c main deck (post off/wld-1)

block -1 -3 -4 -12 -15 -23 -24 -26;
      -1 9;
      -1 4;
      -4.4 -2.4 -1.4 6.6 9.6 17.6 18.6 20.6
       80.3 87.8
       0 3
thic 0.014;
mate 2;
c along x-axis
 jbmi 1 8;1 2;1 1;26 2 1 v 1 0 0 1;
c along z-axis
 jbmi 1 1;1 2;1 2;1 4 1 v 0 0 1 1;
 jbmi 8 8;1 2;1 2;1 4 1 v 0 0 1 1;
c along y-axis
 kbmi 1 8;1 2;1 2;2 9 1 v 0 1 0  1;
c along x-axis
 kbmi 1 8;1 1;1 2;26 1 1 v 1 0 0 1;
c along y-axis
 ibmi 1 8;1 2;1 1;9 1 1 v 0 1 0  1;
c along z-axis
 ibmi 1 8;1 1;1 2;1 4 1 v 0 0 1 1;


c main deck (enlisted berth./uuv workshop)

block -1 -13 -14 -26;
      -1 -23;
      -1 -4;
      -4.4 7.6 8.6 20.6
       87.8 110
       0 3
thic 0.014;
mate 2;
c along x-axis
 jbmi 1 4;1 2;1 2;26 2 1 v 1 0 0 1;
c along z-axis
 jbmi 1 1;1 2;1 2;1 4 1 v 0 0 1 1;
 jbmi 4 4;1 2;1 2;1 4 1 v 0 0 1 1;
c along y-axis
 kbmi 1 4;1 2;1 2;2 23 1 v 0 1 0  1;
c along x-axis
 kbmi 1 4;1 2;1 2;26 2 1 v 1 0 0 1;
c along y-axis
 ibmi 1 4;1 2;1 2;23 2 1 v 0 1 0  1;
c along z-axis
 ibmi 1 4;1 1;1 2;1 4 1 v 0 0 1 1;
 ibmi 1 4;2 2;1 2;1 4 1 v 0 0 1 1;
```

109

```
c left hull

block -1 -10;
      -1 -9 -22 -37 -52 -67 -82 -90 -98 -113;
       1 -8;
      -4.4 4.4
       0 7.80 20.3 35.3 50.3 65.3 80.3 87.8 95.3 110
       0 -7.48
thic 0.014;
mate 2;

c along z-axis
 jbmi 1 1;1 10;1 2;1 8 1 v 0 0 1 2;
 jbmi 2 2;1 10;1 2;1 8 1 v 0 0 1 2;
c along y-axis
 kbmi 1 1;1 10;1 2;1 111 1 v 0 1 0 2;
 kbmi 2 2;1 10;1 2;1 111 1 v 0 1 0 2;
c along x-axis
 kbmi 1 2;1 10;1 2;26 2 1 v 1 0 0 2;
c along y-axis
 ibmi 1 2;1 10;2 2;111 1 1 v 0 1 0 2;
c along z-axis
 ibmi 1 2;1 1;1 2;1 8 1 v 0 0 1 2;
 ibmi 1 2;2 2;1 2;1 8 1 v 0 0 1 2;
 ibmi 1 2;3 3;1 2;1 8 1 v 0 0 1 2;
 ibmi 1 2;4 4;1 2;1 8 1 v 0 0 1 2;
 ibmi 1 2;5 5;1 2;1 8 1 v 0 0 1 2;
 ibmi 1 2;6 6;1 2;1 8 1 v 0 0 1 2;
 ibmi 1 2;7 7;1 2;1 8 1 v 0 0 1 2;
 ibmi 1 2;8 8;1 2;1 8 1 v 0 0 1 2;
 ibmi 1 2;9 9;1 2;1 8 1 v 0 0 1 2;
 ibmi 1 2;10 10;1 2;1 8 1 v 0 0 1 2;


c projection of left hull

edge 1 10 2 2 10 2 91.2
edge 1 10 1 1 10 2 91.2
edge 2 10 1 2 10 2 91.2
edge 1 10 2 2 10 2 91.2
edge 1 10 1 2 10 1 91.1
sfi 1 2; -10; 1 2;sd 91
sfi -1 0 -2; 1 10; 1 2;sd 3
edge 1 1 2 2 1 2 3.1
sfi 1 2; 1 10; -2;sd 3

c right hull

block -1 -10;
      -1 -9 -22 -37 -52 -67 -82 -90 -98 -113;
       1 -8;
      11.8 20.6
      0 7.80 20.3 35.3 50.3 65.3 80.3 87.8 95.3 110
      0 -7.48
thic 0.014;
mate 2;
```

```
c along z-axis
 jbmi 1 1;1 10;1 2;1 8 1 v 0 0 1 2;
 jbmi 2 2;1 10;1 2;1 8 1 v 0 0 1 2;
c along y-axis
 kbmi 1 1;1 10;1 2;1 111 1 v 0 1 0 2;
 kbmi 2 2;1 10;1 2;1 111 1 v 0 1 0 2;
c along x-axis
 kbmi 1 2;1 10;1 2;26 2 1 v 1 0 0 2;
c along y-axis
 ibmi 1 2;1 10;2 2;111 1 1 v 0 1 0 2;
c along z-axis
 ibmi 1 2;1 1;1 2;1 8 1 v 0 0 1 2;
 ibmi 1 2;2 2;1 2;1 8 1 v 0 0 1 2;
 ibmi 1 2;3 3;1 2;1 8 1 v 0 0 1 2;
 ibmi 1 2;4 4;1 2;1 8 1 v 0 0 1 2;
 ibmi 1 2;5 5;1 2;1 8 1 v 0 0 1 2;
 ibmi 1 2;6 6;1 2;1 8 1 v 0 0 1 2;
 ibmi 1 2;7 7;1 2;1 8 1 v 0 0 1 2;
 ibmi 1 2;8 8;1 2;1 8 1 v 0 0 1 2;
 ibmi 1 2;9 9;1 2;1 8 1 v 0 0 1 2;
 ibmi 1 2;10 10;1 2;1 8 1 v 0 0 1 2;

c projection of right hull

edge 1 1 2 2 1 2 86.1
edge 1 1 1 1 1 2 86.1
edge 2 1 1 2 1 2 86.1
edge 1 10 2 2 10 2 94.2
edge 2 10 1 2 10 2 86.3
edge 1 10 1 1 10 2 94.2
edge 1 10 2 2 10 2 94.2
edge 1 10 1 2 10 1 94.1
sfi -1 0 -2; 1 10; 1 2;sd 86
sfi 1 2; 1 10; -2;sd 86

c left bow

block -1 -10;
      1 -8;
     -1 -8;
     -4.4 4.4
      0 -7.48
      0 -7.48
thic 0.014;
mate 2;
c along y-axis (problem with i)
 kbmi 1 1;1 2;1 2;1 8 1 v 0 1 0 2;
 kbmi 2 2;1 2;1 2;1 8 1 v 0 1 0 2;
c along z-axis
 jbmi 1 1;1 2;1 2;1 8 1 v 0 0 1 2;
 jbmi 2 2;1 2;1 2;1 8 1 v 0 0 1 2;

c along y-axis
 ibmi 1 2;1 2;1 2;8 2 1 v 0 1 0 2;
 ibmi 1 2;2 2;2 2;1 1 1 v 0 0 1 2;
 ibmi 1 2;2 2;1 1;1 1 1 v 0 0 1 2;
```

```
c projection of left bow

edge 1 2 1 2 2 1 5.1
edge 2 2 1 2 2 2 5.1
edge 2 1 1 2 2 1 5.1
edge 1 1 1 2 1 1 93.2
edge 1 1 1 1 2 1 5.1
sfi 1 2; 1 2; -1;sd 93
sfi -2; 1 2; 1 2;sd 5
sfi 1 2; 1 2; -2;sd 5
sfi -1; 1 2; 1 2;sd 5
sfi -2; 1 2; 1 2;sd 5
sfi 1 2; -2; 1 2;sd 5


c right bow

block -1 -10;
       1 -8;
      -1 -8;
      11.8 20.6
       0 -7.48
       0 -7.48
thic 0.014;
mate 2;
c along y-axis (problem with i)
 kbmi 1 1;1 2;1 2;1 8 1 v 0 1 0 2;
 kbmi 2 2;1 2;1 2;1 8 1 v 0 1 0 2;
c along z-axis
 jbmi 1 1;1 2;1 2;1 8 1 v 0 0 1 2;
 jbmi 2 2;1 2;1 2;1 8 1 v 0 0 1 2;

c along y-axis
 ibmi 1 2;1 2;1 2;8 2 1 v 0 1 0 2;
 ibmi 1 2;2 2;2 2;1 1 1 v 0 0 1 2;
 ibmi 1 2;2 2;1 1;1 1 1 v 0 0 1 2;


c projection of right bow

edge 1 2 1 2 2 1 92.1
edge 2 1 1 2 2 1 92.1
edge 1 1 1 1 2 1 92.1
sfi -1; 1 2; 1 2;sd 88
sfi -2; 1 2; 1 2;sd 88
sfi 1 2; 1 2; -1;sd 92
sfi 1 2; 1 2; -2;sd 88
sfi 1 2; -2; 1 2;sd 88


c 1st platform port

block 1 9;
       1 118;
       1 ;
      -3.89 3.89
      -7.48 110
      -3.5
thic 0.014;
mate 2;
```

```
c along x-axis (problem with i)
 jbmi 1 2;1 2;1 1;9 1 1 v 1 0 0 2;

c along y-axis
 ibmi 1 2;1 2;1 1;118 1 1 v 0 1 0 2;

c projection of 1st platform port

edge 1 1 1 2 1 1 90.1
edge 2 1 1 2 2 1 90.1
edge 1 1 1 1 2 1 90.1
edge 1 2 1 2 2 1 90.2
sfi 1 2; 1 2; -1; sd 90

c 1st platform starboard

block 1 9;
      1 118;
      1;
      12.31 20.09
    -7.48 110
    -3.5
thic 0.014;
mate 2;
c along x-axis (problem with i)
 jbmi 1 2;1 2;1 1;9 1 1 v 1 0 0 2;

c along y-axis
 ibmi 1 2;1 2;1 1;118 1 1 v 0 1 0 2;

c projection of 1st platform starboard

edge 1 1 1 2 1 1 89.1
edge 2 1 1 2 2 1 89.1
edge 1 1 1 1 2 1 89.1
edge 1 2 1 2 2 1 89.1
edge 1 2 1 2 2 1 89.2
sfi 1 2; 1 2; -1; sd 89
ztol 0.0001;
merge

delem lbm 8839 8838 8837 8836 8835 8834;
delem lbm 9145 9144 9143 9142 9141 9140;
delem lbm . .  . .  . .  . .  . . ;

fset hull = ls
c linear shells
12999:13030 13094:13165 13205:13256 13320:13436 13482:13541 13605:13739
...        ...       ...        ...       ...       ...
sd 999 faceset hull ;

abaqus

c  output file name is trugrdo

c  creating ABAQUS input deck

write
```

THIS PAGE INTENTIONALLY LEFT BLANK

APPENDIX C. FLUID MODELING OF SEA TENTACLE MODEL USING ABAQUS/CAE

This appendix covers the process for generating the fluid finite element mesh by using ABAQUS. ABAQUS is an advanced finite element analysis that provides complete and powerful solutions for linear and nonlinear engineering problems. It is a suite of finite element analysis modules. ABAQUS/CAE, having a modern graphical user interface (GUI) of menus, icons, and dialog boxes, provides the most complete interface with the ABAQUS solver programs available [Ref. 22]. The fluid mesh generation in ABAQUS/CAE is described as follows. In order to understand the process, the user should be familiar with the components of the ABAQUS/CAE and the appearance of the window. Figure 77 shows the components that appear in the main window.
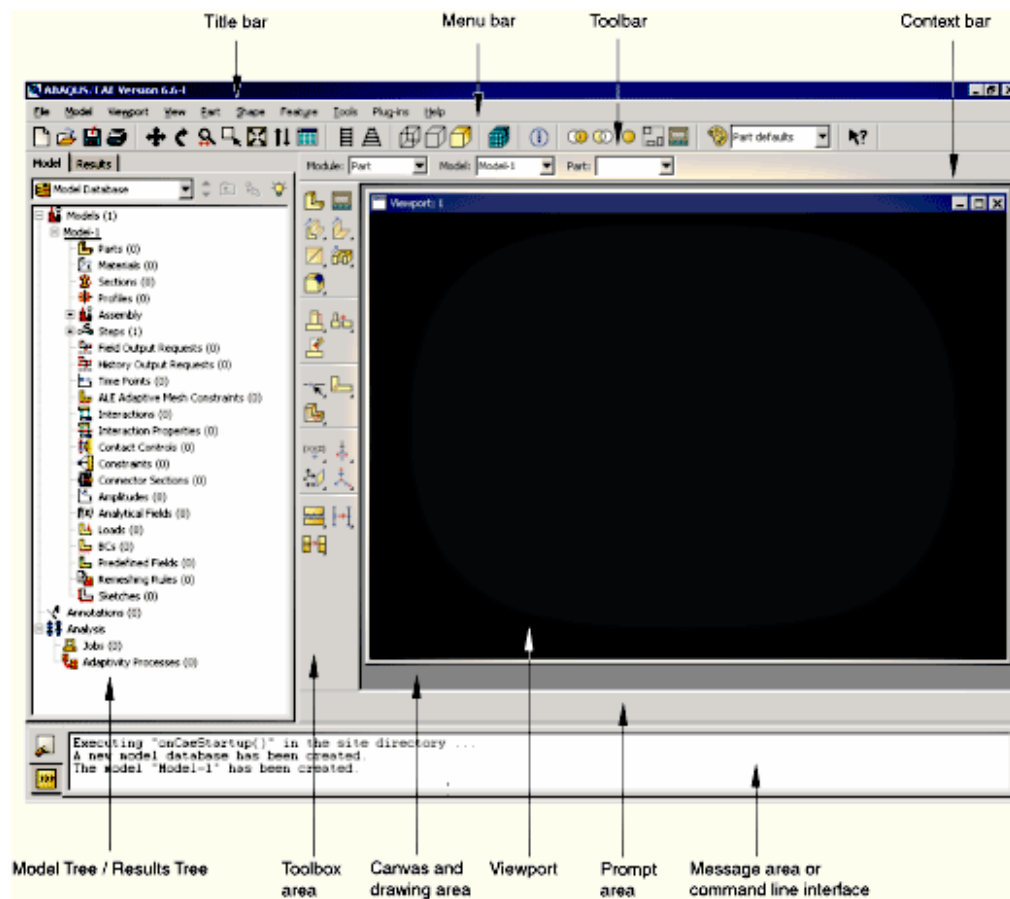

Figure 77.   Components of the main window in ABAQUS/CAE [Ref. 22]

1. Geometry can be imported from other packages with several file formats in ABAQUS/CAE. The best choice for importing geometry is importing it as an SAT file. From the main menu bar:

    File → Import → Part → Input the SAT file → Accept the conversion to precise representation → Select the solid topology → Click OK (Figure 78)
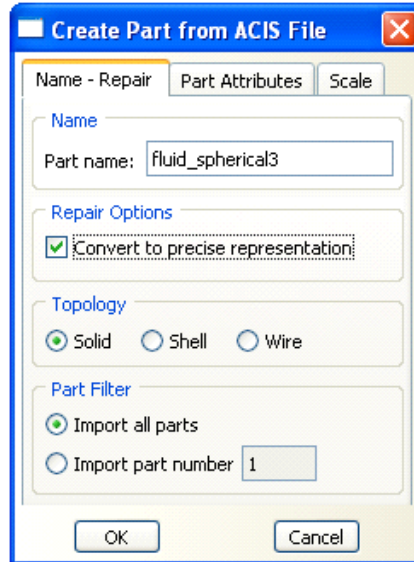

Figure 78.   Creating Part Dialog Box

2. The surfaces should be created in Part phase since they will be used in the Interaction phase. As shown in Figure 79, the nonreflecting circular and spherical surfaces are created in order to define the acoustic impedance in the Interaction phase. From the main menu bar:

    Tools → Surface → Create → Name the geometry → Select the regions interactively → Click DONE in the prompt area
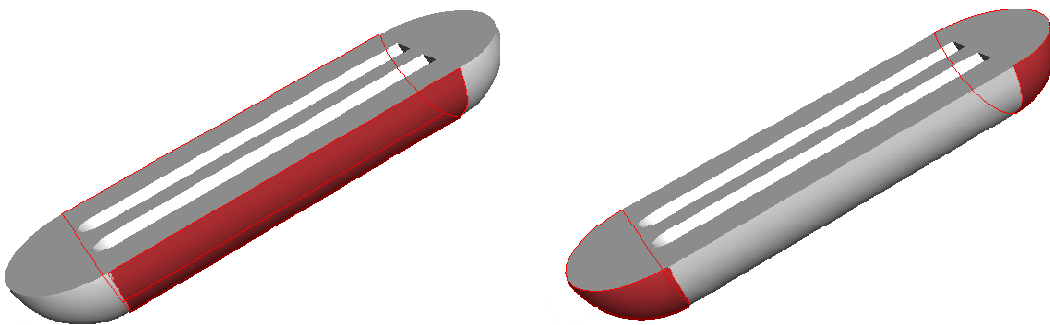

Figure 79.   Nonreflecting circular and spherical surfaces

116

3.　　The fluid material should be defined as an acoustic medium. From the tool bar, go to the Property Module and from the main menu bar:

Material → Create → Name the material → Select Other menu → Acoustic Medium → Enter the Bulk Modulus → Select General menu → Enter the mass density (Figure 80)

4.　　The section properties of a model can be defined by creating a section in the Property Module. Since the fluid mesh should have solid elements, a homogeneous solid section should be created. A homogeneous solid section is the simplest section type that the user can define. It includes only a material reference and a plane stress/plane strain thickness. From the main menu bar:

Section → Create → Select Solid Category → Accept Homogeneous as the default category section → Click Continue (Figure 81)

The solid section editor appears. In the Edit Section dialog box:

Select Material → Accept the default value of 1 for Plane stress/strain thickness → Click OK (Figure 81)
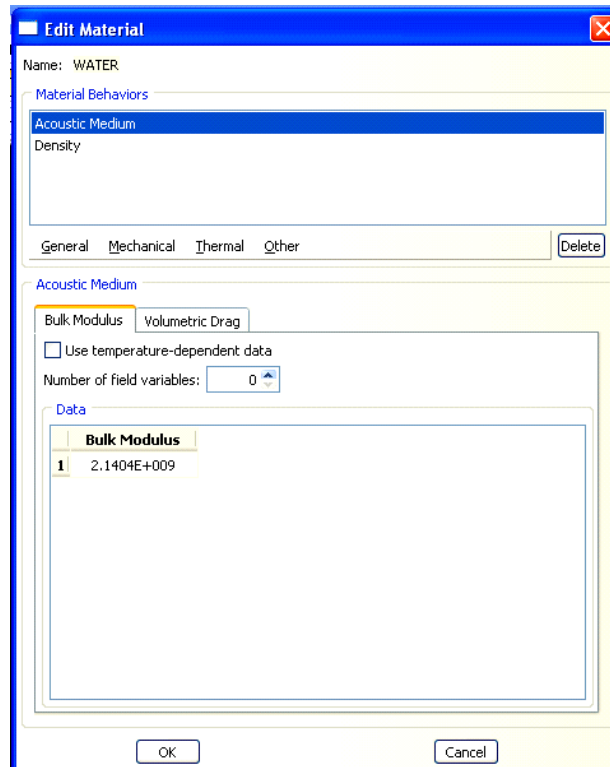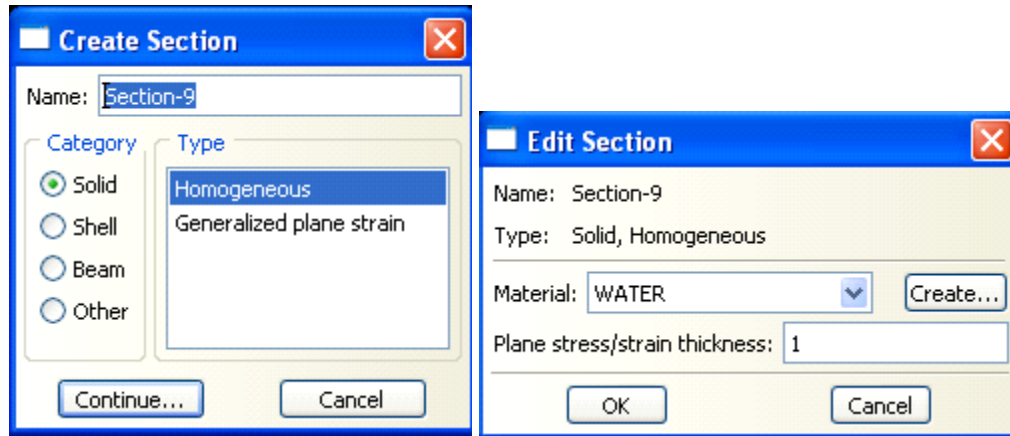

Figure 80.　Material Editor Dialog Box

Figure 81. Creating and Editing Section

5. Each part created is oriented in its own coordinate system and is independent of the other parts in the model. The Assembly module is used to define the geometry of the finished model by creating instances of a part. Although a model may contain many parts, it contains only one assembly. From the tool bar, go to the Assembly Module and from the main menu bar:

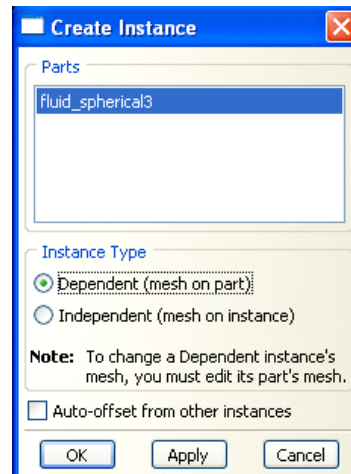**Instance → Create → Select the dependent instance type → Click OK**

Figure 82. Creating Instance

6. The Mesh module is used to generate the finite element mesh. The meshing techniques, which ABAQUS/CAE will use to create the mesh, the element type and shape can be chosen. For the Sea TENTACLE model, the element type of the fluid mesh should be the acoustic type. From the tool bar, go to the Mesh Module and select the fluid part from the Object menu. From the main menu bar:

Mesh → Element Type → Select Acoustic Finite Element → Select Tetrahedral Element (AC3D4) → Click OK (Figure 83)

118

7.   The Mesh Controls dialog box is used to examine the technique that ABAQUS/CAE will use. After assigning this element shape, the color of the part should be turned to purple. From the main menu bar:

Mesh → Mesh Controls → Select Tetrahedral as the element shape → Click OK (Figure 84)
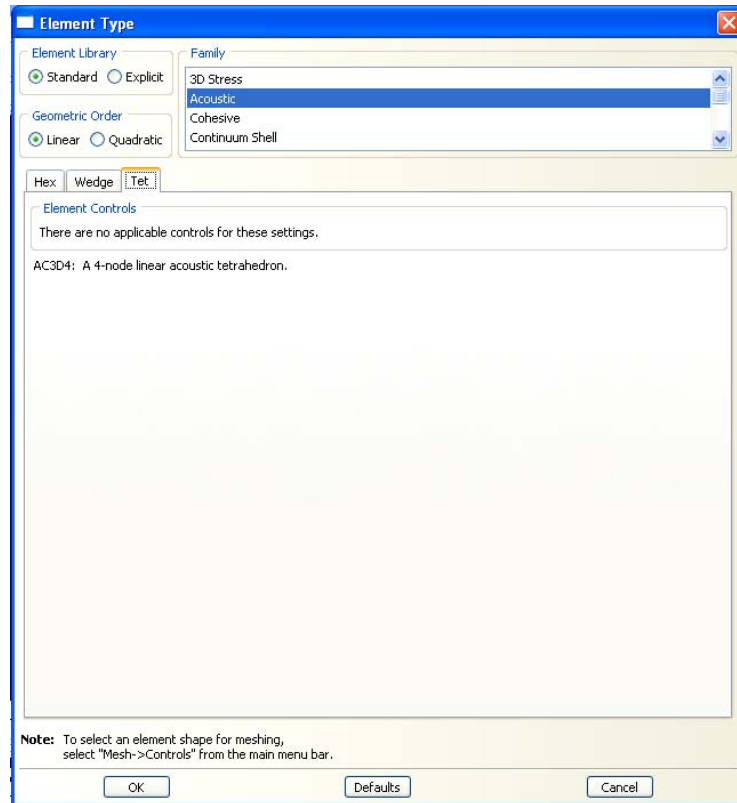

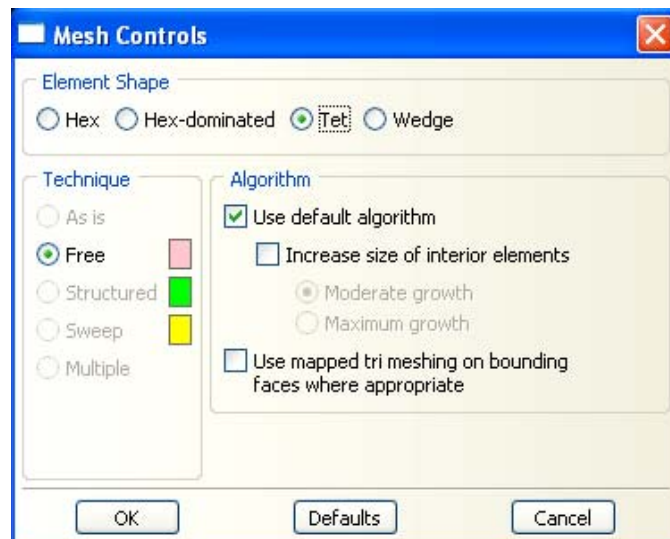**Figure 83.**   Selecting the Element Type

Figure 84.   Mesh Control Dialog Box

119

8.   The number of seeds should be selected prior to the meshing process. It can be accomplished by entering the approximate global seed size. For the Sea TENTACLE model, 1 m was input as the global element size. From the main menu bar:

Seed → Part → Enter the approximate global size of the element → Accept the other values as default → Click Apply and OK
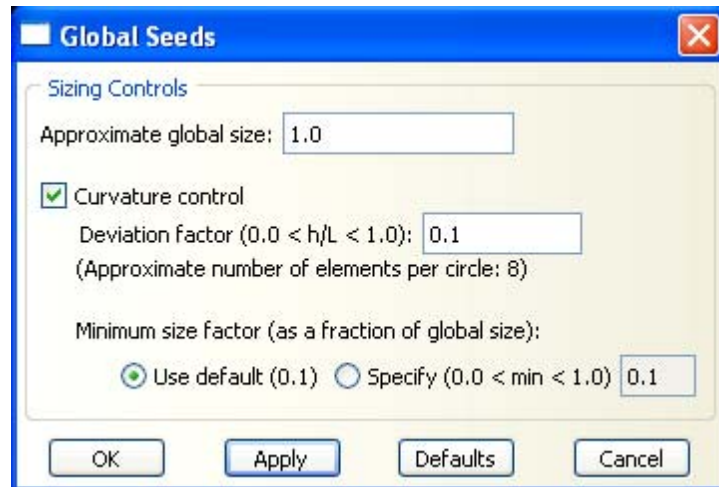

Figure 85.   Defining the Element Size

9.   In order to finish the meshing process, from the main menu bar:

Mesh → Part → Click Yes to confirm the meshing in the prompt area

The final mesh of the fluid mesh is displayed and the information about the mesh is given at the message prompt of ABAQUS/CAE.

APPENDIX D.   COUPLING THE FLUID/STRUCTURAL MESH AND UNDEX ANALYSIS OF SEA TENTACLE MODEL BY USING ABAQUS/CAE

ABAQUS/CAE incorporates the analysis modules into a **C**omplete **A**BAQUS **E**nvironment for modeling, managing, and monitoring ABAQUS analyses and visualizing results. It also introduces the generalized force on acoustic and solid media associated with the arrival of dilatational waves. Since the fluid mechanics is assumed to be linear, the wave fields in the fluid can be superimposed in a dynamic problem excited by a propagating wave in the fluid arriving from outside the domain [Ref. 22].

The fluid mesh and structural mesh should be coupled in order to couple the response of the structure to that of the fluid. This can be done by creating a TIE constraint in ABAQUS/CAE. This appendix covers the coupling process and UNDEX analysis for the Sea TENTACLE model.

1. The structural input file created in TrueGrid can be imported as a model in ABAQUS/CAE. From the main menu bar:

   File → Import → Model → Select the ABAQUS input file for the structural model

2. After importing the model, checking the features, sets, sections, and profiles of the structural model is strongly encouraged. From the model tree:

   Click Parts → Click PART-1 → Check the desired features

3. The fluid mesh can be created under the imported model tree as described in Appendix C.

4. After creating the fluid mesh, some surfaces of the fluid part should be defined prior to UNDEX analysis steps. The surface that will be coupled with the wetted surface of the ship and the exterior face of the fluid part that interacts with the charge should be defined as surfaces. These surfaces will be used in the Interaction Module for easier accessibility. In the Mesh Module:

   Tools → Surface → Create → Name the surface → Click OK → Select the region which will be coupled with the wetted surface of the ship (Do the same process for the exterior fluid surface)
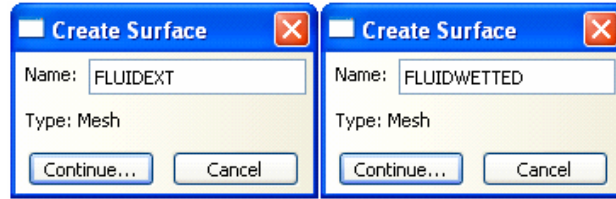
Figure 86.   Creating Surface Dialog Box

5. Coupling the fluid and structural mesh can be done by the TIE option. From the tool bar, go to the Interaction Module and from the main menu bar:

Constraint → Select TIE → Click OK → Choose the wetted surface of the ship as the master surface from the Surfaces option in the prompt area → Click Continue → Choose the fluid surface, FLUIDWETTED which was created in Step 4 as the slave surface from the Surfaces option in the prompt area → Click Continue → Click OK in the Edit Constraint window
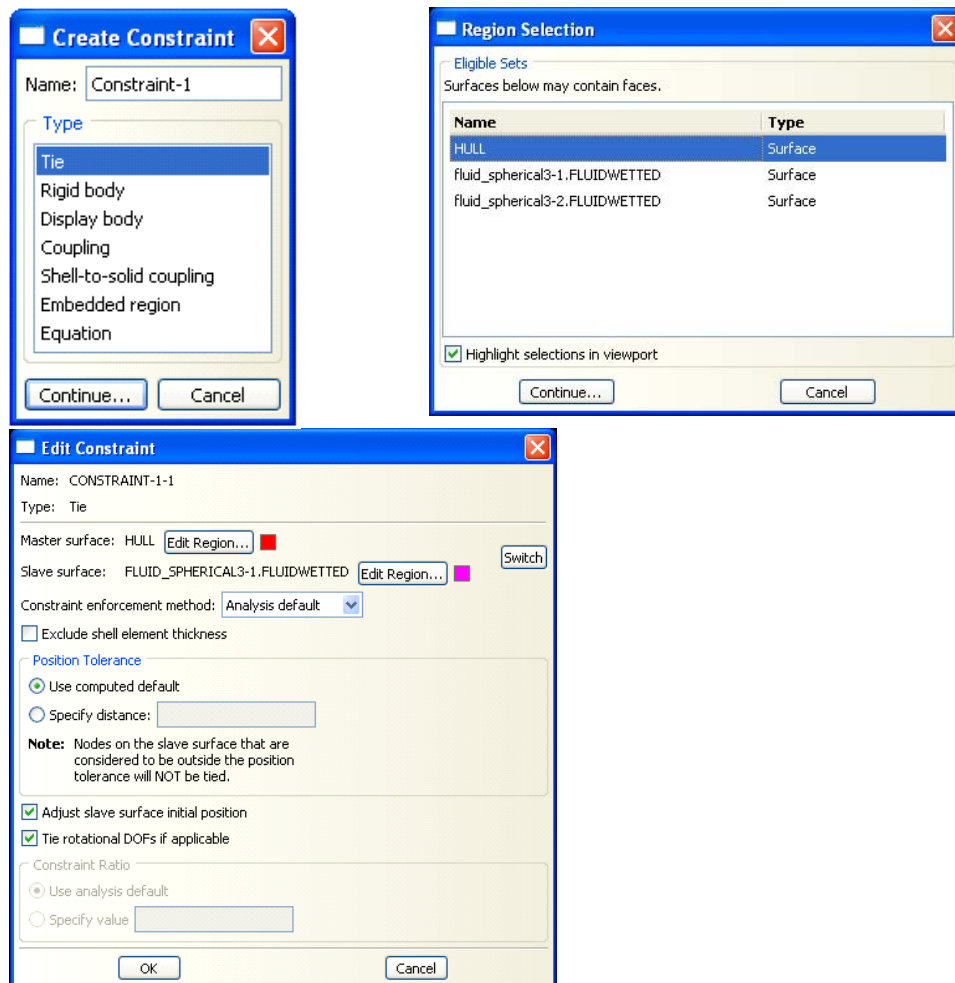

Figure 87.   Applying Constraint on the Model

122

6. After coupling the fluid-structural meshes, the next step is to create a specific analysis step. ABAQUS/CAE creates a special initial step at the beginning of the model's step sequence that allows the user to define the boundary conditions, fields and interactions that are applicable at the beginning of the analysis. The initial step is followed by one or more specific analysis steps. Incident wave loads are supported only in transient dynamic procedures. From the tool bar, go to the Interaction Module and from the main menu bar:

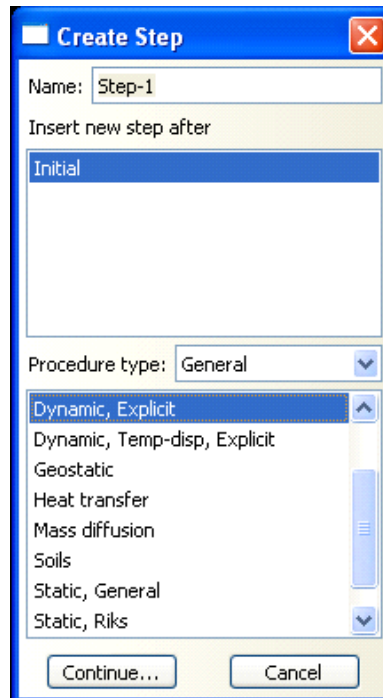**Step → Create → Select Dynamic, Explicit**

Figure 88.   Creating the Step

7. The step editor appears. In the editor window, the step properties should be defined. The incrementation of the step is of considerable interest. ABAQUS automatically subdivides a large time step into several smaller increments if it finds that the solution is nonlinear by using the Newton-Raphson iteration. This process is completely automatic, and ABAQUS will always take the largest possible time increments that will reach the end of the step and still give an accurate, convergent solution.

Select Basic tab → Name the step → Enter the desired time period (In Sea TENTACLE model, it was input as 0.5 seconds) → Select Incrementation tab → Select automatic type → Accept the default value of 1 for time scaling factor → Select Other tab → Enter the linear and quadratic bulk viscosity parameters (default values are shown in the figure)
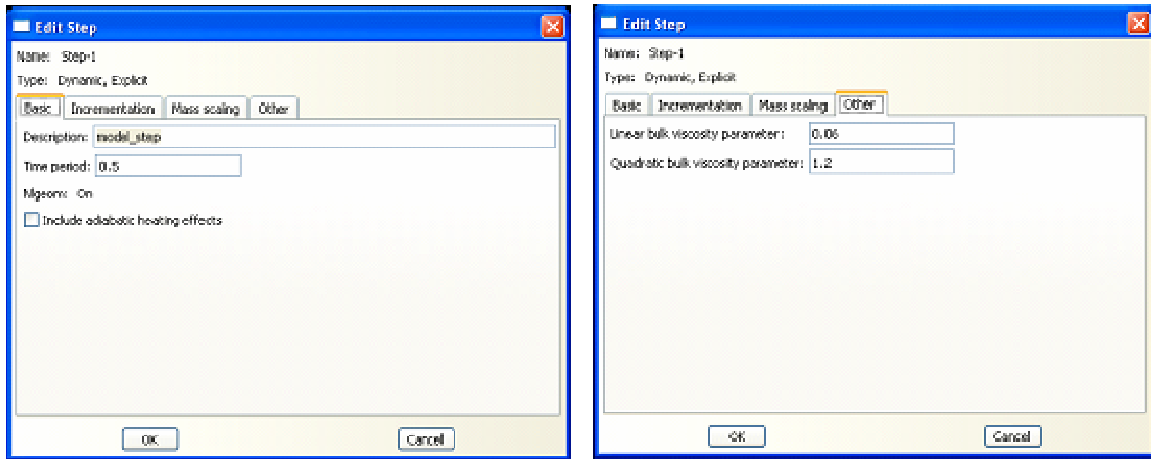
Figure 89.   Defining the Dynamic Step

8. The location of the charge and the stand-off point should be defined as reference points prior to the interaction. From the main menu bar:

Tools → Reference Point → Enter the location of the point at where the charge locates in the prompt area → Enter (Do the same process for the stand off point)
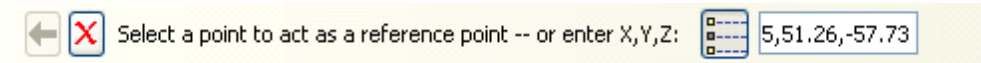

Figure 90.   Defining a Reference Point in the Prompt Area

9. The explosive load is specified with an incident wave load in UNDEX analysis. The load is applied on both the structure and the fluid at their common interface. The load is similar to a distributed load and the charge can be located outside the acoustic domain in ABAQUS/CAE. UNDEX analysis is tracked beginning at the standoff point. From the main menu bar:

Interaction → Create → Select Incident Wave → Click Continue → Select the type of region → Click on the first reference point and second reference point in the viewport interactively → Select the exterior fluid surface from the Surfaces option in the prompt area (Figure 91)

10. Interaction editor appears. In the interaction editor window:

Select the UNDEX from definition tab → Create Wave property → Select Incident Wave → Click OK (Figure 91)
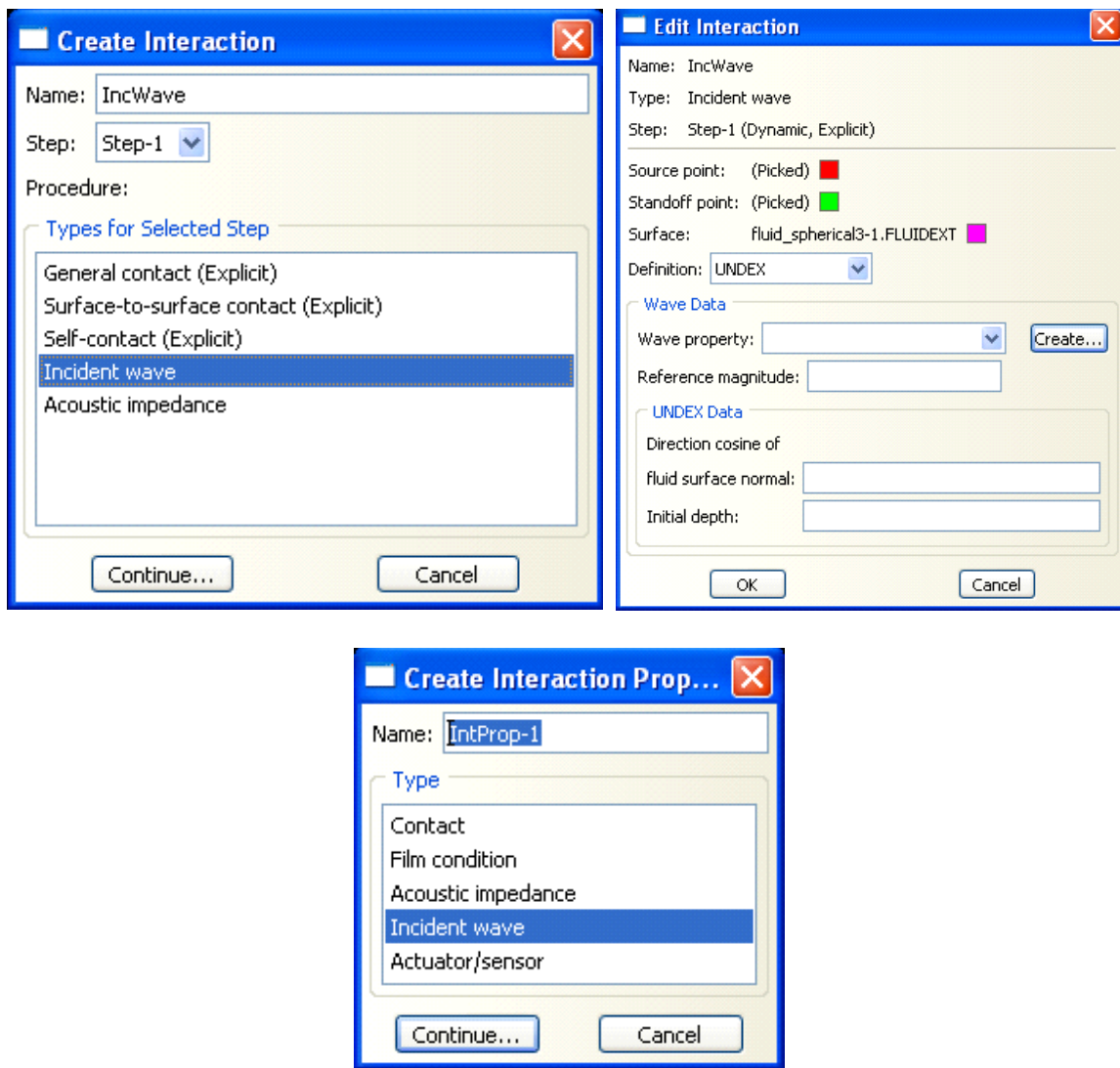
124

Figure 91.   Creating Incident Wave Interaction for the Model

11. Continue with the interaction editor. The charge used in the Sea TENTACLE model analysis is TNT. Since the metric system was used in the Sea TENTACLE model, all the values in Figure 92 are in metric system except the constants A and B that are dimensionless.

    Input the speed of sound and fluid mass density → Select the Spherical Wave definition → Click on the Use UNDEX Charge → Input the physical, material and bubble model step data

Figure 92. Defining the Properties of TNT Charge

12. Acoustic impedance is used to provide surface impedance information or nonreflecting boundaries for acoustic and coupled fluid-structural analysis. It states that acoustic energy leaves the mesh through a nonreflecting boundary. The nonreflecting type depends on the boundary geometry. In this thesis, fluid mesh consists of two spherical and one circular surface that were created separately in the Part phase. Therefore, the boundary type should be spherical and circular. From the main menu bar:

Interaction → Create → Name the interaction → Select Step-1 from the Step menu → Select Acoustic Impedance option → Click Continue → Select the one of the exterior surface of the fluid mesh as the boundary from the Surfaces option → Click Continue → Select Nonreflecting impedance definition in the Interaction editor window → Select Circular/Spherical as nonreflecting type and enter the radius of the geometry → Click OK (Repeat this process for each boundary surfaces)
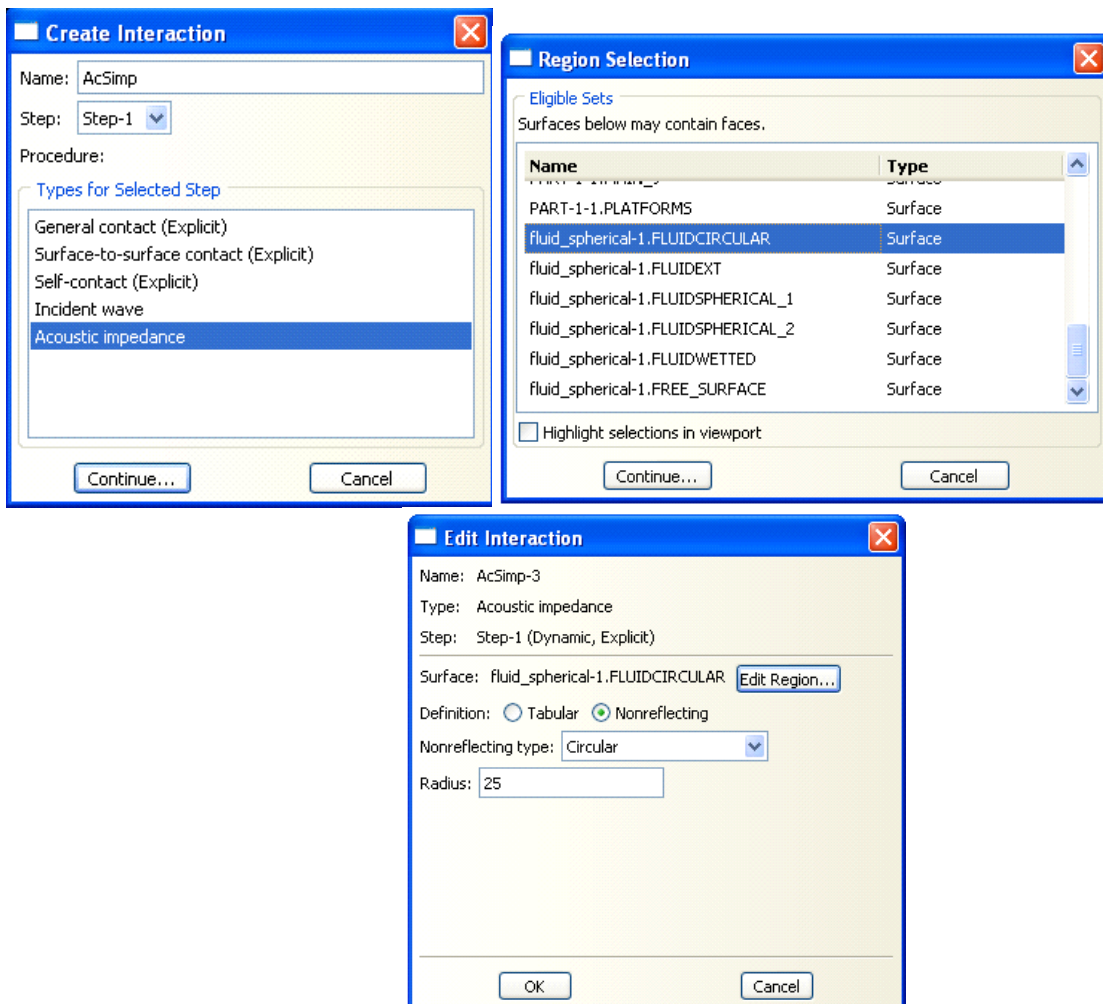

Figure 93.   Creating Acoustic Impedance Interaction

127

13. The dynamic acoustic pressure boundary condition on the free surface requires a zero pressure boundary condition on this surface in UNDEX phenomena. From the tool bar, go to the Load module and from the main menu bar:

BC → Create → Select Other from Category option → Select Acoustic pressure as the BC type → Click Continue → Select the free surface of the fluid as the BC location in the viewport interactively → Input 0 as the magnitude of the pressure at the free surface → Click OK
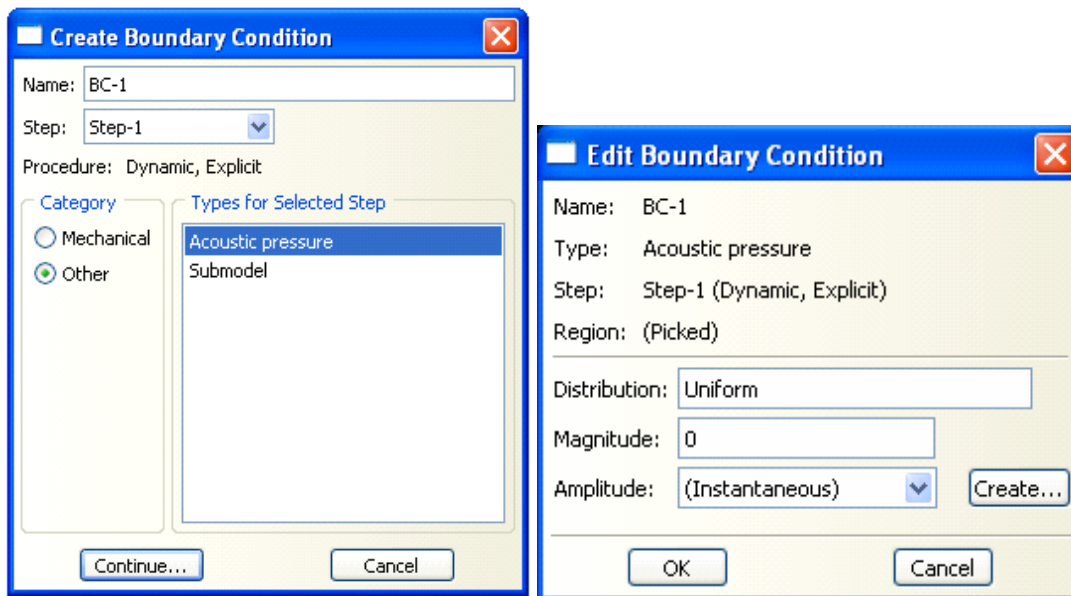
Figure 94. Creating the Boundary Condition at the Free Surface

14. The next step is to create the output requests. Field output variables are generally written at relatively low frequencies to the output database for the entire model. The velocity, acceleration and acoustic pressure are the main important field output variables for UNDEX analysis. The dynamics of the shock front can easily be seen in the plots by selecting the acoustic pressure variable as an output. From the tool bar, go to Step module and from the main menu bar:

Output → Field Output Resuests → Create → Select the whole model as the domain → Select Evenly Spaced Time Intervals as the frequency of obtaining the output → Input the desired time interval → Select Output at approximate times for timing → Select the desired output variables seperately (Displacement/Velocity/Acceleration, Acoustics and Stress etc) → Click OK
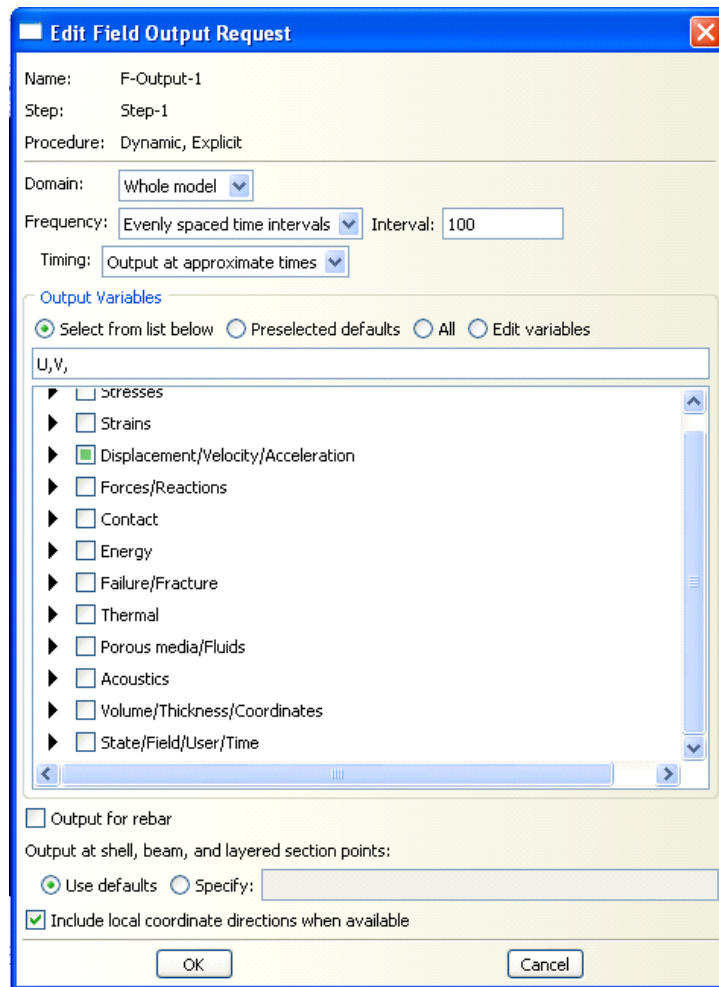
Figure 95.   Field Output Request

15. History output variables are generally written at relatively high frequencies to the output database for a small portion or node of the model. The velocity/acceleration is the main important history output variable for UNDEX analysis. The velocity history at critical points in the structure indicates the severity with which the shock has influenced the structure. From the main menu bar:

Output → History Output Requests → Create → Select the set as domain → Select the desired point/node → Pick every n time increments as the frequency → Input 1 as n value → Select the desired output variables (Displacement/Velocity/Acceleration) → Click OK
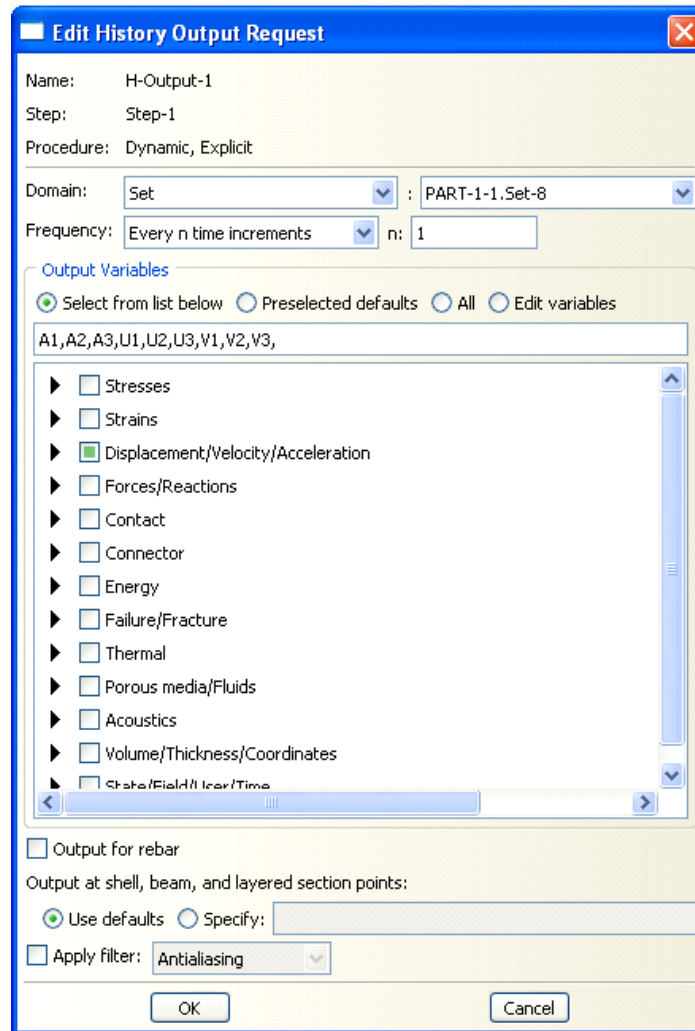
Figure 96. History Output Request

16. The next step is to edit the attribute of the model. The formulation type should be defined at this step. Total wave formulation was used in the Sea TENTACLE model. From the model tree:

Right Click on the model name → Click Edit Attributes → In the editor window, specify acoustic wave formulation (Figure 97)
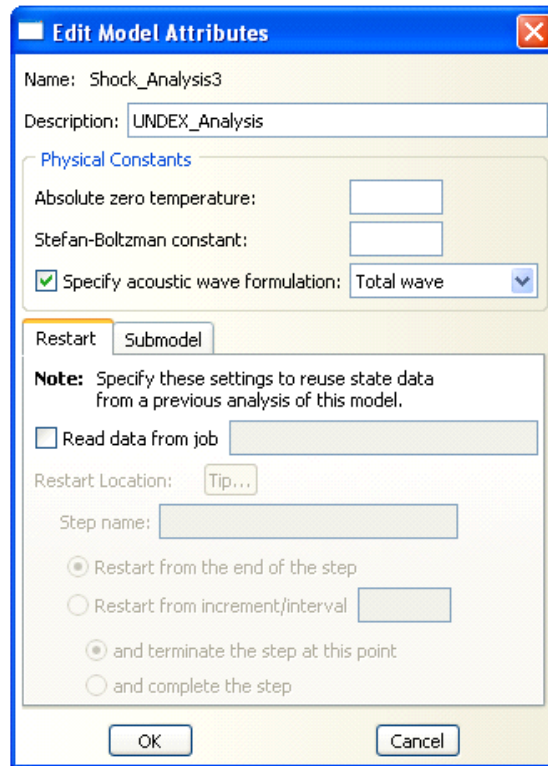
Figure 97. Specifying Total Wave Formulation

17. Some of the functions in UNDEX analysis are not supported in ABAQUS/CAE. Therefore, they have to be invoked by using keywords editor. From the model tree:

Right Click on the model name → Click Edit Keywords → In the editor window:

Define the cavitation limit in pressure magnitude under the Materials option:

```
*Acoustic Medium, Cavitation Limit

0.0,
```

Define the bubble loading in order to visualize the bubble history under the Interactions option:

```
*Amplitude, Definition=Bubble, Name=Bubble,
Time=Total
```

131

First Line:

Charge material constant K, k, A, B, adiabatic charge constant K_c, ratio of specific heats for gas, density of charge material, mass of charge material, charge depth

```
52.1E6,9E-005,0.18,0.185,839600000,1.27,1500,
3401.94, 57.0
```

Second Line:

Fluid mass density, sound speed in fluid, X-direction of cosine of fluid surface normal, Y-direction of cosine of fluid surface normal, Z-direction of cosine of fluid surface normal

```
1025.0, 1500.0, 0.0, 0.0, 1.0
```

Third Line:

Gravitational acceleration, atmospheric pressure, wave effect parameter, flow drag coefficient

```
9.8066, 101320, 1.0, 2.0
```

Fourth Line:

Time duration, maximum number of time steps, relative step size, absolute step size, step size control exponent

```
1.5, 1500, 1E-011, 1E-011, 0.2
```

Define the acoustic static pressure at two reference points as an initial condition:

```
*Initial Conditions, Type=Acoustic Static
Pressure
fluid_spherical-1.FLUID,0,8.08768177,-
30.5471306, -2.75, 251381.25, 8.10000038, -
7.48000002, -27.75
```

18. The Job module is used to create and configure the analysis jobs. Submitting a job to ABAQUS/Standard or ABAQUS/Explicit for analysis generates the input files and submits them as analysis jobs. The input file can be created without submitting the job. From the tool bar, go to the Job module and from the main menu bar:

Job → Create → Select the model → Click Continue → Name the description of the job → Select the Full Analysis from the Submission tab → Input the file processor memory as the maximum memory of the machine that will be used for the analysis. **(Figure 98)**

19. The final step is submitting the job and running the analysis. From the main menu bar:

Job → Manager → Click on Submit (Click on Write Input in order to create the input file without running the analysis) (Figure 99)
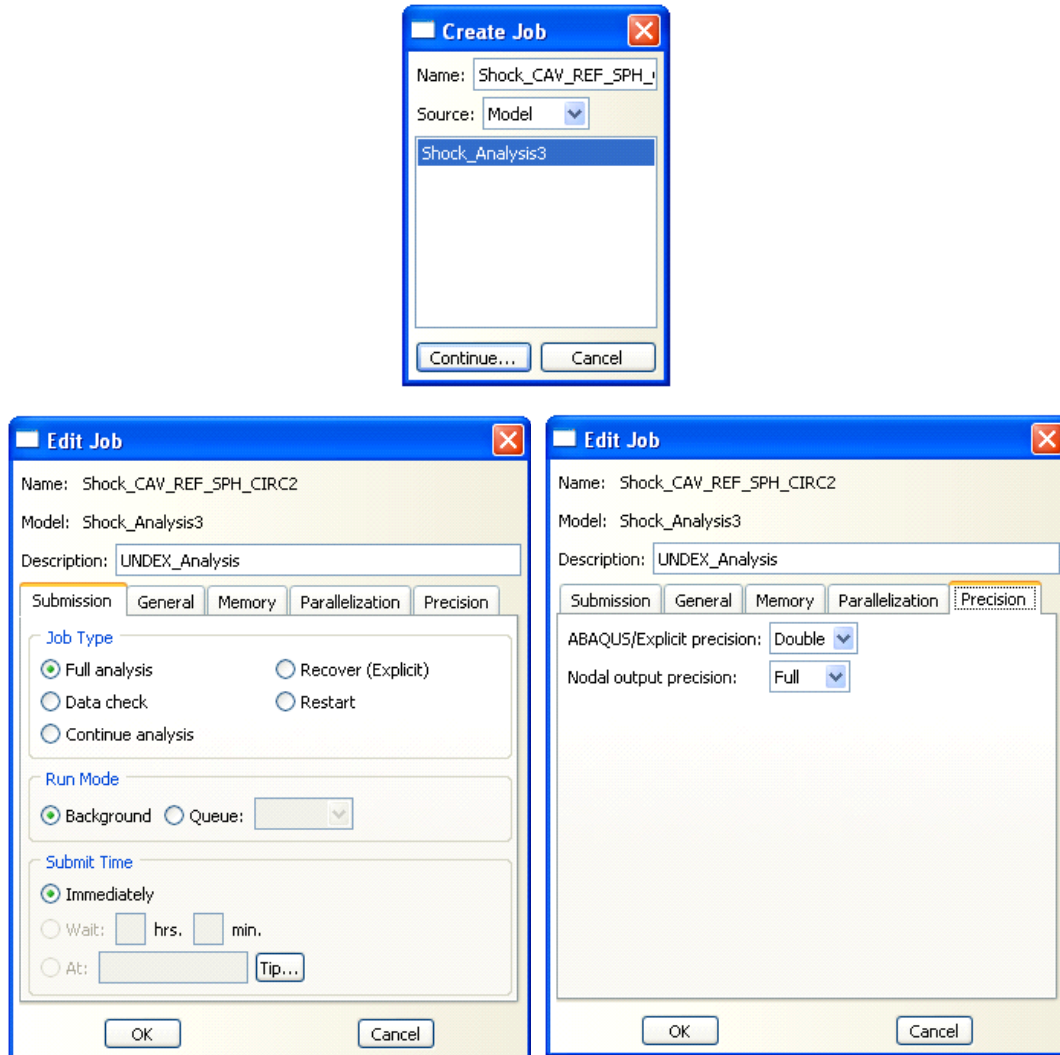
Figure 98. Creating the Job for Simulation
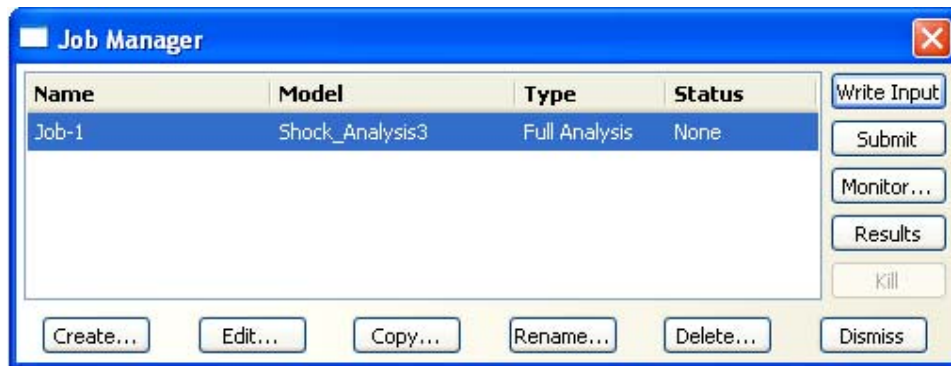
Figure 99. Job Manager Dialog Box

The input file of the model is summarized as follows.

```
**
** MATERIALS
**
*Material, name=M1
*Damping, alpha=19.2, beta=2.09e-06
*Density
7850.,
*Elastic
 2.07e+11, 0.3
*Material, name=M2
*Damping, alpha=19.2, beta=2.09e-06
*Density
7850.,
*Elastic
 2.07e+11, 0.3
*Material, name=WATER
*Acoustic Medium
 2.1404e+09,
*Density
1025.,
**
** INTERACTION PROPERTIES
**
*Incident   Wave   Interaction   Property,   name=INTPROP-1,
type=SPHERE
1500., 1025.
*UNDEX Charge Property
5.21e+07, 9e-05, 0.18, 0.185, 8.396e+08, 1.27
1500., 3401.94, 9.8066, 101320., 1.0, 2.
1.5, 1500, 1e-11, 1e-11, 0.2
57., 0., 0., 1.
```

```
**
** PHYSICAL CONSTANTS
**
*Acoustic Wave Formulation, type=TOTAL WAVE
** -------------------------------------------------------
*Initial Conditions, Type=Acoustic Static Pressure
fluid_spherical-1.FLUID, 0, 8.08768177, -30.5471306, -2.75,
251381.25, 8.10000038, -7.48000002, -27.75
**
** STEP: Step-1
**
*Step, name=Step-1
model_step
*Dynamic, Explicit
, 1.5
*Bulk Viscosity
0.06, 1.2
**
** BOUNDARY CONDITIONS
**
** Name: Aco-BC-1 Type: Acoustic pressure
*Boundary
FLUID_SPHERICAL-1.FREESURFACE, 8, 8
**
** INTERACTIONS
**
** Interaction: AcSimp-1
*Simpedance, nonreflecting=SPHERICAL
FLUID_SPHERICAL-1.FLUIDSPHERICAL_1, 25.
** Interaction: AcSimp-2
*Simpedance, nonreflecting=SPHERICAL
FLUID_SPHERICAL-1.FLUIDSPHERICAL_2, 25.
** Interaction: AcSimp-3
*Simpedance, nonreflecting=CIRCULAR
FLUID_SPHERICAL-1.FLUIDCIRCULAR, 25.
** Interaction: IncWave-1
*Incident wave interaction, UNDEX, property=INTPROP-1
FLUID_SPHERICAL-1.FLUIDEXT,_PICKEDSET28,_PICKEDSET29, 1.
**
** OUTPUT REQUESTS
**
*Restart, write, number interval=1, time marks=NO
**
** FIELD OUTPUT: F-Output-1
**
*Output, field, number interval=100
```

```
*Node Output
PABS, POR
**
** FIELD OUTPUT: F-Output-2
**
*Element Output, directions=YES
S,
**
** FIELD OUTPUT: F-Output-3
**
*Node Output
U, V
**
** HISTORY OUTPUT: H-Output-1
**
*Output, history, frequency=1
*Node Output, nset=PART-1-1.GAP_MAIN01
A1, A2, A3, U1, U2, U3, V1, V2
V3
**
```

LIST OF REFERENCES

1.   NAVSHIPS 250-660-26, "Mechanical Shock on Naval Vessels," March 1946

2.   NSWCCD/UERD, www.dt.navy.mil/sur-str-mat/sur-wea-eff/his, September 2006.

3.   OPNAV Instruction 9072.2, "Shock Hardening of Surface Ships," 12 January 1987.

4.   NAVSEA 0908-LP-000-3010A, Shock Design Criteria for Surface Ships, October 1994.

5.   Military Specification, MIL-S-901D, Shock Tests, High Impact Shipboard Machinery, Equipment and Systems, Requirements for, March 1989.

6.   USS John Paul Jones (DDG-53) Shock Trial Final Report, AEGIS Program Manager (PMS-400), November 1994.

7.   DOT&E FY97 Annual Report, www.globalsecurity.org/military/library/budget/fy1997/dot-e/navy/97ddg51.html, September 2006.

8.   Shin, Y. S. and Schneider, N. A., "Ship Shock Trial Simulation of USS Winston S. Churchill (DDG-81): Modeling and Simulation Strategy and Surrounding Fluid Volume Effects" Proceedings of the 74th Shock and Vibration Symposium, San Diego, CA, 27-31 October 2003.

9.   Shin, Y. S., "Ship Shock Modeling and Simulation for Far-field Underwater Explosion," Computers & Structures, 82 (2004) 2211-2219.

10.   Shin, Y. S., "Naval Ship Shock and Design Analysis" Course Notes for Underwater Shock Analysis, Naval Postgraduate School, Monterey, California, 2006.

11.   Cole, R. H., *Underwater Explosions*, pp. 1-15, Princeton University Press, 1948.

12.   DeRuntz, Jr., J. A., *The Underwater Shock Analysis (USA) Manual*, Unique Software Applications, Colorado Springs, Colorado, May 1996.

13.   Arons, A. B., et al., "Long Range Shock Propagation in Underwater Explosion Phenomena II," Underwater Explosion Compendium, Vol. 1, October 1949.

14.   Didoszak, J. M., "Parametric Studies of DDG-81 Ship Shock Trial Simulations," Master's Thesis, Naval Postgraduate School, Monterey, California, 2004.

15.   Shin, Y. S., "LS-DYNA Training Guide: Nonlinear Dynamic Analysis of Structures in 3-D Code Coupled with Underwater Shock Analysis Code for Ship Shock Modeling and Simulation," Naval Postgraduate School, July 2002.

16.   DeRuntz, Jr., J. A. "The Underwater Shock Analysis Code and Its Applications," 60th Shock and Vibration Symposium, Vol. I, pp. 89-107, November 1989.

17.   Geers, T. L., "Doubly Asymptotic Approximations for Transient Motions of Submerged Structures," Journal of the Acoustical Society of America, Vol. 64, pp 1500-1508, 1978.

18.   DeRuntz, Jr. J. A. and Rankin, C.C., "Applications of the USA-STAGS-CFA Code to Nonlinear Fluid-Structure Interaction Problems in Underwater Shock of Submerged Structures," Proceedings of the 60th Shock and Vibration Symposium, 1989.

19.   Shin, Y. S. and Santiago, L. D., "Surface Ship Modeling and Simulation: 2D Analysis," Journal of Shock and Vibration, Vol. 5, No. 2, 1998, John Wiley & Sons, Inc.

20.   Naval Postgraduate School Technical Report, "Sea TENTACLE," January 2006.

21.   XYZ Scientific Applications, Inc., *TrueGrid Manual*, Livermore, California, 1997.

22.   Hibbitt, Karlsson & Sorensen, Inc., *ABAQUS User's Manual*, Version 6.6

23.   Shin, Y. S. and Ham, I., "Damping Modeling Strategy for Naval Ship System," Proceedings of the 74th Shock and Vibration Symposium, San Diego CA, 27-31 October 2003.

24.   Schneider, N. A., "Prediction of Surface Ship Response to Severe Underwater Explosions Using a Virtual Underwater Shock Environment," Master's Thesis, Naval Postgraduate School, Monterey, California, 2003.

INITIAL DISTRIBUTION LIST

1.   Defense Technical Information Center
        Ft. Belvoir, Virginia

2.   Dudley Knox Library
        Naval Postgraduate School
        Monterey, California

3.   Mechanical Engineering Department Chairman, Code ME
        Naval Postgraduate School
        Monterey, California

4.   Naval/Mechanical Engineering Curriculum Code 74
        Naval Postgraduate School
        Monterey, California

5.   Prof. Young S. Shin, Code ME/Sg
        Department of Mechanical and Astronautical Engineering
        Naval Postgraduate School
        Monterey, California

6.   Research Assistant Prof. Jarema M. Didoszak, ME/Di
        Department of Mechanical and Astronautical Engineering
        Naval Postgraduate School
        Monterey, California

7.   LTjg Hakan Ucar
        Turkish Navy
        Istanbul, Turkey

8.   Dr. Jeff Cipolla
        ABAQUS, Inc.
        Providence, Rhode Island

9.   Karl D'Souza
        ABAQUS, Inc.
        Providence, Rhode Island

10.   Dibyendu Datta
        ABAQUS, Inc.
        Providence, Rhode Island

11.   Frederick A. Costanzo
Underwater Explosion Research Department (UERD)
Naval Surface Warfare Center – Carderock Division
West Bethesda, Maryland

12.   Hans U. Mair
Institute for Defense Analysis
Alexandria, Virginia